TALLINN UNIVERSITY OF TECHNOLOGY
School of Information Technologies
Thomas Johann Seebeck Department of Electronics

Akmalidin Alisher O'g'li Alimov, 177321IVEM

PHASED ARRAY ANTENNA DESIGN FOR MIMO AND BEAMFORMING TECHNOLOGIES ON 5G

Master's Thesis

Supervisor: Yannick Le Moullec
PhD

Tallinn 2019

TALLINNA TEHNIKAÜLIKOOL
Infotehnoloogia teaduskond
Thomas Johann Seebecki elektroonikainstituut

Akmalidin Alisher O'g'li Alimov, 177321IVEM

FAASINIHUTUSEGA VÕREANTENNI DISAIN 5G MIMO JA SUUNATUD SIGNAALIEDASTUSE TEHNOLOOGIAS

Magistritöö

Juhendaja: Yannick Le Moullec

PhD

Tallinn 2019

Author’s declaration of originality

I hereby certify that I am the sole author of this thesis. All the used materials, references to the literature and the work of others have been referred to. This thesis has not been presented for examination anywhere else.

Author: Akmalidin Alisher O’g’li Alimov

04.05.2019

Abstract

Phased Array Antenna Design For MIMO and Beamforming Technologies on 5G

The application of phased array antennas is expanding rapidly with the introduction of 5G technology where MIMO and beamforming technologies are key enablers of high data rate exchange. Among others, 5G technology is creating new business opportunities in logistics, for example, using delivery drones and robots that exploit a low latency remote control to deliver items. To benefit from a high data rate exchange and real-time control, such drones and robots need to be equipped with array antennas. However, designing a compact antenna that would support MIMO and beamforming technologies is a challenging task since these technologies require different antenna element spacing in the phased array antenna construction.

In this thesis, a 6x6 (16 active elements) phased array antenna is proposed with MIMO performance prioritized over beamforming since beam shaping requires intensive signal processing, which may rapidly drain the battery of e.g. the delivery robot.
Prior to array antenna design and simulation, a state-of-the-art on beamforming and MIMO technologies, as well as mutual coupling reduction between elements and impact of the main beam steering to the antenna operational impedance, are discussed.
Several design approaches are presented (common ground plane, individual ground plane, an individual ground plane with metallic slots, for 4x4 and 6x6 configurations) and their respective performances are analysed.

Although the proposed 6x6 (16 active elements) phased array antenna beamforming performance does not satisfy the requirements in terms of steering the main beam to +45° to -45°on φ and θ planes, its MIMO metrics such as correlation coefficient and diversity gain results are within the required limits. Maximum beamforming of 7° on azimuth and elevation planes has been accomplished even though 20° main lobe steering phase distribution has been applied between elements. The simulated MIMO performance for correlation coefficients between antenna elements is below 0.005, while diversity gain results in the frequency range of 2.5 GHz - 2.7 GHz are above 9.95 dB, which meets the requirements set in the thesis.

Overall, the results are encouraging and pave the way for further development of such phased array antennas.

The thesis is in English and contains 78 pages of text, 6 chapters, 79 figures, 6 tables.

Annotatsioon

Faasinihutusega võreantenni disain 5G MIMO ja suunatud signaaliedastuse tehnoloogias

Faseeritud maatriksantennide kasutamine on kiires kasvutrendis tänu 5G-tehnoloogia arengule, kus ülikiire andmeside on võimalik peamiselt tänu MIMO-le ja suunatud raadiolevile. Näitena paljude hulgast võib tuua 5G tehnoloogia loodavad uued ärivõimalused logistika vallas, kus andmeside madal latentsusaeg võimaldab lihtsamalt juhtida kauba kättetoimetamiseks kasutatavaid droone ja roboteid. Et kasutada ülikiire andmeside eeliseid ja reaalajas toimivat juhtimist tuleb taolised robotid ja droonid varustada maatriksantennidega. Ometi on sellise kompaktse antenni väljatöötamine, mis toetaks samaaegselt nii MIMO-t kui ka suunatud raadiolevi, keerukas ülesanne. Seda peamiselt seetõttu, et kumbki neist tehnoloogiaist vajab isesugust vahekaugust antenni elementide vahel.

Käesolevas töös on käsitletud 6x6-elemendise (neist 16 on aktiivelemendid) ringpolariseeritud faseeritud maatriksantenni väljatöötlust. Seejuures on MIMO jaoks olulised parameetrid eelisseisus suunatud raadiolevi jaoks oluliste parameetrite ees, kuna raadiokiire moodustamiseks vajalik intensiivne signaalitöötlus on energiamahukas ning võib vähendada seadmete, näiteks kaubarobotite akude kestvust.

Enne antenni väljatöötluse juurde asumist leiavad käsitlemist raadiokiire juhtimise ning MIMO tehnoloogiate kaasaegne tipptase, samuti meetodid soovimatute sidestuste vähendamiseks antenni elementide vahel ja antenni peakiire juhtimisest tulenevad antenni tööimpedantsi muutused.

Käsitlust leiavad mitmed väljatöötlusvariandid koos nende parameetrite võrdleva analüüsiga – näiteks ühise maatasemega, eraldatud maatasemetega, eraldatud maatasemetega metall-piluantennid, 4x4- ja 6x6-maatriksite juhud.

Kuigi väljapakutud 16 aktiivelemendiga 6x6-elemendiline faseeritud antennimaatriks ei võimalda saavutada peakiire kallutatavust vahemikus +45 kuni -45° φ- ja θ-sihtides, on tema MIMO-parameetrid nagu korrelatsioonitegur ja hajusvõimendus siiski etteantud piirides. Saavutatav on maksimaalne kallutuse väärtus 7° asimuudi ja tõusutasandites, kuigi kasutatav elementidevaheline pealehe faasijaotuse väärtus on kuni 20°. Simuleerimistulemustest saadud MIMO-parameetrite väärtused on järgmised: antenni elementidevahelised korrelatsioonitegurid jäävad alla 0.005, samas kui saavutatav hajusvõimendus ületab 9.95 dB, mis on kooskõlas antud tööle esitatud nõudmistega. Saavutatud tulemused on üldiselt paljutõotavad ning sillutavad teed edasisele tööle taoliste faseeritud antennimaatriksite väljatöötlusel.

Töö on kirjutatud inglise keeles ning sisaldab 78 lehekülge, 6 peatükki, 79 joonist ja 6 tabelit.

Acronyms

BS base station. 13

CCL channel capacity loss. 25

DL downlink (Base station to user communication link). 14

ECC envelope correlation coefficient. 21–23, 25

eMBB enhanced mobile broadband. 16

GDS grounded dielectric slab. 35

IoT The Internet of Things. 13

LOS line-of-sight. 49

MIMO multiple-input-multiple-output. 13

MTC machine type communication. 16

RX receiver. 48

SISO single-input-single-output. 48, 49

SNR signal-to-noise-ration. 48

TX transmitter. 13, 48

UL uplink (User to base station communication link). 14

URLLC ultra-low latency. 16

List of Figures

1.1 Spatial multiplexing using 2x2 antenna configuration parallel signals S1 and S2 transmission with channel matrix H and received signals r1,r2 [5]. 14

1.2 5G End-to-End communication using Beam Steering [11]. 16

1.3 Main beam scanning from -45 degree to +45 degree. If the beam goes to lower angles close to elements (fillet with red), it may affect elements' radiation and bandwidth of under it. 19

2.1 (a) Configuration of the two-port multiband MIMO antenna; (b) Detailed configuration of the hybrid strips [18]. 21

2.2 Comparison of the measured and simulated reflection coefficients of the MIMO antenna proposed in [18]. 22

2.3 Comparison of the measured and simulated mutual coupling coefficient of the MIMO antenna proposed in [18]. 23

2.4 (a) UWB MIMO antenna geometry proposed dimensions: L=42 mm, W=25 mm, L_{SA}=21 mm, W_{SA}=8 mm, L_{f1}=8 mm, L_{f2}=9 mm, W_f=2 mm, W_{f1}=1.2 mm, L_1=4.6 mm, W_1=2.3 mm, L_2=0.8 mm, W_2=2.3 mm, L_3=3.2 mm, W_3=1.6 mm, L_4=0.6 mm, W_4=1.4 mm, L_5=3 mm, d_1=4.8 mm, d= 7 mm, g=11.2 mm (b) Fabricated antenna top and bottom view [19] 24

2.5 Simulated and measured S-parameters comparison of the four-element MIMO antenna proposed in [19]. S_{11} coefficient is shown for the 1^{st} element and S12, S13, S14 represents 50 Ω terminated 2^{nd}, 3^{rd} and 4^{th} elements' coupling effects on the 1^{st} element, respectively [19]. 26

2.6 The distance between antenna elements (g parameter) impact on S-parameters. The increase of g parameter, lowers the mutual coupling between elements [19]. 27

2.7 3-D radiation pattern of Ant_1 and Ant_2 at 6GHz (a) Ant_1 radiation on $-y$ axis and (b) Ant_2 radiation on $+y$ axis. When Ant_1 and Ant_2 are excitepd, other ports are terminated with 50 Ω matched load [19]. 27
2.8 The Vertical distance between antenna elements (d parameter) impact on S-parameters. Increasing the d parameter lowers the mutual coupling between elements [19]. 28
2.9 UWB MIMO antenna measured ECC and CCL values from 3GHz to 12 GHz. The values are lower than the limits [19]. 28
2.10 Array factor of four column antenna with a half-wavelength spaced. the beam is not steered keeping at 0 degree and sidelobes are suppressed [6]. . 29
2.11 90°ideal standard base station column patterns [6]. 30
2.12 The array factor and column patter overlay. The mean beam and two sidelobes get amplified and other parts are cancelled [6]. 31
2.13 Final pattern accomplished by summing the array factor and column pattern [6]. 31
2.14 Main beam steering 30°and 25dB sidelobe suppression achieved by amplitude tapering. [6] 32
2.15 The array factor and column pattern summed. Sidelobe levels are 25dB down but grating lobes at the edge of column pattern is not suppressed. [6]. 33
2.16 A beam steered 20° to the right and the secondary beam falls into the column pattern results in having 3dB difference between main beam and grating lobe on the left [6]. 33
2.17 Periodic fractal defected ground structure between elements. The dimensions of etched FDGS from the ground plane can be calculated to reject the desired frequency range and reduce mutual coupling. [27] 35
2.18 Reflection coefficient of the 1^{st} element (S_{11}), mutual coupling between the 1^{st} and 2^{nd} element (S_{12}), and reflection coefficient of the 2^{nd} element (S_{22}), with and without defected ground structure[27] 36
2.19 Proposed structure on E-plane for mutual coupling reduction [20] 36
2.20 Current distribution on the patch element. The slots placed between the elements reflect the surface wave, reducing the coupling of radiated element to the adjacent element [20] 37

2.21 Proposed structure mutual coupling effect on E-plane (L = W = 9.3 mm, y_f = 1.55 mm, ϵ_r = 2.2, ϵ_{r2} = 10.2, L_s = 5.8 mm, W_s = 0.3 mm , S = 14.99 mm, h_1 = h_2 = 0.787 mm, t = 0.02 mm). (a) The effect of slots' spacing variation on mutual coupling between 2 elements, (b) The conventional versus proposed structure reflection coefficient of the 1^{st} element (S_{11}) and mutual coupling between 2 elements (S_{12}) [20] 39

3.1 Uniform excitation of 4x4 phased array antenna with the same amplitude level set to form a directed beam in a particular direction (Uniform excitation does not support side lobe level reduction) 44
3.2 Taylor excitation of 4x4 phased array antenna elements with various amplitude values assigned to form a directed beam in a particular direction with at least -30 dB side lobe levels 45
3.3 2D Phased array pattern with "Taylor" (green curve) and "Uniform" (red curve) excitation. Taylor excitation uses amplitude tapering which tailors amplitude levels to elements individually [45] 45
3.4 The cumulative distribution function of equation (2.5), showing the diversity gain obtained as a function of the increase in the number of antenna elements [40] 48

4.1 Taylor pattern excitation signals for the phased array antenna elements (16 active elements) with various amplitude levels 51
4.2 Square truncated capacitively pin-fed circularly polarized patch antenna top view [46] 52
4.3 Square truncated capacitively pin-fed circularly polarized patch antenna side view [46] 53
4.4 Reflection coefficient of the patch element with dimensions indicated in Table 4.1, assuming center frequency being 2.5 GHz 53
4.5 3D radiation pattern of square truncated capacitively pin-fed circularly polarized patch antenna [46] 54

4.6 S11 parameters of an 6x6 array antenna whose elements are designed setting the center frequency at 2.6 GHz. All active elements' reflection coefficients are shown with 100 MHz shift from 2.5 GHz to 2.6 GHz on a -10 dB level) 54

4.7 Front (On the right) and back (on the left) views of the 4x4 phased array antenna (16 elements' numbers indicated) with shared ground plane between elements. 56

4.8 Reflection coefficients of the 16 elements with a shared ground plane between them. The curves are not below the -10 dB level within the B7 frequency range 56

4.9 Mutual coupling results for 8 elements. The coupling levels are high between the 5^{th},6^{th},7^{th},8^{th},9^{th},10^{th},11^{th}, and 12^{th} elements because of high amplitude levels; on the other hand, the impact of the 5^{th} and 6^{th} elements is low on the 1^{st} element 57

4.10 Surface wave caused by internal reflection of electromagnetic waves on two different medias: metal and air [47] 57

4.11 Excitation signals for the 1^{st}, 6^{th}, 7^{th},10^{th}, 10^{th}, and 16^{th} elements of the phased array antenna 58

4.12 Surface wave flow between the 16 elements of the shared ground plane antenna at 2.5 GHZ frequency with 0° beamforming. The amplitudes of the elements located at the edge are low so does the surface wave flow intensity 59

4.13 Front and back view of the 6x6 (16 active elements) phased array antenna with only active elements numbered on the shared ground plane 60

4.14 6x6 phased array antenna "Taylor" excitation view. The highest amplitude levels are at the four elements at the centre; the other elements have lower amplitudes 60

4.15 Simulation results for (6x6 phased array) 16 active elements reflection coefficients with shared ground plane between elements with ϕ , θ=0° direction beamforming. The elements exhibit below -10 dB levels within the B7 frequency range 61

4.16 6x6 phased array's 8^{th} and 29^{th} elements at the edge, each assigned with 0.4 $W^{\frac{1}{2}}$ 62

4.17 Surface wave flow of common ground plane array antenna on 2.5 GHz frequency with ϕ , θ = 0° beamforming. The array has 36 elements but only 16 of them are active, the rest is passive but surface wave leaks to passive elements too. 62

4.18 Radiation and total efficiency of 6x6 phased array within the desired frequency band B7 (2.5 GHz - 2.7 GHz) with linear scale, 1 being 100 % efficiency. 63

4.19 6x6 phased array 16 active element impedance representation. All the active elements' impedance values (load impedance) are close to 50Ω (input impedance) 63

4.20 2D radiation pattern of 6x6 phased array antenna with the blue lines representing the angular width of the beam at 2.625 GHz frequency (Downlink Frequency of B7 band [7]). The main beam directed to 0° with magnitude achieves 17.2 dBi and a side lobe level of -19.7 dB 64

4.21 Reflection coefficients of the (6x6 phased array) 16 elements with shared ground plane between the elements with 5° beamforming. 65

4.22 2D radiation pattern of 6x6 phased array antenna with blue lines representing the angular width of the beam at 2.625 GHz frequency (Downlink Frequency of B7 band [7]). The main beam is directed to 2° even though 5° beamforming phase distribution is applied for each element. The achieved magnitude is 15.7 dBi and the side lobe level is -19.3 dB 65

4.23 Surface wave flow of common ground plane array antenna on 2.5 GHz frequency with ϕ , θ = 5° beamforming. The array has 36 elements but only 16 of them are active; the other ones are passive but surface wave still leaks to passive elements. 66

5.1 Simulation results of the reflection coefficients for the 4x4 phased array with individual ground planes (16 active elements) on ϕ, θ= 0° beamforming with 2.5 GHz- 2.7 GHz frequency range that of interest. 69

5.2 Mutual coupling results for 8 elements within 2.5 GHz - 2.7 GHz. The coupling levels are high between the the 5^{th}, 6^{th}, 7^{th}, 8^{th}, 9^{th}, 10^{th}, 11^{th}, and 12^{th} elements because of high amplitude levels; on the other hand, the impact of the 5^{th} and 6^{th} elements is low on the 1^{st} element 69

5.3 Front and back views of 4x4 (16 active elements) phased array antenna with only active elements numbering on an isolated ground plane 70

5.4 Surface wave flow between individual ground planes used in the 16 element array antenna on 2.5 GHZ frequency with 0° beamforming. 70

5.5 4x4 phased array radiation on x-axis component of H-plane. The magnetic field distribution is low on the 4^{th} and 13^{th} elements compared to the 1^{st} and 16^{th} elements 71

5.6 A Patch antenna element with metallic slots on the bottom as well as on the right-hand side, which is used to make a 6x6 array antenna 72

5.7 4x4 isolated ground plane phased array antenna with metallic slots placed between the elements. 73

5.8 4x4 isolated ground plane phased array antenna reflection coefficients of each element. The frequency range of interest is 2.5 GHz - 2.7 GHz . . . 73

5.9 Mutual coupling results for 8 elements. The coupling levels are high between the 5^{th}, 6^{th}, 7^{th}, 8^{th}, 9^{th}, 10^{th}, 11^{th}, and 12^{th} elements because of high amplitude levels; on the other hand, the impact of the 5^{th} and 6^{th} elements is low on the 1^{st} element within 2.5 GHz - 2.7 GHz 74

5.10 Front and back view of 6x6 (16 active elements) phased array antenna with only active elements numbering and isolated ground planes 75

5.11 Reflection coefficients of (6x6 phased array) 16 elements with individual ground planes on each patch with ϕ , θ= 0° beamforming. 75

5.12 Radiation and total efficiency of 6x6 phased array within desired frequency band B7 (2.5 GHz - 2.7 GHz) with linear scale, 1 being 100 % efficiency 76

5.13 A surface wave flow of isolated ground plane array antenna on 2.5 GHz frequency with ϕ , θ= 0° beamforming. The array has 36 elements but only 16 of them are active, the rest is passive but surface wave leaks to passive elements too. 76

5.14 2D radiation pattern of 6x6 phased array antenna with blue lines representing the angular width of the beam at 2.625 GHz frequency (Downlink Frequency of B7 band [7]). The phase distribution is applied for each element to steer the beam in ϕ, θ= 0° direction. The achieved main lobe magnitude is 17 dBi and the side lobe levels are -18.4 dB 77

5.15 Reflection coefficients of (6x6 phased array) 16 elements with individual ground planes on each patch with ϕ , θ= 5° beamforming. 78

5.16 2D radiation pattern of 6x6 phased array antenna at 2.625 GHz frequency (Downlink Frequency of B7 band [7]). The main beam is directed to 2° even though 5° beamforming phase distribution is applied for each element. The achieved magnitude is 15.5 dBi and the side lobe level is -18.4 dB 78

5.17 Reflection coefficients of (6x6 phased array) 16 elements with individual ground planes on each patch with ϕ , θ = 10° beamforming. 79

5.18 2D radiation pattern of 6x6 phased array antenna at 2.625 GHz frequency (Downlink Frequency of the B7 band [7]). The main beam is directed to 4° even though 10° beamforming phase distribution is applied for each element. The achieved magnitude is 13.6 dBi and the side lobe level is -18.5 dB 80

5.19 Single patch element truncation length impact on reflection coefficient [46]. The green line shows 6.6 mm and the red line 5.8 mm truncation length. The two resonant frequencies are brought closer with truncation length = 5.8 mm (Red curve) 81

5.20 6x6 phased array antenna with isolated ground plane as well as with metallic slots between elements 82

5.21 Reflection coefficients of 6x6 phased array antenna with isolated ground plane as well as with metallic slots between elements on ϕ , θ = 10° beamforming 82

5.22 A surface wave flow of isolated ground plane array antenna with metallic slots placed between elements on 2.5 GHz frequency with ϕ , θ= 10° beamforming. The array has 36 elements but only 16 of them are active, the rest is passive but surface wave leaks to passive elements too. 83

5.23 2D radiation pattern of 6x6 phased array antenna at 2.625 GHz frequency (Downlink Frequency of the B7 band [7]). The main beam is directed to 4° even though 10° beamforming phase distribution is applied for each element. The achieved main lobe magnitude is 13.7 dBi and the side lobe level is -18.0 dB 84

5.24 Reflection coefficients of 6x6 phased array antenna with isolated ground plane as well as with metallic slots between elements on ϕ, θ = 20° beamforming 85

5.25 2D radiation pattern of 6x6 phased array antenna at 2.625 GHz frequency (Downlink Frequency of the B7 band [7]). The main beam is directed to 7° even though 20° beamforming phase distribution is applied for each element. The achieved main lobe magnitude is 11.2 dBi and the side lobe level is -17.9 dB 85

5.26 Correlation coefficients of 16 elements in 6x6 phased array antenna with isolated ground and the metallic slots between elements 86

5.27 Diversity gain of 16 elements in 6x6 phased array antenna with isolated ground and the metallic slots between elements. The graph shows diversity between one element and neighboring elements on the right and the top. . 87

6.1 Stacked pin-fed rectangular patch antenna element. The active radiating element is placed between two different substrate materials. There is a passive radiator which is capacitively coupled to the active radiator 91

List of Tables

2.1 ECCs calculated for different frequencies at three desired bands, i.e., 900 MHz, 2 GHz and 3.5/5 GHz 24

3.1 32 Active element phased array antenna parameter requirements 41

4.1 Square truncated capacitively pin-fed circularly polarized patch antenna element dimensions and performance parameters [46] 55

5.1 Square truncated capacitively pin-fed circularly polarized patch antenna element's single ground plane size (each element ground plane size is identical). 68

5.2 Square truncated capacitively pin-fed circularly polarized patch antenna element's modified parameters 72

5.3 Square truncated capacitively pin-fed circularly polarized patch antenna element single ground plane size (each element individual ground plane's size is identical). 74

Contents

1 Introduction **13**

1.1 Motivation to study 5G 16

1.2 Problem Statement 16

1.2.1 Mutual coupling reduction 17

1.2.2 Surface current impact on the main beam scanning angle 17

1.2.3 Optimization of array antenna element parameters for an acceptable MIMO and beamforming 18

1.3 Approach followed in this thesis 18

2 State-of-the-Art on Antenna Design for MIMO and Beamforming Technologies **20**

2.1 "Closely-spaced Multi-band MIMO Antenna for Mobile Terminals" paper review 21

2.2 "Compact MIMO Slot Antenna for UWB Applications" paper review . . 23

2.3 "Beamforming Antenna Spacing Variations" paper review 29

2.4 "Wide scan phased array patch antenna with mutual coupling reduction" paper review 32

2.4.1 Defected ground structures [25]–[27] 34

2.4.2 Grounded dielectric slab loaded by slot [20] 35

3 MIMO and Beamforming Antenna Design Requirements **40**

3.1 General Parameter Goals 41

3.1.1 S-Parameter Goals 41

3.1.2 Antenna Polarization Goals 42

3.1.3 The phased array antenna element spacing for beamforming and MIMO technologies 42
3.2 Beamforming requirements and performance metrics 43
3.2.1 Total Active Reflection Coefficient (TARC) metric 44
3.3 MIMO antenna requirements and performance metrics 46
3.3.1 Correlation Coefficient 46
3.3.2 Diversity Gain 47
3.3.3 Channel Capacity 48

4 Initial Results : Antenna Design, Simulation, and Analysis 50
4.1 Square truncated capacitively pin-fed circularly polarized patch antenna dimensions 52
4.2 Common Ground Plane 4x4 (16 active elements) Phased Array Antenna Simulation Results 54
4.3 Common Ground Plane 6x6 (16 active elements) Phased Array Antenna Simulation Results 59
4.3.1 ϕ , $\theta = 0°$ beamforming simulation results and analyses 61
4.3.2 ϕ , $\theta = 5°$ beamforming simulation results and analysis 64

5 Optimized Results: Antenna Design, Simulation and Analysis 67
5.1 4x4 (16 active elements) Phased Array Antenna Simulation Results and Analysis 68
5.1.1 Individual Ground Plane 4x4 (16 active elements) Phased Array Antenna Simulation Results 68
5.1.2 Individual Ground Plane with Metallic Slots 4x4 (16 active elements) Phased Array Antenna Simulation Results 71
5.2 6x6 (16 active elements) Phased Array Antenna Simulation Results 73
5.2.1 Individual Ground Plane 6x6 (16 active elements) Phased Array Antenna Simulation Results 74
5.2.2 Individual Ground Plane with Metallic Slots 6x6 (16 active elements) Phased Array Antenna Simulation Results 80

6 Conclusion and Future Work 88
6.1 The future steps 90

Chapter 1

Introduction

Wireless communication is one of the fastest growing fields attracting various businesses, media and empowering people's imagination. Exponential growth in cellular networks over the last decade resulted in achieving 4.7 billion users worldwide in 2018 [1]. In fact, mobile and smartphones have become a vital tool for business and everyday life in most countries, not only for communication but also for data acquisition, analysis and The Internet of Things (IoT) .

Antennas are one of the key elements of a wireless communication system; they convert signals into an electromagnetic wave for transmission and the other way around for the reception. Antenna systems play an important role in terms of achieving base station (BS) coverage area, high data rate transmission and high energy efficiency. Currently, 4G base station (BS)s are equipped with multiple antennas ranging from 2 up to 16 branch antennas [2] and upcoming 5G technology requires massive MIMO with various combinations starting from 16 elements transmitter (TX), 4x4 (16 elements), 8x4 (32 elements), 8x8 (64 element), etc. antennas and up [3] that are used to transmit and receive information, which is known as multiple-input-multiple-output (MIMO) technology [4].

MIMO technology requires multiple antennas on both the transmitter and receiver sides, which can benefit in various scenarios. A number of antennas at the receiver and transmitter sides simultaneously can be used for parallel communication, creating independent channels between antenna elements, as illustrated in **Figure 1.1**. Such implementation known as spatial multiplexing gives a possibility for high data rate exchange in limited bandwidth radio channel without degradation of power efficiency, and the data rate in-

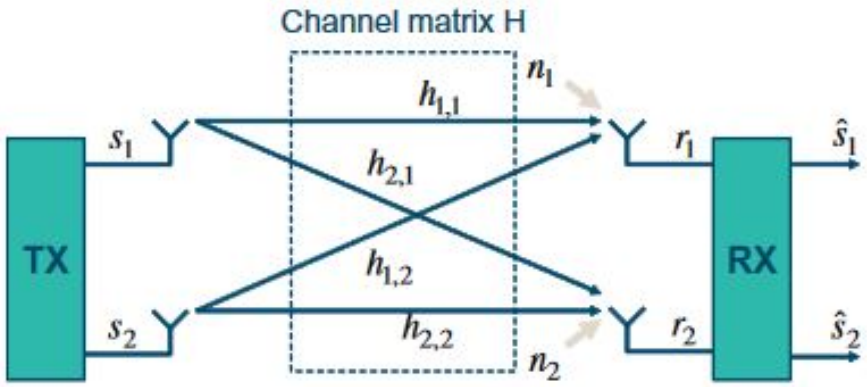

Figure. 1.1. Spatial multiplexing using 2x2 antenna configuration parallel signals S1 and S2 transmission with channel matrix H and received signals r1,r2 [5].

creases linearly based on the number of antennas [5]. Another beneficial use-case is to avoid multi-path fading on the radio channel where the same information signal is received with multiple antennas at the receiver side. Furthermore, multiple antenna techniques can also be used to shape the electromagnetic beam of the antenna to a specific target direction. Consequently, beamforming maximizes the total gain of the array antenna at receiver/transmitter sides and suppresses the interfering signals in the radio channel, increasing network capacity as shown in **Figure 1.1**.

Diverse requirements of spatial multiplexing and beamforming in antenna structure make that it is one of the intensively researched topics [6]. This MSc thesis is in line with such ongoing research and focuses on antenna module design for the 5G networks sub-6-GHz N7 band frequency range where uplink (User to base station communication link) (UL) is 2500 – 2570 MHz and downlink (Base station to user communication link) (DL) is 2620 – 2690 MHz [7]. The investigation is aimed at achieving balanced antenna spacing and mutual coupling where both functionalities, MIMO and beam shaping, can be implemented at an acceptable level using the same antenna. The reason for particularly choosing the N7 band is related to the overall antenna size in which antenna element dimensions and spacing are considerably smaller compared to lower frequency bands. Other factors are relatively higher bandwidth in both UL and DL sides and a better possibility of achieving higher antenna bandwidth in higher frequency.

There are many antenna manufacturing companies [8], [9] developing array antennas

for various applications such as base stations, fixed point to point and point to multiple point communications, cars that will support autonomous driving, etc. The antennas mentioned in the fields above require high power and intensive signal processing. Thus, within the thesis, the design and integration of the array antenna for low power mobile devices are carried out. Especially, the antenna design proposed in this thesis is tailored for a few applications in autonomous vehicles operating on 5G networks such as drones and autonomous delivery robots (A well-known example of such delivery robots are that of Starship [10]). Thus, compactness of the antenna module, low latency communication and high speed of information exchange are considered during the design. Multiple antenna designs with different element sizes and properties are discussed throughout the thesis where the one most suitable for a given application is selected .

This thesis work is structured to give a brief introduction to the next generation 5G, key enablers, motivation to the study, and problem statement in Chapter 1. Chapter 2 presents background material related to recent developments in phased array antenna type usage for spatial multiplexing, beamforming, reduction of the mutual coupling between antenna elements, and element spacing parameters. Chapter 3 presents the requirements set for phased array in terms of antenna beamforming and MIMO performance which should be taken into account while designing the antenna. The phased array antennas are designed from square truncated capacitively pin-fed circularly polarized patch antenna. Therefore, in Chapter 4 simulation analyses of 4x4 and 6x6 phased array antennas that are simulated without any changes to the patch element (originally acquired parameters remained) are presented. Chapter 5 presents 4x4 and 6x6 phased array antennas which were constructed from the patch element whose parameters and dimensions were modified and metallic slots were added to achieve better MIMO and beamforming performances. Chapter 5 also covers simulation analyses of the array antennas and proposes the final choice of the antenna with proper parameters. Finally, Chapter 6 concludes the thesis and suggest possible future work.

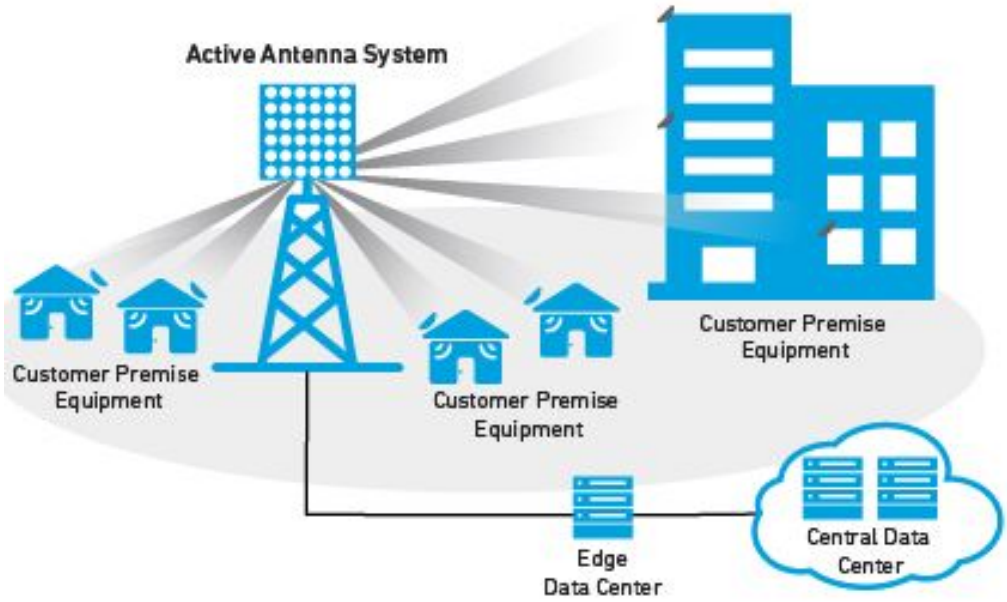

Figure. 1.2. 5G End-to-End communication using Beam Steering [11].

1.1 Motivation to study 5G

Introduction of upcoming 5G technology is considered to cover all the gaps that the previous generations had, offering high-quality service to users and empowering new technologies with enhanced mobile broadband (eMBB), ultra-low latency (URLLC) and machine type communication (MTC). The motivation for investigating the problems of upcoming technology is the opportunities it opens up in the tech world, easing the everyday life of people and empowering new inventions. uMTC and MTC of 5G will enable new technologies to be introduced and developed. uMTC use case will correspond to the industrial manufacturing, doing surgery remotely and increased safety for autonomous driving with its high throughput and latency. Meanwhile, MTC scenarios ensure efficient connectivity of massive IoT devices at low-cost [12]. The antenna design proposed in the thesis can find its usage in uMTC scenarios for drones' and delivery robots' future communication systems to enable new services through base stations.

1.2 Problem Statement

As mentioned in the introduction, MIMO and beamforming are part of the key enabling technologies of 5G where an array of antenna elements are required to enable the performance of spatial multiplexing and beam shaping [12]. However, problems such as mutual

coupling between antenna and array antenna element parameters that are not optimized hinder the effective operation of beamforming and MIMO features. Therefore, this thesis focuses on tackling the following problems and detailed procedures to address these problems are described in the subsections that follow.

- Mutual coupling effect between elements on the array set
- Surface current flow impact on operational bandwidth of the phased array antenna when the main beam is steered on ϕ and θ planes
- Optimization of array antenna element parameters for an acceptable MIMO and beamforming

1.2.1 Mutual coupling reduction

One of the reasons for eliminating mutual coupling is its negative effect on the reflection coefficient (S11) [13] of the antenna and the fact that it can be complicated to control in phased array antennas since array antennas can have each element fed individually or using one feeding port. Besides the S11 parameter, beamforming may not reach the desired beam shape because of high inter-element radiation interference [14].

To deal with this problem, this thesis proposes the design of individual feeding of each antenna element since, in spatial multiplexing, information received from each antenna elements are individually processed. To reduce the impact of mutual coupling, a design where each antenna element has a separate ground plane instead of one for all elements, as well as metallic slots placement between elements on the array antenna, are proposed. The possible reason for this could be that, when one ground plane is shared with all antenna elements, their back lobe radiation intensity may be different causing a small voltage difference on the plane, which may lead to current flow on the ground plane and thus changing the S11 parameters and radiation pattern of the elements.

1.2.2 Surface current impact on the main beam scanning angle

The phased array antennas discussed in this thesis are designed on a dielectric substrate. The substrate is physical support which separates the radiator element from the ground plane and it has a considerable effect on the performance of the phased array antenna. One

of the negative effects is the surface waves. Surface waves are guided waves that propagate on the substrate parallel to the surface which impacts negatively on the scanning angle of the main beam when it is steered on azimuth and elevation planes (ϕ and θ planes) [15].

To reduce the surface wave flow on the substrate and its negative impact on the antenna operation bandwidth, metallic slots placement is proposed. These metallic slots with proper parameters reflect and absorb the surface waves, leading to significantly minimized the effect on the reflection coefficient of individual elements.

1.2.3 Optimization of array antenna element parameters for an acceptable MIMO and beamforming

It is known that array antennas tailored for MIMO systems have elements spaced one wavelength apart, resulting in higher diversity not to cause coupling effect between elements and increase the gain [6]. When the signal is transmitted from the BS and if the receiver is equipped with multiple antennas, it benefits from the diversity whereby the receiver sensitivity is increased [6].

However, a design difference can be seen in beamforming antennas as compared to MIMO wherein beamforming elements are located close to each other with only half-wavelength distance and possess wide beam width with high antenna gain stability. In this case, the mutual coupling is higher, which can be pre-calculated before the antenna design to take into account the impact on beamforming and bandwidth of the antenna. It is obvious that the phased array optimized for beamforming will not give effective operation in MIMO applications.

To deal with the element spacing and acceptable beamforming and MIMO performance problem, in this thesis circular polarized antennas with 0.7 λ element spacing are simulated and analyzed to achieve the desired diversity and the main beam angle. Several geometrical compromises are practised by varying antenna element parameters to improve both beamforming and MIMO [6].

1.3 Approach followed in this thesis

The overall approach followed in this thesis includes:

A) Square truncated capacitively in-fed circularly polarized patch array antenna design

and analysis are completed using CST studio software including the results of calculated each element diversity gains, correlation coefficients, S11 parameters, mutual coupling, total and radiation efficiencies and beamforming.

B) Two types of array antennas: 4x4 (16 active elements) and 6x6 (16 passive, 16 active elements) phased arrays are simulated and analyzed. Array antenna element parameters have been optimized to achieve wider beamforming and higher diversity gain between elements, keeping the compactness of the antenna module.

C) It is aimed to perform beamforming simulation in the range of -45 degree to +45 degrees in both elevation and azimuth plane since in lower angles of the main beam, the energy of the beam may be coupled to elements in close proximity changing the bandwidth and radiation of elements and overall antenna, as shown in **Figure 1.3** .

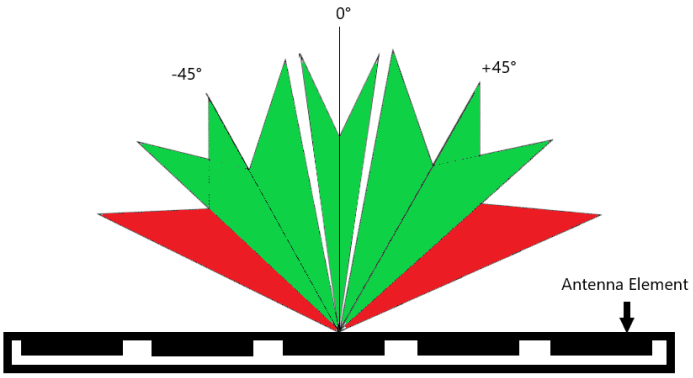

Figure. 1.3. Main beam scanning from -45 degree to +45 degree. If the beam goes to lower angles close to elements (fillet with red), it may affect elements' radiation and bandwidth of under it.

Chapter 2

State-of-the-Art on Antenna Design for MIMO and Beamforming Technologies

This chapter represents recent developments and research efforts conducted by various research groups to identify antenna types and their geometrical constellations used for MIMO and beamforming technologies and the methodologies for reducing mutual coupling between the antenna elements. The geometrical constellation refers to the shape of the antenna element, its size and the placement of elements in a particular order. The main focus is towards antenna element spacing, the geometrical shape of MIMO antenna elements, scattering parameters, and diversity performance.

The design of a MIMO antenna array may implement different kinds of antenna elements, depending on the application. Frequently, a single antenna element is studied for its performance, radiation pattern, surface wave distribution, and the effective bandwidth before constructing an array from it. When it comes to 5G NR applications, both printed circuit board (PCB) antennas [16] in frequency range 2 (FR2), which is above 26 GHz [7], and dual polarized dipole antennas in frequency range 1 (FR1) sub-6GHz frequencies [7] are commonly used [17]. The following sub-sections review prime examples of two papers dealing with MIMO antenna design metrics including the element spacings("Closely-spaced Multi-band MIMO Antenna for Mobile Terminals"[18],"Compact MIMO Slot Antenna for UWB Applications" [19]) , one paper of beamforming antenna element spacing consideration("Beamforming Antenna Spacing Variations" [6])and finally, mutual coupling reduction methods ("Methods to Reduce Mutual Coupling Affect" [20]) .

2.1 "Closely-spaced Multi-band MIMO Antenna for Mobile Terminals" paper review

The current section content refers to the research paper [18] that describes a MIMO antenna with 2 elements which support three bands namely 900 MHz, the 2 GHz and the 3.5/5 GHz. The size of each element is 29 mm x 16 mm x 0.8 mm with mutual coupling being lower than -10 dB within the bands and a protruded strip connected to the ground resulted in the reduction of the envelope correlation coefficient (ECC).

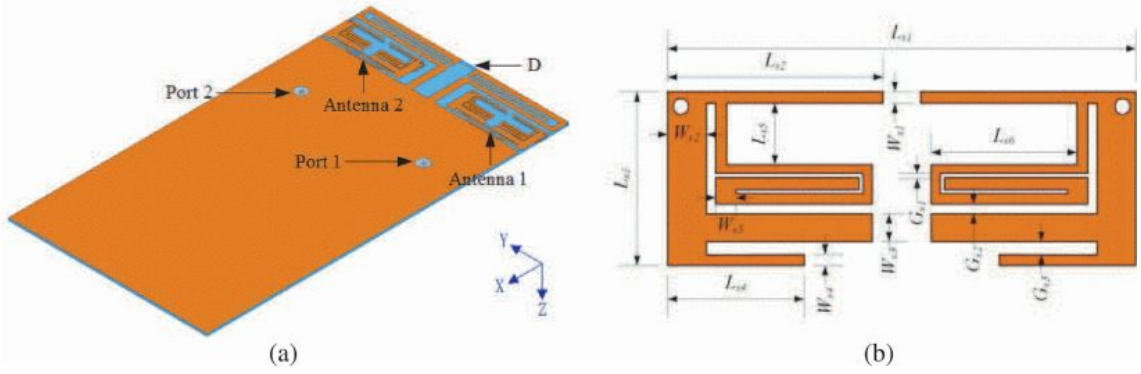

Figure. 2.1. (a) Configuration of the two-port multiband MIMO antenna; (b) Detailed configuration of the hybrid strips [18].

The MIMO antenna depicted in **Figure 2.1** is fabricated on an FR-4 substrate with a thickness of 0.8 mm and a dielectric constant of 4.4. The PCB board size is 115 x 60 mm^2 where 60 x 16 mm^2 area is a ground clearance with two symmetrically duplicated elements are placed. The antenna 1 and antenna 2 on the PCB are separated D=3 mm apart and are fed by 50Ω coaxial line each. The designed antenna is proposed for handset mobile devices which operate in GSM900/PCS/UMTS/LTE2300, WLAN/WiMAX and lower UWB technologies. From a technical perspective, three bands operation of the MIMO antenna is accomplished with the protruded folded strip, the hybrid strips and monopole parts of each element for the low (900MHz), the middle (2GHz) and the high band (3.5/5GHz) frequencies, respectively [18]. [1].

Scattering parameters such as reflection coefficient and mutual coupling coefficients are measured and compared with simulated results of a 2 antenna MIMO module, as

[1]The qualities of the figures discussed in "Closely-spaced Multi-band MIMO Antenna for Mobile Terminals" are restricted in the original source

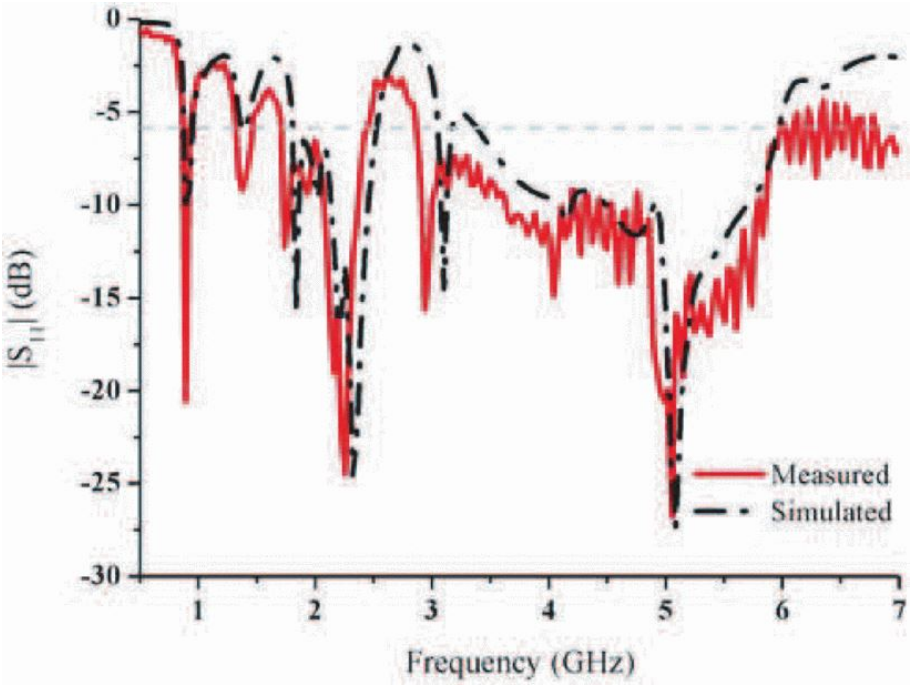

Figure. 2.2. Comparison of the measured and simulated reflection coefficients of the MIMO antenna proposed in [18].

shown in **Figure 2.2** and **Figure 2.3**, respectively [2]. The measured result is presented as a red line and the simulated one as a dash-dotted line. The **Figure 2.2** shows the impedance bandwidth of the antenna for each frequency (900 MHz, 2 GHz, 3.5/5 GHz)where for the low band 11% of the operation frequency (860-960 MHz), for the middle band 36% (1710-2450 MHz) and for the high band 70% (2870-5990 MHz). Meanwhile, as **Figure 2.3** shows, the coupling coefficient is below -10 dB for the whole band and the values decrease as the frequency increases, which consolidates the element isolation issue [18].

Diversity performance of the 2-antenna MIMO system is evaluated using envelope correlation coefficient (ECC). When the envelope correlation coefficient (ECC) is low, isolation and diversity gain would be high; hence, for MIMO system applications envelope correlation coefficient (ECC) is 0.5. Current research paper [18] calculated the envelope correlation coefficient (ECC) of 2-element MIMO antenna based on S-parameters results since this method is faster and more convenient compared to the method where far-field patterns are used. However, radiation efficiency (which has a linear effect) is not taken

[2]The qualities of the figures discussed in "Closely-spaced Multi-band MIMO Antenna for Mobile Terminals" are restricted in the original source

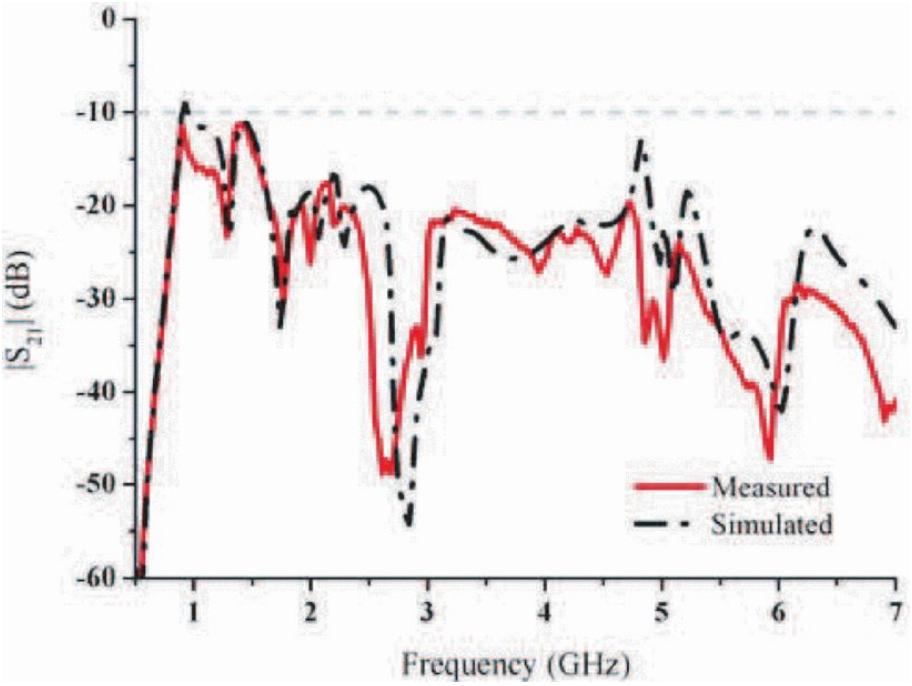

Figure. 2.3. Comparison of the measured and simulated mutual coupling coefficient of the MIMO antenna proposed in [18].

into account in the calculation. The envelope correlation coefficient (ECC)s calculated over the range of 0.5 GHz to 7 GHz is less than 0.2, as listed in Table 2.1, which is less than the criterion 0.5.

2.2 "Compact MIMO Slot Antenna for UWB Applications" paper review

All the content in this section is extracted from the research paper about the MIMO antenna system described in [19] that contains 4 elements with similar polarization, the size being 42 x 25 mm^2. The slot antennas are used as MIMO antenna elements where high isolation among elements is achieved by 1) placing the antenna elements asymmetrically and 2) due to directional radiation properties of the slot antennas. The stepped slot design implemented on elements which were excited with 50 Ω microstrip lines, and this design choice, make the multiple resonant mode transitions smooth since each slot has its resonant frequency based on the slot length. The substrate used to fabricate the antenna is low-cost FR4 with dielectric constant 4.4 and a thickness of 1.6 mm, as shown in **Figure 2.4**.

The MIMO antenna elements are fed with the line on one side of the substrate, the

Bands	Frequency (GHz)	ECC
Low	0.89	0.0027
	0.92	0.101
	0.96	0.029
Middle	1.8	0.0002
	2	0.0026
	2.2	0.0003
High	3	0.0007
	4	0.0003
	5	0.0002

Table 2.1: ECCs calculated for different frequencies at three desired bands, i.e., 900 MHz, 2 GHz and 3.5/5 GHz

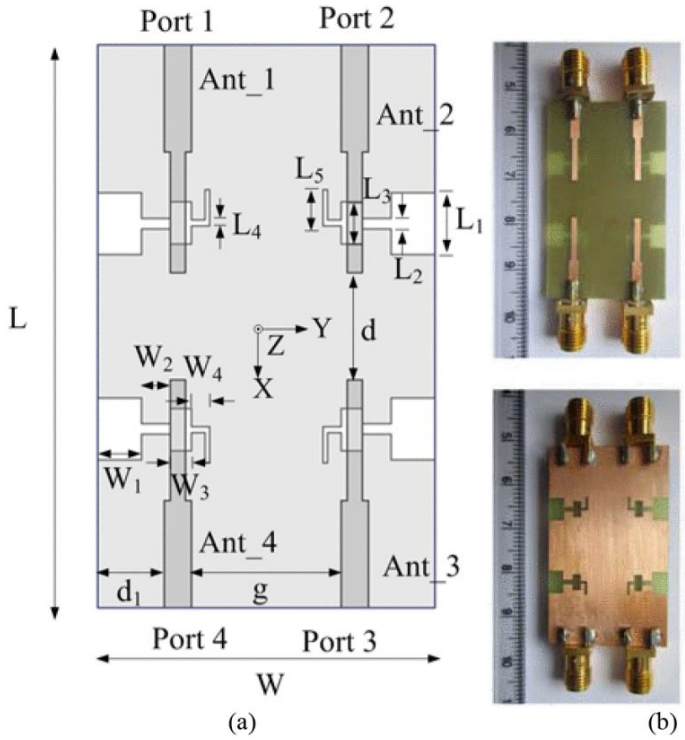

Figure. 2.4. (a) UWB MIMO antenna geometry proposed dimensions: L=42 mm, W=25 mm, L_{SA}=21 mm, W_{SA}=8 mm, L_{f1}=8 mm, L_{f2}=9 mm, W_f=2 mm, W_{f1}=1.2 mm, L_1=4.6 mm, W_1=2.3 mm, L_2=0.8 mm, W_2=2.3 mm, L_3=3.2 mm, W_3=1.6 mm, L_4=0.6 mm, W_4=1.4 mm, L_5=3 mm, d_1=4.8 mm, d= 7 mm, g=11.2 mm (b) Fabricated antenna top and bottom view [19]

other side being the ground plane. Antenna ports are numbered from 1 to 4 and scattering parameters of the UWB MIMO system are shown in **Figure 2.5** where 1st elements reflection coefficient and other 3 neighbour elements' coupling effects are plotted. The antenna has the bandwidth lower than -10 dB from 3.1 GHz to 12 GHz and the isolation of 1^{st} element from the other 3 elements is lower than -22 dB without the utilization of any kind of decoupling network. Significant reduction of coupling effect is accomplished by radiation pattern [21] and asymmetrical structure of elements [19].

The horizontal separation distance (g) between elements impacts the isolation, where increasing g decreases the effect of the elements between each other [19]. The horizontal separation distance was chosen to be $g = 11.2mm$ as an optimal design parameter that satisfies the requirement of isolation of -20dB on the desired spectrum [22].

The stepped slot design followed in [19] acts as a radiator and placing the elements asymmetrical forces them to radiate in the opposite direction, leading to negligible coupling as depicted in **Figure 2.7**. The radiation of Ant_1 is on $-y$ axis whereas Ant_2 radiation is on $+y$ axis, which eliminates the Ant_1 and Ant_2 maximum electric field overlap and reduces the correlation coefficient [19].

The mutual coupling of Ant_1 and Ant_4 which are located vertically to each other depends on the distance d between them. As the value of d increases, the coupling effect between Ant_1 and Ant_4 decreases, as shown in **Figure 2.8**. The distance of d=7 mm improves the isolation of elements since the surface wave on Ant_4 is almost negligible when Ant_1 is excited and other elements are terminated with 50 Ω load [19].

Important parameters that define the performance of a MIMO antenna are envelope correlation coefficient (ECC) and channel capacity loss (CCL). Their acceptable limits are ECC < 0.5 [23] and CCL < 0.4 [22], which can be obtained from the S-parameters and radiation efficiency of the MIMO antenna, as shown in formula 2.1 [19].

$$\rho_e = |\rho_{ij}|^2 = \frac{|S_{ii}S_{ij} + S_{ji}S_{jj}|^2}{(1 - |S_{ii}|^2 - |S_{ji}|^2)(1 - |S_{jj}|^2 - |S_{ij}|^2)} \tag{2.1}$$

Figure 2.9 shows the measured ECC and CCL values where ECC < 0.01 while CCL < 0.4 bits/Hz/s from 3GHz to 12GHz [19].

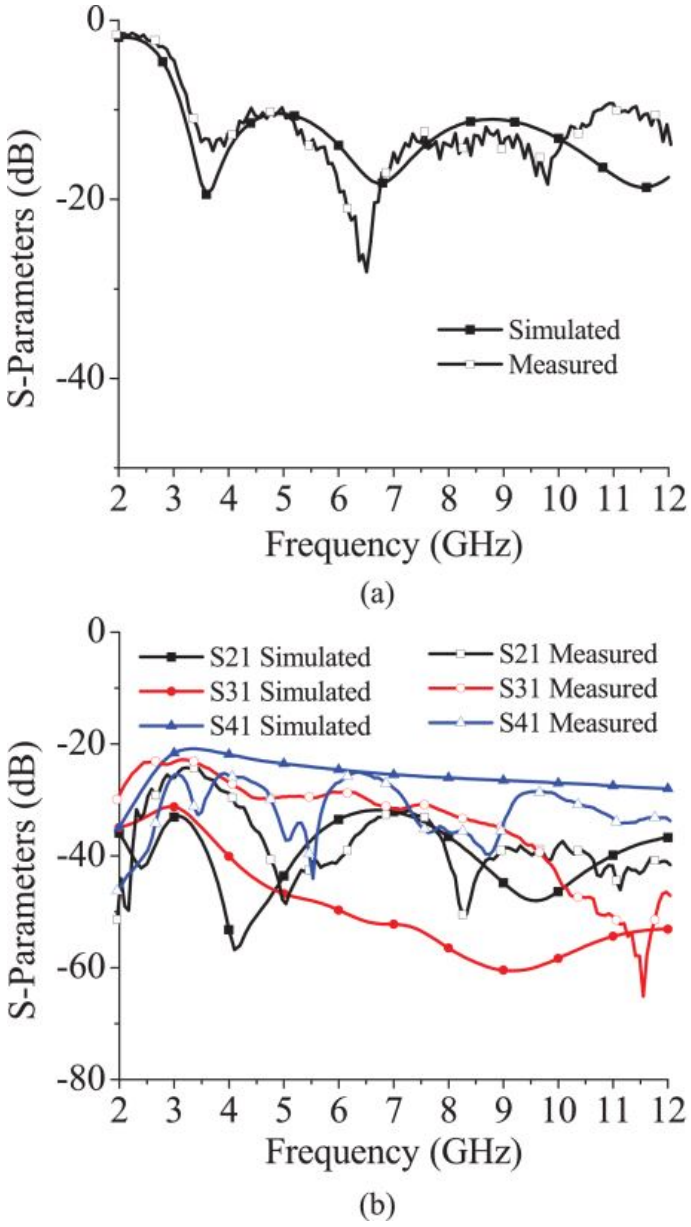

Figure. 2.5. Simulated and measured S-parameters comparison of the four-element MIMO antenna proposed in [19]. S_{11} coefficient is shown for the 1^{st} element and S12, S13, S14 represents 50 Ω terminated 2^{nd}, 3^{rd} and 4^{th} elements' coupling effects on the 1^{st} element, respectively [19].

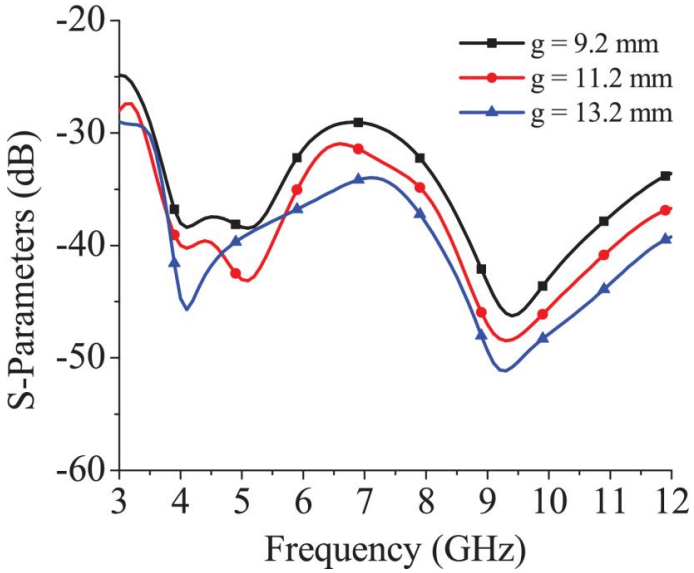

Figure. 2.6. The distance between antenna elements (g parameter) impact on S-parameters. The increase of g parameter, lowers the mutual coupling between elements [19].

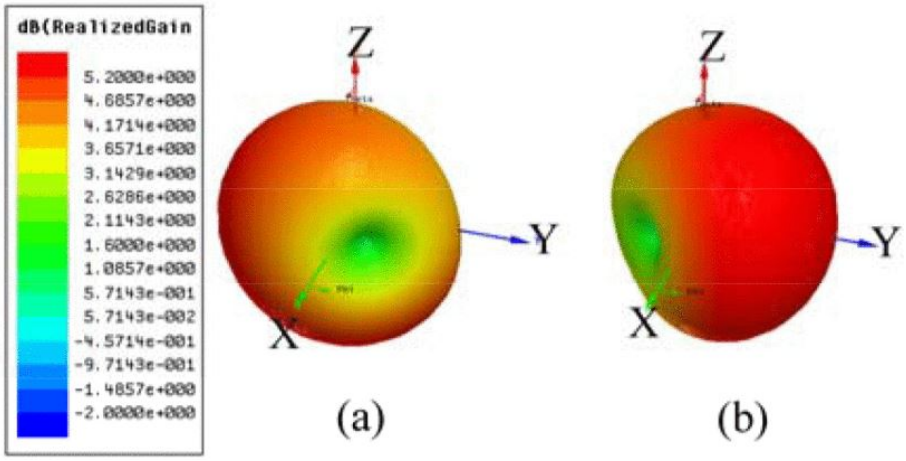

Figure. 2.7. 3-D radiation pattern of Ant_1 and Ant_2 at 6GHz (a) Ant_1 radiation on $-y$ axis and (b) Ant_2 radiation on $+y$ axis. When Ant_1 and Ant_2 are excitepd, other ports are terminated with 50 Ω matched load [19].

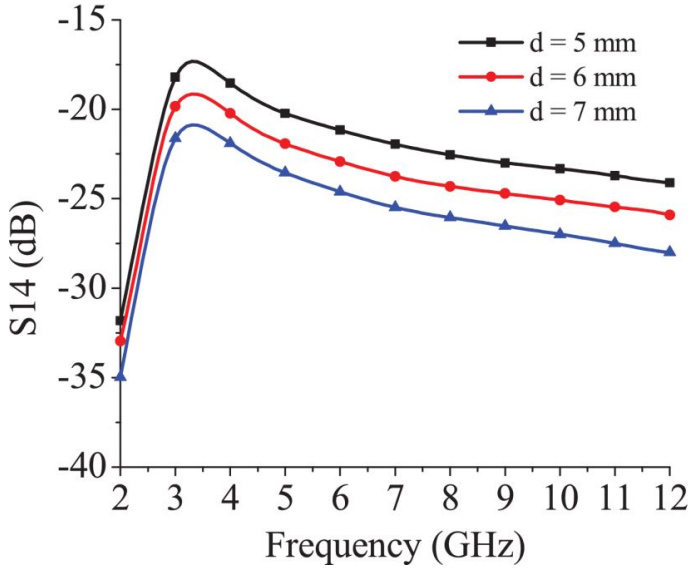

Figure. 2.8. The Vertical distance between antenna elements (*d* parameter) impact on S-parameters. Increasing the *d* parameter lowers the mutual coupling between elements [19].

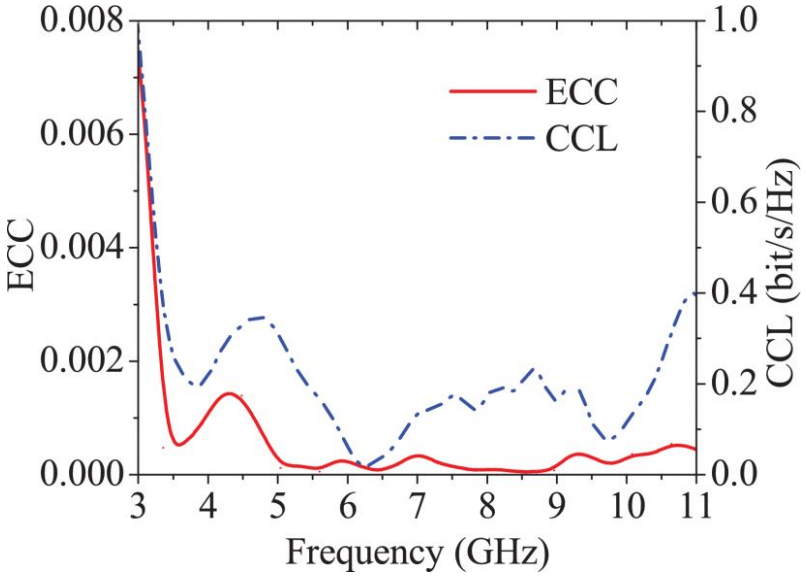

Figure. 2.9. UWB MIMO antenna measured ECC and CCL values from 3GHz to 12 GHz. The values are lower than the limits [19].

2.3 "Beamforming Antenna Spacing Variations" paper review

In beamforming, phased antenna characteristics such as the array factor and the element pattern are known to be key to achieve the desired beam with the right parameters. Amplitude, the phase distribution, and the column spacing determine the array factor. **Figure 2.10** shows the four column antenna's array factor receiving equal phases and amplitudes with columns spaced half-wavelength apart. Having multiple peaks in **Figure 2.10** is due to the sinusoidal nature of the equations where dipoles add up in the phase constructively, and lower sidelobes are created when phases add up destructively [6].

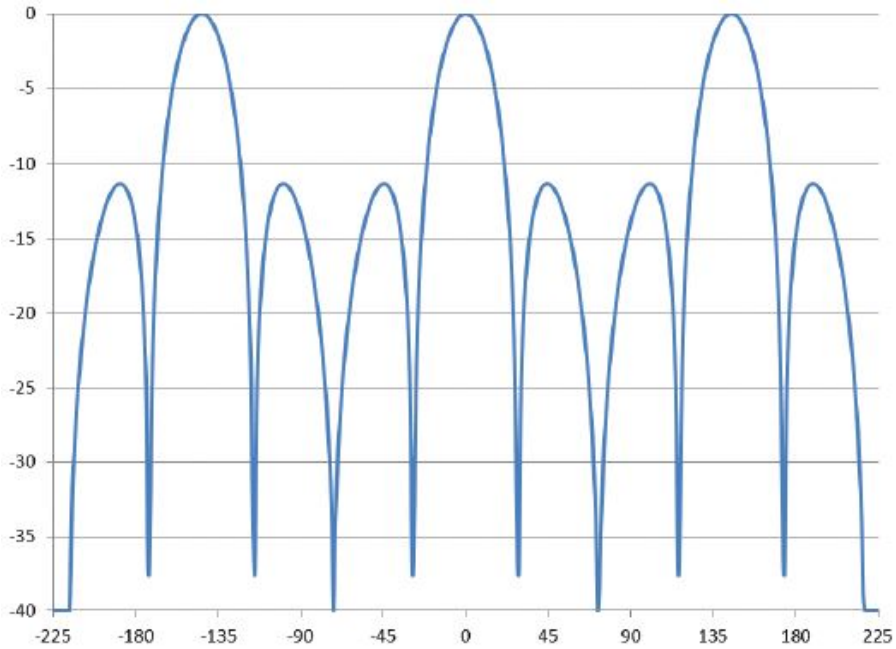

Figure. 2.10. Array factor of four column antenna with a half-wavelength spaced. the beam is not steered keeping at 0 degree and sidelobes are suppressed [6].

Physical features of a phased array antenna such as column spacing, the height of dipole element, the width of chassis and internal wall structure create the element or column pattern. The representation of standard base station array "fan-beam" pattern is depicted in **Figure 2.11**, where a change in phase or amplitude does not effect on the column pattern, and a 3dB beamwidth of the column pattern limits the main beam scanning angle range [6].

In the system terminology, the array factor is viewed as an "angular amplified" and

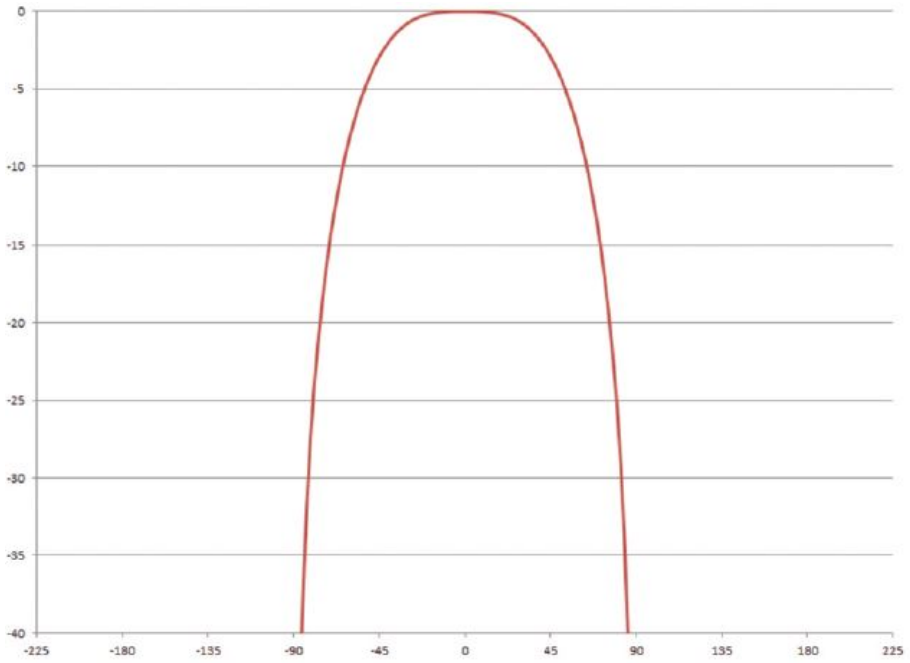

Figure. 2.11. 90°ideal standard base station column patterns [6].

the column pattern is the original signal that gets amplified, leading to creating a stronger signal with more gain in the angular region of the array factor. In the case of array factor amplifying outside the original signal, nothing is created due to the absence of the original signal (column pattern) [6]. [3]

The column pattern act as a filter that cuts off the secondary main beams and their sidelobes, as shown in **Figure 2.13**. The array type discussed in [6] has a column pattern with a range of 90°to 110°, which makes it perfect for beamforming but not for MIMO application as the column gain drops. Steering the beam can be accomplished by implementing phase progression on the columns which shift the array factor phase while the column pattern remains unchanged. During the beam steering, sidelobes may reach unacceptable levels; hence, implementation of the amplitude tapering across the columns suppresses the levels of undesired sidelobes since it distributes tailored amplitudes to each element in the array [24], as shown in **Figure 2.14**, where -25 dB suppression level is achieved. Even though the element pattern is 90°, 45°scanned angle may introduce -3 dB degradation of the main beam, and beyond that, the pattern falls abruptly [6].

0.5λ spacing of the element satisfies the beamforming features of the antenna, but MIMO performance is degraded significantly as the coupling between columns increase.

[3]The qualities of the Figures 2.11 2.13 discussed in "Beamforming Antenna Spacing Variations" are restricted in the original source

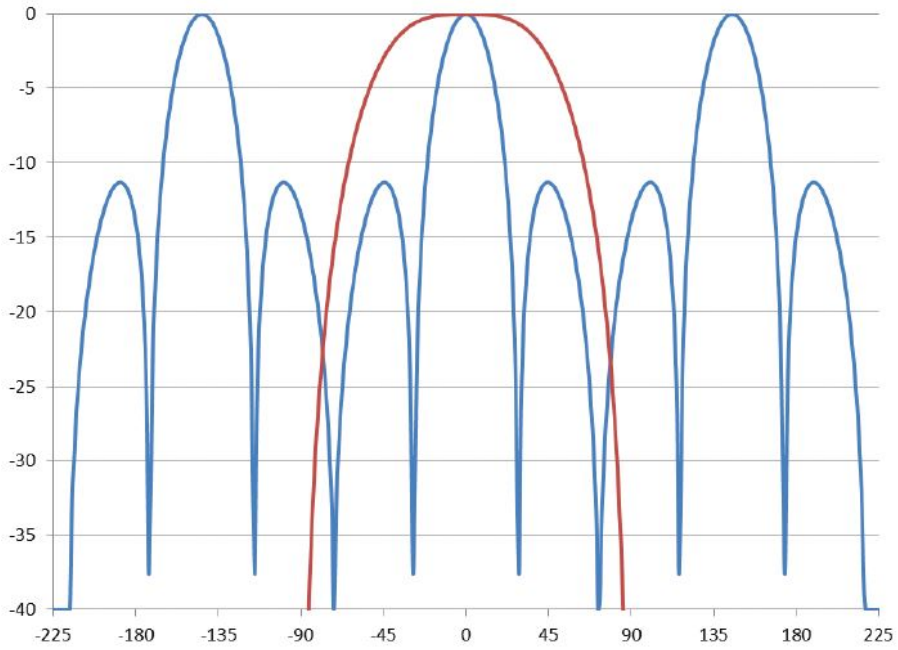

Figure. 2.12. The array factor and column patter overlay. The mean beam and two sidelobes get amplified and other parts are cancelled [6].

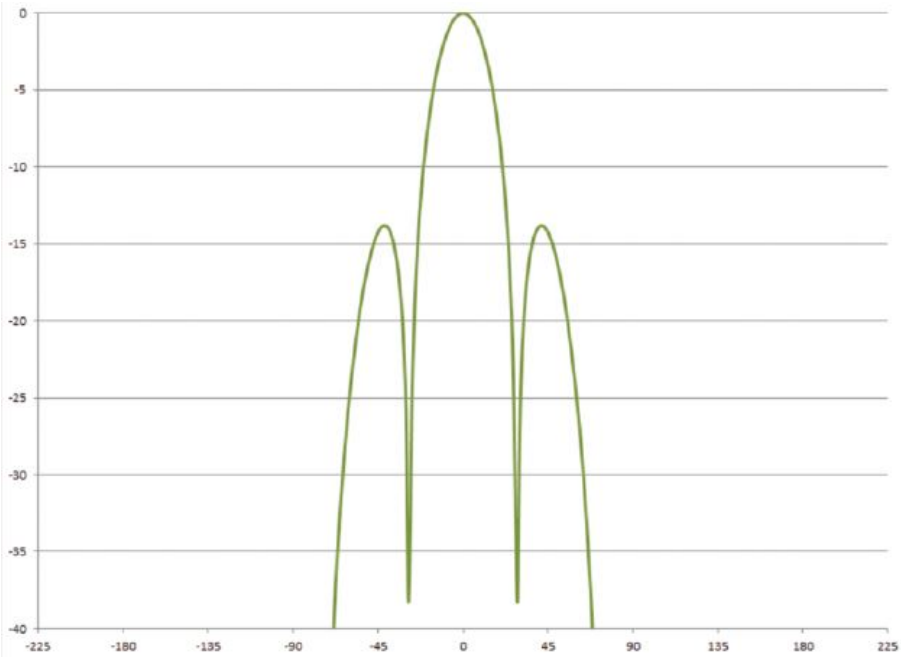

Figure. 2.13. Final pattern accomplished by summing the array factor and column pattern [6].

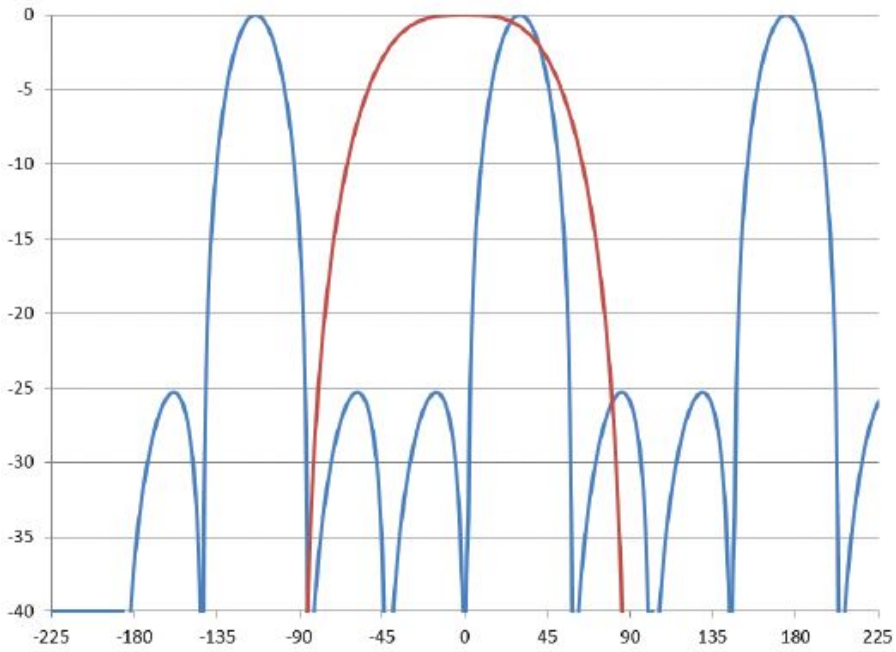

Figure. 2.14. Main beam steering 30°and 25dB sidelobe suppression achieved by amplitude tapering. [6]

Therefore, four-column dual polarized antenna one wavelength spaced and 90° column pattern antenna has experimented. Widening the space between elements leads to the secondary solution main beams to move into the column pattern which is known as grating lobes. The amplitude tapering method can be implemented to reduce the sidelobe levels 25 dB down but it does not impact the grating lobes, as shown in **Figure 2.15**. When the main beam is at 0°, grating lobes are at about -13 dB from the beam peak. However, during the process of steering, for instance, to 20°, the grating lobe level is down only about 3 dB from the main peak. This results in having two main beams as represented in **Figure 2.16** that confuse the system, i.e. to identify whether the user is to the right or to the left of the antenna.

2.4 "Wide scan phased array patch antenna with mutual coupling reduction" paper review

The paragraphs in this section including subsections that are not referenced are extracted from [20] paper and additional sources are referenced accordingly.

The demand for phased array antennas is increasing as radar systems evolve as well

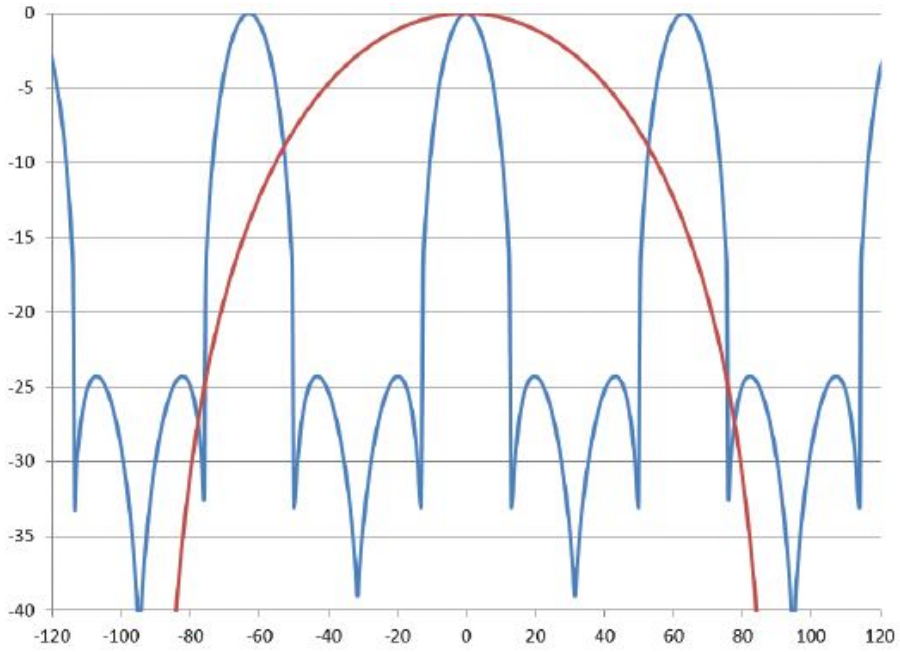

Figure. 2.15. The array factor and column pattern summed. Sidelobe levels are 25dB down but grating lobes at the edge of column pattern is not suppressed. [6].

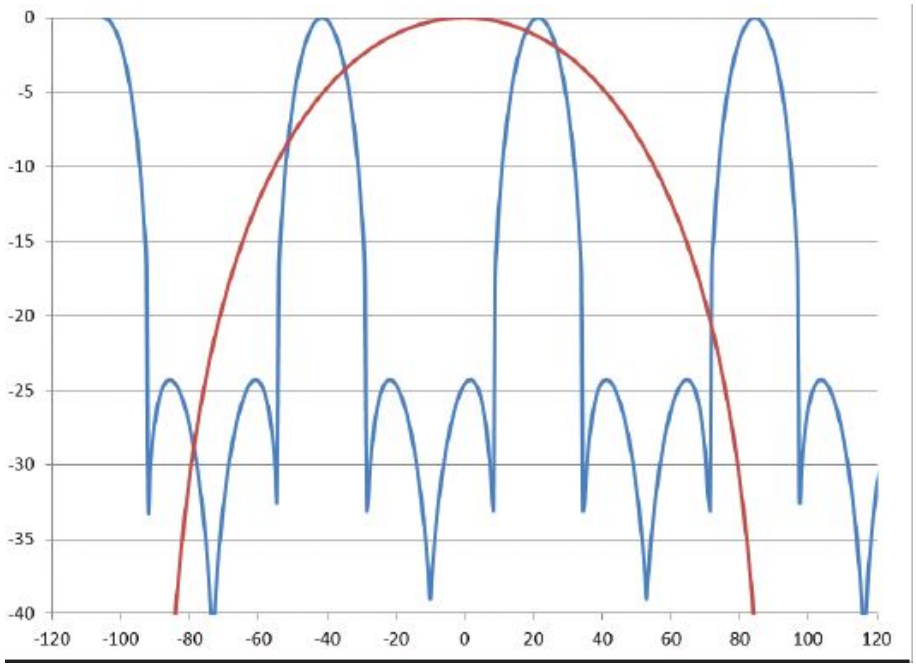

Figure. 2.16. A beam steered 20° to the right and the secondary beam falls into the column pattern results in having 3dB difference between main beam and grating lobe on the left [6].

as with the introduction of 5G technology where massive MIMO systems require the implementation of phased array antennas. In recent years, phased array antennas printed on PCB with compact size, light weight and ease of fabrication are being widely used in various applications [20]. However, surface wave excitation leads to high mutual coupling between elements if the microstrip antenna is chosen as an element in the array. Mutual coupling increases when the elements are placed close to each other; but, in order to avoid the appearance of grating lobes, spacing should be balanced in the range of 0.5λ and 1λ. Moreover, mutual coupling impacts the input impedance of elements in large arrays as the scanning angles of the antennas change. During the last few years, a number of techniques have been experimented to bring down mutual coupling between elements. The following techniques are recently researched to reduce the surface wave as well as mutual coupling; however, some of them may not apply for linear or planar arrays if the inter-element spacing is low:

- Defected ground structures in the ground plane [25]–[27]
- Electromagnetic band gap structures in between the patches [28]–[30]
- Cavity-backed patch elements [31]
- Usage of metameterial structure in between patches[32]–[34]
- Usage of coplanar wall [35]–[38]
- Grounded dielectric slab loaded by slot [20]

The next section discusses only "Defected ground structures in the ground plane [25]–[27]" and "Narrow slot placement between antenna elements [20]" methods as they are the most relevant ones for the method the author proposes in later chapters.

2.4.1 Defected ground structures [25]–[27]

"The compact geometrical slots embedded on the ground plane of microwave circuits are referred to as Defected Ground Structure (DGS). A single defect (unit cell) or a number of periodic and aperiodic defects configurations may be comprised in DGS."[39]. The shape that is periodic or nonperiodic acts as a band-gap filter rejecting some frequency range, which leads to mutual coupling reduction [27]. The etched DGS on the ground plane is

shown in **Figure 2.17**. This results in a slight shift on the operation frequency of the patch antenna, but S_{12} parameter is improved by about 30 dB; mutual coupling is reduced from -15 dB to -46 dB, as depicted in **Figure 2.18** . The back lobe level is higher when DGS is implemented but the main polarization radiation patterns do not experience a significant difference between the original patch and that with DGS.

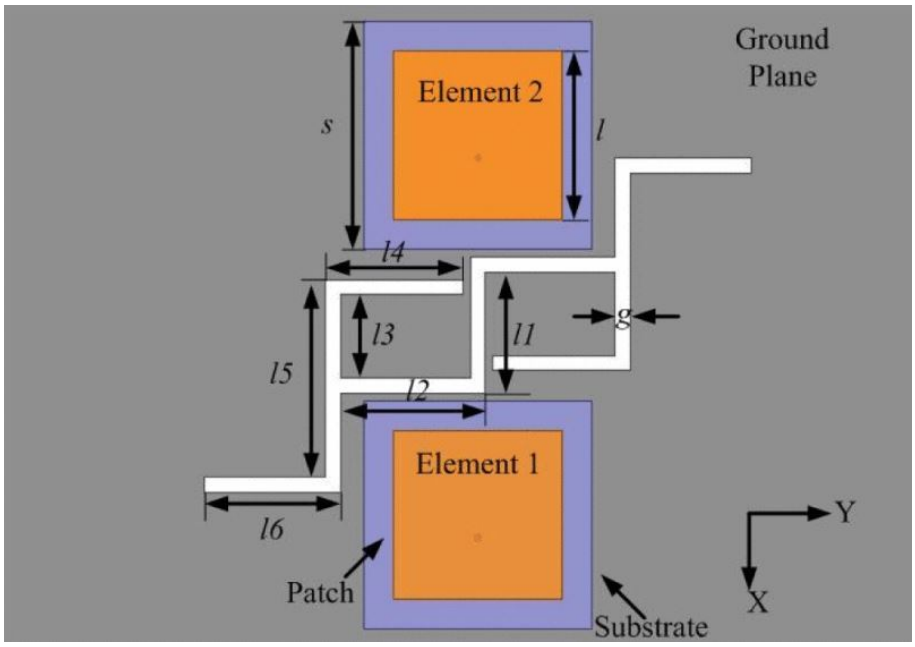

Figure. 2.17. Periodic fractal defected ground structure between elements. The dimensions of etched FDGS from the ground plane can be calculated to reject the desired frequency range and reduce mutual coupling. [27]

2.4.2 Grounded dielectric slab loaded by slot [20]

The space between patch antenna elements in the array can be considered as a waveguide by which surface wave can travel and cause mutual coupling between the patches. The surface waves couple from one element to each other, leading to the change in the input impedance of the elements and degrades the scanning performance of the array. One of the ways of preventing surface wave travelling through grounded dielectric slab (GDS) is to place slots in the ground plane in between the patch elements (**Figure 2.19**).

The slot provides an impedance loading since the space between the patch elements is considered as a transmission line. If appropriate slots' dimensions are chosen, the

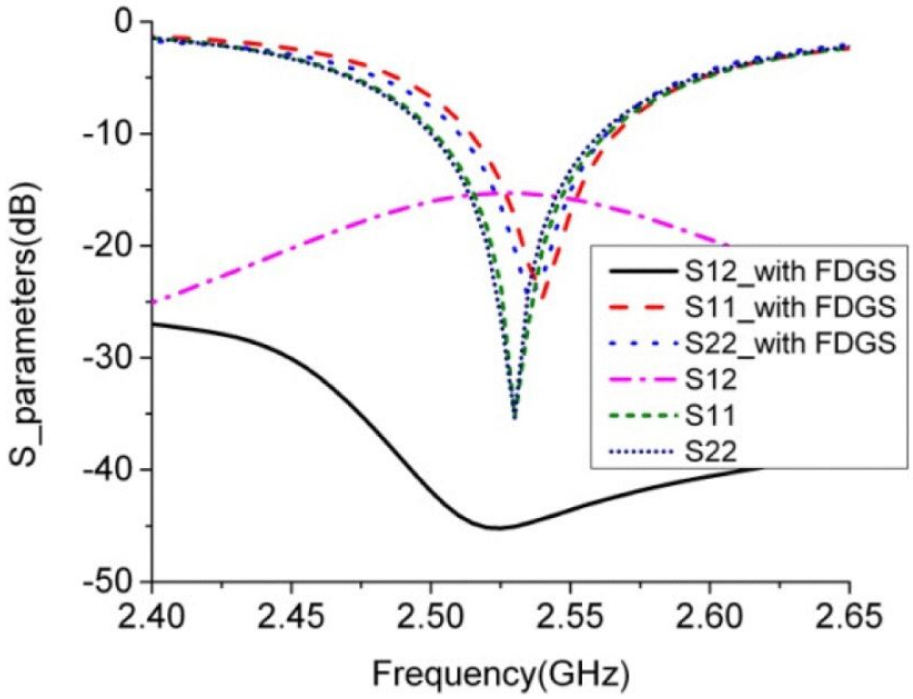

Figure. 2.18. Reflection coefficient of the 1^{st} element (S_{11}), mutual coupling between the 1^{st} and 2^{nd} element (S_{12}), and reflection coefficient of the 2^{nd} element (S_{22}), with and without defected ground structure[27]

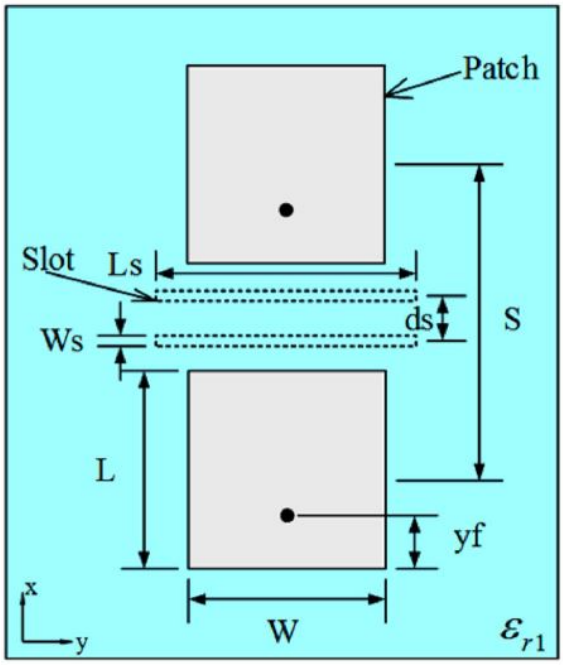

Figure. 2.19. Proposed structure on E-plane for mutual coupling reduction [20]

impedance loading characteristics reflect or absorb some part of the surface wave, as depicted in **Figure 2.20**. One of the important parameters to reduce coupling is the series impedance of the slots. The maximum mutual coupling reduction can be achieved if the proper impedance values of the slots are set. The slots' series impedance value can be adjusted by offsetting the position of the slots, the spacing between the slots, and their lengths. If the spacing between the slots is set accordingly, back lobe in the broadside direction can be reduced. The length of the slots are half wavelength $\lambda_{eff}/2$ and can be computed using Equation (2.2):

$$L_s = \lambda_{eff} = \frac{c}{(\sqrt{\epsilon_{eff}} * f) * 2}; \qquad \epsilon_{eff} = (\epsilon_{r1} + \epsilon_{r2})/2 \tag{2.2}$$

where ϵ_{r2} is the permittivity of air and ϵ_{r1} is the substrate relative permittivity and it determines the lengths of the slot.

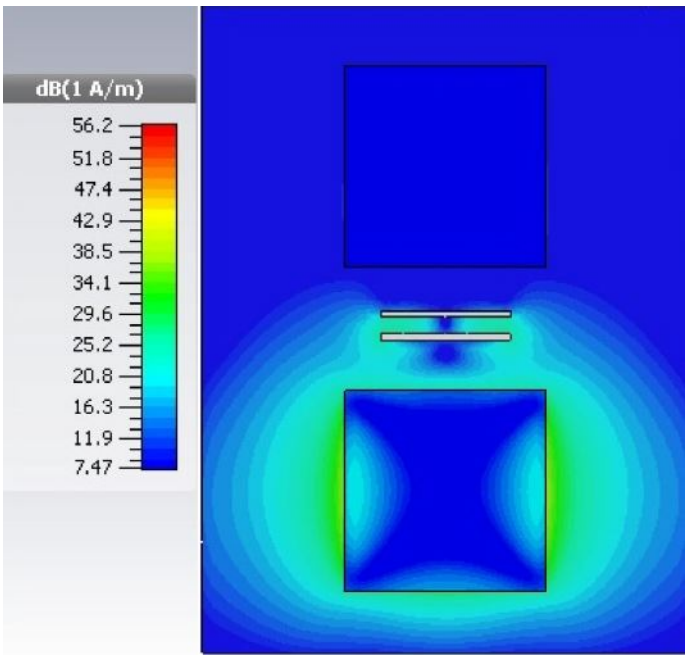

Figure. 2.20. Current distribution on the patch element. The slots placed between the elements reflect the surface wave, reducing the coupling of radiated element to the adjacent element [20]

The impact of spacing between slots on mutual coupling and the proposed structure results are simulated with centre frequency being 10 GHz, as shown in **Figure2.21**. It can be seen that mutual coupling is improved to about -44 dB with slots spaced 1 mm apart from each other. Varying the space between slots shifts the operation frequency and slightly increases the antenna bandwidth, as **Figure2.21** (b) shows. Comparing the mutual

coupling of the conventional structure (red curve) with the proposed structure where slots are placed in between the elements (green curve), about 22 dB better result is obtained at 10 GHz while (S_{11}) antenna bandwidth increases marginally.

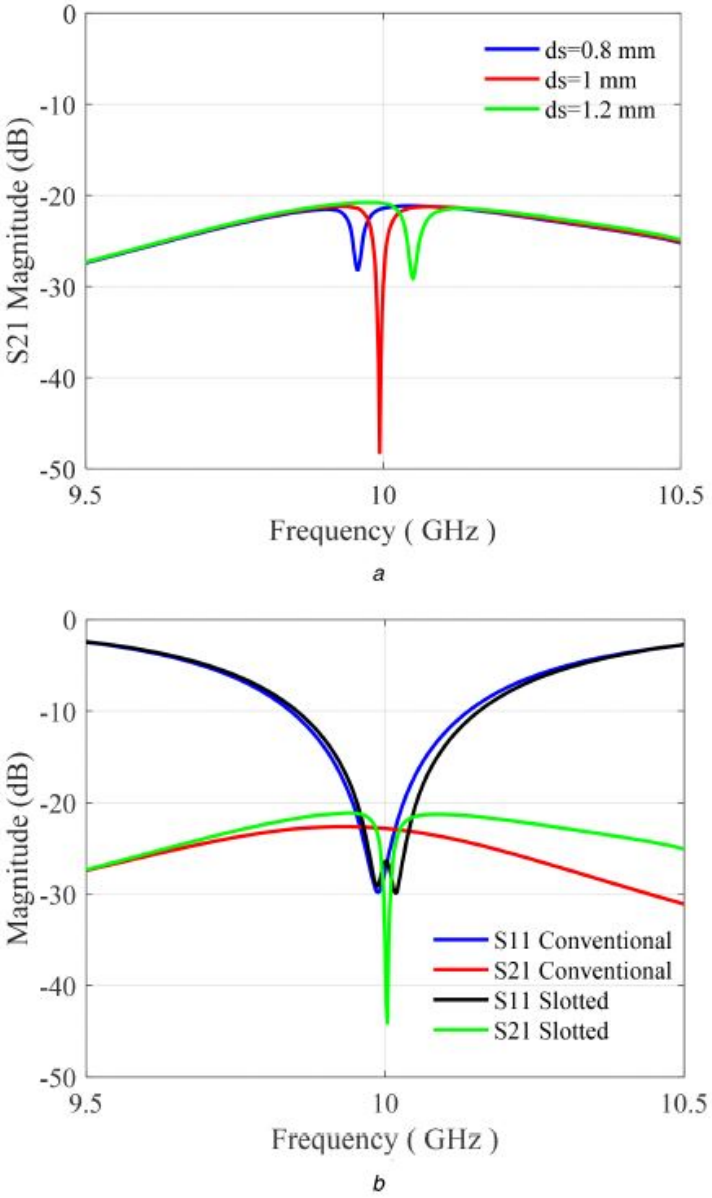

Figure. 2.21. Proposed structure mutual coupling effect on E-plane (L = W = 9.3 mm, y_f = 1.55 mm, ϵ_r = 2.2, ϵ_{r2} = 10.2, L_s = 5.8 mm, W_s = 0.3 mm , S = 14.99 mm, h_1 = h_2 = 0.787 mm, t = 0.02 mm). (a) The effect of slots' spacing variation on mutual coupling between 2 elements, (b) The conventional versus proposed structure reflection coefficient of the 1^{st} element (S_{11}) and mutual coupling between 2 elements (S_{12}) [20]

Chapter 3

MIMO and Beamforming Antenna Design Requirements

It is apparent that upcoming 5G networks require a new set of metrics of antenna systems compared to conventional antennas [4]. Therefore, this chapter of the thesis explains important performance metrics that need to be evaluated in beam-shaping and MIMO design[4] and sets requirements for a beamforming range, an antenna polarization, S-parameters, as well as antenna spacing for MIMO and beamforming of 10x6 (32 active elements phased array) antennas. A number of MIMO metrics are defined in the following sections; note that for beamforming, only element spacing is discussed with a common metric for both beam-shaping and MIMO antenna total active reflection Coefficient (TARC) metrics. Few suggestions presented in the scientific literature are also taken into account to accomplish better S-parameter versus scan angle of the array antenna.

Within this thesis, more attention is paid towards MIMO performance of the antenna rather than beamforming capability. A massive MIMO antenna with a large number of elements serve many subscribers on the same frequency spectrum creating individual channels, which results in increasing capacity of the network almost as many times as the number of antenna elements and serving many users at the same time using a specific channel [40]. Meanwhile, beamforming concentrates the beam to the user with the possible improvement of the SNR, which enables the implementation of high order modulations (QAM-32, QAM-64, QAM-128, etc...) and high data rate exchange.

The general and specific parameters' requirements for a 10x6 phased array antenna that this thesis investigates are represented in **Table 3.1**. Technology-specific metrics are

Parameters	**Beamforming**	**MIMO**
S11, dB	-10	-20
S21, dB	-20	-20
Antenna Polarization	Horizontal,Vertical	Horizontal,Vertical
Element Spacing,λ	0.75	0.75
Correlation Coeff	Not Applicable	0.3
Diversity Gain, dB	Not Applicable	>9 dB
Beam Scan angle,°	-45 to +45	N/A

Table 3.1: 32 Active element phased array antenna parameter requirements

discussed in the dedicated sections and the common ones are highlighted in Section 3.1 with listed goals and explanations. The antenna modelled is simulated and analyzed in the next chapters.

3.1 General Parameter Goals

In this section, general parameters that belong to both MIMO and beamforming antennas are discussed. The requirements for the parameters are listed in **Table 3.1** and the reason behind setting such requirements are explained in this and next sections.

3.1.1 S-Parameter Goals

The antenna module has 16 active elements and all of them are powered at the same time, which increases mutual coupling between elements. The mutual coupling and scanning angle range change the S11 parameters of each antenna element. Therefore, instead of using one common ground plane for a 10x6 phased array antenna, each element has its own ground plane, which leads to a reduction of coupling. Furthermore, metallic slots are placed between elements to limit surface wave flow in the array. With the improvements introduced, the S11 parameters of each element should be below than -10 dB (**Table 3.1**). This is frequently practised among antenna manufacturing vendors since in the case of 3 dB power delivery to the antenna, -7 dB is reflected and the rest is accepted by the antenna [41]. The limit for mutual coupling of elements (S12) should be below -15 dB to -20

dB depending on the distance between elements since antenna element spacing varies in the range of 0.5 λ - 0.75 λ and so does the impact. The final design is simulated with elements' spacing of 0.75 λ thus, the lowest limit is -20 dB for mutual coupling as shown in **Table 3.1**.

3.1.2 Antenna Polarization Goals

The antenna module presented in this thesis is intended to be used as a receiver with both MIMO and beamforming support if the transmitter side implements these features. The transmitter side may be equipped with antennas which emit electromagnetic waves in vertical and horizontal polarization, improving diversity gain of MIMO performance and increasing channel capacity by parallel transmission. Thus, the antenna should be designed to support both polarization even though double polarized antenna may limit the range of beam scanning angle. The antenna is simulated with directing the main beam to various angles in the required range (**Table 3.1**) to monitor the impact on the impedance of the array antenna.

3.1.3 The phased array antenna element spacing for beamforming and MIMO technologies

It has been pointed out that MIMO and beamforming technologies require different antenna element spacing but it is possible to find the distance where MIMO and beamforming are performed at an acceptable level. Therefore, in this thesis, various antenna element spacings are simulated to achieve high diversity gain and at the same time directed antenna pattern with low sidelobe levels. As it has been shown in **Table 3.1**, element spacing is 0.75 λ since it is the middle point between beamforming (which requires 0.5λ separation) and MIMO (which requires 1 λ separation) technologies.

Massive MIMO utilizes a high number of elements in the array. The number of elements in the phased array antenna investigated in this thesis is 60 (10x6) but only 32 (8x4) of them are active and the rest can be considered as an outer shell that possibly creates the same surrounding as the elements in the middle of the array, which leads to less impedance change. Throughout the thesis, two types of array antenna (8x4 without the outer shell and 10x6 with outer shell) are simulated and analyzed. Another reason for

particularly targeting a 10x6 array antenna module is the hardware limitation of the laptop [42] used to simulate the antenna in CST studio.

3.2 Beamforming requirements and performance metrics

Antenna arrays used for beamforming are different from MIMO antenna set where each element in the array gets excitepd with specific amplitude and phase to form a directed beam in the desired direction. In this thesis, beamforming of a 10x6 array antenna is simulated using CST studio. There are a number of excitation patterns (Uniform, Binominal, Taylor, Chebyshev, Gaussian) available for phased arrays in CST simulation software."Chebyshev" distribution has high sidelobe levels for elements spacing less than 0.8λ while sidelobe levels in "Binominal" excitation are very low due to high the excitation coefficients which results in an enormous difference between the main lobe and side lobe. In practice, it is difficult to produce signals with a huge difference between the coefficients [43]. "Similarly, the "Gaussian" excitation pattern has specific amplitude distribution which leads to decaying of the radiation pattern of both main and side lobe [44] which is not desirable for the applications stated in Chapter 1. However, only "Uniform" and "Taylor" distribution excitation patterns are used.

Both excitation patterns ("Uniform" and "Taylor") options in CST studio can be used to shape a beam by varying the phases of elements. However, due to the same amplitude level assignment in "Uniform" distribution, sidelobe levels may be high. Thus, this thesis uses "Taylor" excitation to form the beam, which suppresses the side lobes about 30 dB from the main beam (**Figure 3.3**). As it has been discussed in the introduction part, the phased antenna is configured to form a beam in azimuths plane within -45° to +45° with reflection coefficient (S11) being kept lower than -10 dB.

Since "Uniform" excitation pattern sets the same amplitude for all elements in the array (**Figure 3.1**), it can be thought of a smart antenna system being in a default state. A smart antenna system in the receiver side may be in a default state waiting to be connected when the base station does not allocate a specific beam for it. Once the beam is shaped at the transmitter side, it is directed to the receiver and the receiver should configure the elements' phase accordingly to maximize the reception gain of the directed beam. This configuration state can be simulated by implementing "Taylor" excitation since it sets

amplitude and phase values to elements individually, as shown in **Figure 3.2**.

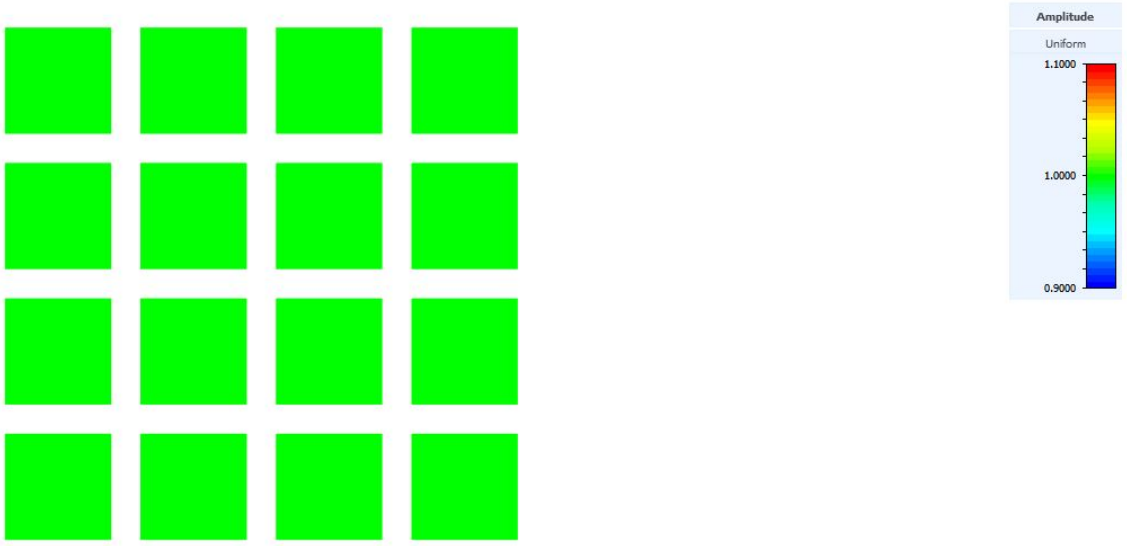

Figure. 3.1. Uniform excitation of 4x4 phased array antenna with the same amplitude level set to form a directed beam in a particular direction (Uniform excitation does not support side lobe level reduction)

3.2.1 Total Active Reflection Coefficient (TARC) metric

In multi-port antennas, the operating bandwidth and efficiency of an antenna are affected by the adjacent element and S-parameters alone do not give enough information to predict the actual system performance. Therefore, a new metric is introduced as total active reflection coefficient (TARC) [4] that is computed using S-parameters of the array antenna; it is the ratio of the square root of the total reflected power divided by the square root of the total incident power in multiport. Formula to compute the N-element antenna is given by [4]:

$$\Gamma_a^t = \frac{\sqrt{\sum_{i=1}^{N} |b_i|^2}}{\sqrt{\sum_{i=1}^{N} |a_i|^2}} \tag{3.1}$$

where b_i and a_i are reflected and incident signals respectively. TARC value ranges from 0 to 1 where zero indicates that all power was radiated while one means all power was reflected. Available power is found by summing the powers of all ports of the antenna. By calculating the TARC, it is possible to determine the effect of various phase feedings, hence the TARC curve shows the resonance frequency and impedance bandwidth of the complete antenna system for the particular phase excitation among ports. The following

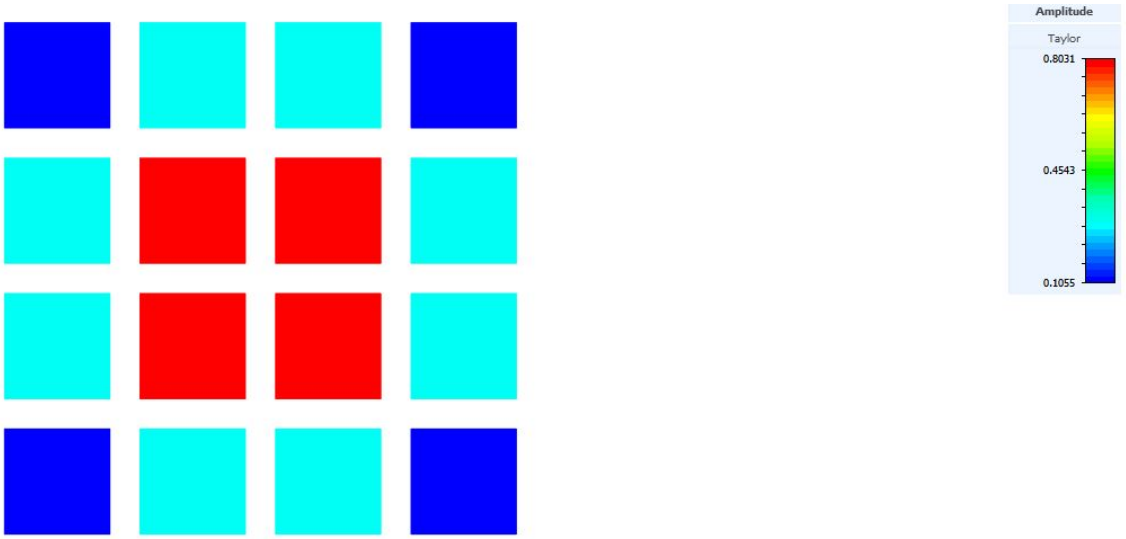

Figure. 3.2. Taylor excitation of 4x4 phased array antenna elements with various amplitude values assigned to form a directed beam in a particular direction with at least -30 dB side lobe levels

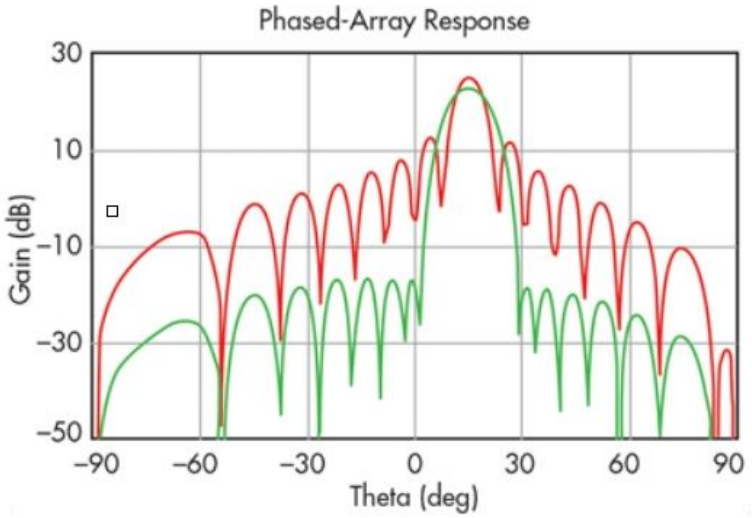

Figure. 3.3. 2D Phased array pattern with "Taylor" (green curve) and "Uniform" (red curve) excitation. Taylor excitation uses amplitude tapering which tailors amplitude levels to elements individually [45]

formula can be used to evaluate 2-port MIMO antenna TARC:

$$\Gamma_a^t = \frac{\sqrt{(|S_{11} + S_{12}e^{j\theta}|^2)} + \sqrt{(|S_{22} + S_{21}e^{j\theta}|^2)}}{\sqrt{2}} \tag{3.2}$$

θ is the feeding phase and S_{xx} and S_{xy} are reflection coefficient and coupling between two ports within the antenna systems [4].

3.3 MIMO antenna requirements and performance metrics

It has been mentioned that mutual coupling between elements is a critical point in MIMO antenna technology and needs to be reduced by placing elements about one wavelength apart. Within the thesis key parameters such as the correlation coefficient and diversity gain are calculated using S-parameters' results with acceptable limits being for the correlation coefficient 0.3 (**Table 3.1**) (5G wireless system standard limit has been set yet) even though it is for 4G wireless systems (3GPP TS 36.101, 2008). For diversity gain, which defines the improvement in signal-to-interference ratio due to the diversity of receivers and the received signals, the limit should be below than -10 dB (**Table 3.1**).

The primary required metrics that differentiate the MIMO antennas with traditional antennas are total active reflection coefficient (TARC) for multi-port antenna systems which is presented in the previous sub-section, diversity gain, correlation coefficient, and channel capacity that characterizes the desired MIMO performance.

3.3.1 Correlation Coefficient

The factor that describes the isolation of communication channels and how they are correlated is called correlation coefficient (ρ) [4]. This parameter takes into account the radiation pattern of each element in the array and their effect when they are excited simultaneously. The correlation coefficient for single mode and lossless antenna can be calculated using s-parameters. The concept of enveloping correlation can be found by squaring the correlation coefficient and the efficiency effect on the envelope correlation can also be computed using s-parameters:

$$|\rho_{ij}| = \rho_{eij} = |\frac{|S_{ii}^* S_{ij} + S_{ji}^* S_{jj}|}{|(1 - |S_{ii}|^2 - |S_{ji}|^2)(1 - |S_{jj}|^2 - |S_{ij}|^2)\eta_{radi}\eta_{radj}|^{0.5}}|^2 \tag{3.3}$$

ρ_{ij} represents the correlation coefficient between i and j elements, ρ_{eij} is the envelop correlation coefficient, S_{ij} is the coupling s-parameters, and $\eta_{radi}\eta_{radj}$ are the i and j elements' radiation coefficient [4]. The acceptable correlation coefficient value for 4G wireless system is 0.3 (3GPP TS 36.101, 2008).

3.3.2 Diversity Gain

Diversity is accomplished when antennas receive a number of identical streams coming from various radio channel paths. In the case of uncorrelated signals at the receiver, better signal reception is achieved by combining the signals which results in increased signal-to-noise-ratio [40]. Since diversity gain identifies the effect of heterogeneity communication system, it is defined as "the difference between the time-averaged SNR of the combined signals within the diversity antenna system and that of a single antenna system in one diversity channel, provided the SNR is reference level" [40]. Mathematically diversity gain can be found using the following formula:

$$DiversityGain = \left[\frac{\gamma_c}{SNR_c} - \frac{\gamma_1}{SNR_1}\right]_{P(\gamma_c<\gamma_s/SNR)} \tag{3.4}$$

where γ_c is the instantaneous SNR and SNR_c is the mean signal-to-noise-ratio for diversity system, and γ_1 and SNR_1 refer to antenna single branch with reference being γ_s/SNR. Considering the signals are not correlated, the possibility of the instantaneous mean SNR of the diversity system being lower than the reference level can be computed with[40]:

$$P\left(\gamma_c < \frac{\gamma_s}{SNR}\right) = \left[1 - e^{-\frac{\gamma_s}{SNR}}\right]^M \tag{3.5}$$

where M stands for the amount of antenna. The combined power of a diversity system (MIMO system) can be increased by increasing the number of antennas and **Figure 2.1** shows the effective diversity gain versus the number of antennas based on equation (2.5).

It can be seen from **Figure 2.1**, as the number of antenna elements increase, that the gain obtained also increases non linearly. In multiple antenna systems, metrics such as the diversity gain and correlation coefficient are related where the higher the diversity, the lower the correlation coefficient [40].

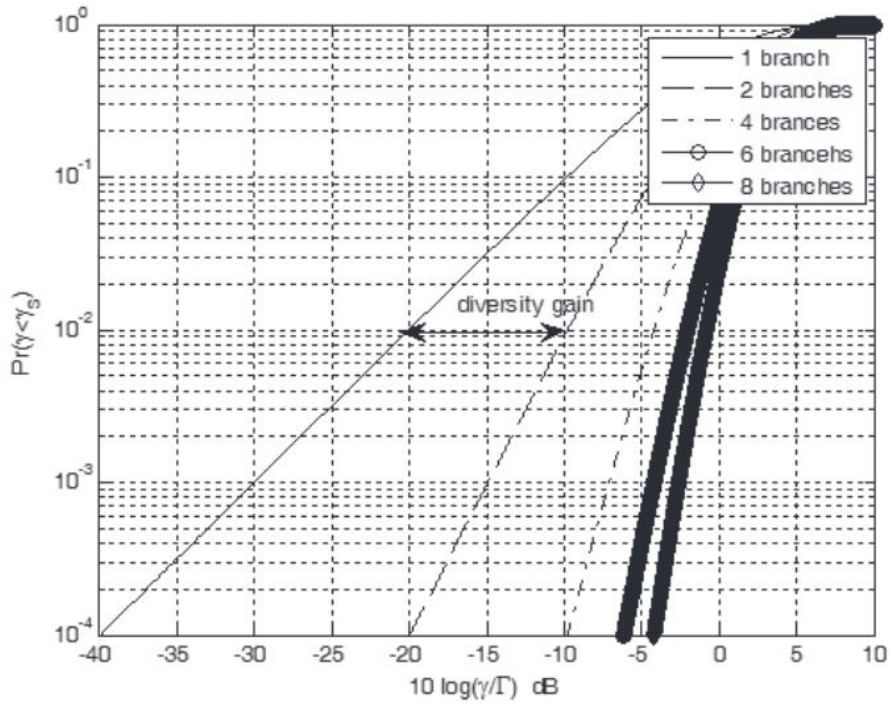

Figure. 3.4. The cumulative distribution function of equation (2.5), showing the diversity gain obtained as a function of the increase in the number of antenna elements [40]

3.3.3 Channel Capacity

The advantage of a MIMO system over single-input-single-output (SISO) antenna system is the improvement of channel capacity in the multipath channel communication environment. The advantage of a MIMO system over a SISO antenna system is the improvement of channel capacity in multipath channel communication environments. The communication channel environment and the antenna radiation characteristics are functions of the channel matrix and play an important role to achieve high channel capacity [40]. The transmitter side should have information about the channel environment so that it powers the antenna elements accordingly. In the case of unknown channel conditions, the transmitter allocates equal power for each element in the N-element MIMO antenna system and the following formula represents the channel capacity of unknown channel condition in bits/sec/Hz [40]

$$C = \log_2 \left[det \left(I_N + \frac{\rho}{N} H H^T \right) \right] \tag{3.6}$$

where N stands for number of antenna elements in both transmitter (TX) and receiver (RX) side, I_N is the NxN identity matrix, ρ represents the average signal-to-noise-ration (SNR) and H is the normalized channel covariance matrix.

The channel capacity can be linearly increased compared to a SISO system if the transmitting/receiving signals are uncorrelated, having zero correlation at both transmitter and receiver side resulting in similar power usage leading to mean effective values normalize as shown in the equation 3.7:

$$C = Nx \log_2 \left(1 + \frac{\rho}{N}\right) \tag{3.7}$$

In real-world conditions, it is not possible to achieve a zero correlation between antenna elements in multi-antenna systems. A high correlation between antenna elements is caused by high mutual coupling between the elements, which degrades the MIMO antenna system performance. In the case of line-of-sight (LOS) communication, a MIMO antenna can be seen as a single-input-single-output (SISO) system with effective aperture increased. However, wireless communication channels in the real world are multipath, hence different channels' correlation information due to i) MIMO antenna operating in a specific environment and ii) propagation environment are contained in the channel coefficient matrix,H, thus calculating it correctly is important.

Chapter 4

Initial Results : Antenna Design, Simulation, and Analysis

Throughout the previous chapters, the antenna types, technologies such as MIMO and beamforming, various performance metrics and lastly, the antenna design requirements that lead to the desired outcome of this thesis have been described. Striving to achieve the requirements listed in Chapter, over 30 different antenna designs have been modelled during the course of this thesis. However, this chapter presents only two types of array antenna simulations since their beam shaping, MIMO performance as well as physical size were close to the requirements. These phased array antennas are constructed from the patch antenna element acquired from Antenna Magus library (Section 4.1).

There are two sections discussed in this chapter. The first section presents the simulation results and analysis of a 4x4 (16 active elements) array antenna; the second section presents the results of 6x6 (36 elements) array antenna but only 16 of them are active while the rest is passive (not excited) with beamforming in the range of -45°to +45°and MIMO performance. These two arrays are made from the patch antenna element without any adjustments to its original parameters (that were calculated in the Antenna Magus tool). In the next chapter, additional parts are added to the patch antenna element and modifications to the parameters are performed for both the 4x4 and 6x6 phased array antenna modules.

As mentioned in Chapter 1, the application of the phased array antenna presented in this thesis is to support both MIMO and beamforming technologies for drones and delivery robots that operate in low power. Thus, the MIMO performance of the antenna is

prioritized over beamforming since beamforming requires heavy signal processing which may consume high power.

The phased array elements are excited with a multitone signal, as shown in Figure 4.1. The amplitude of signals varies since the "Taylor" excitation pattern is used, as discussed in Chapter 3.

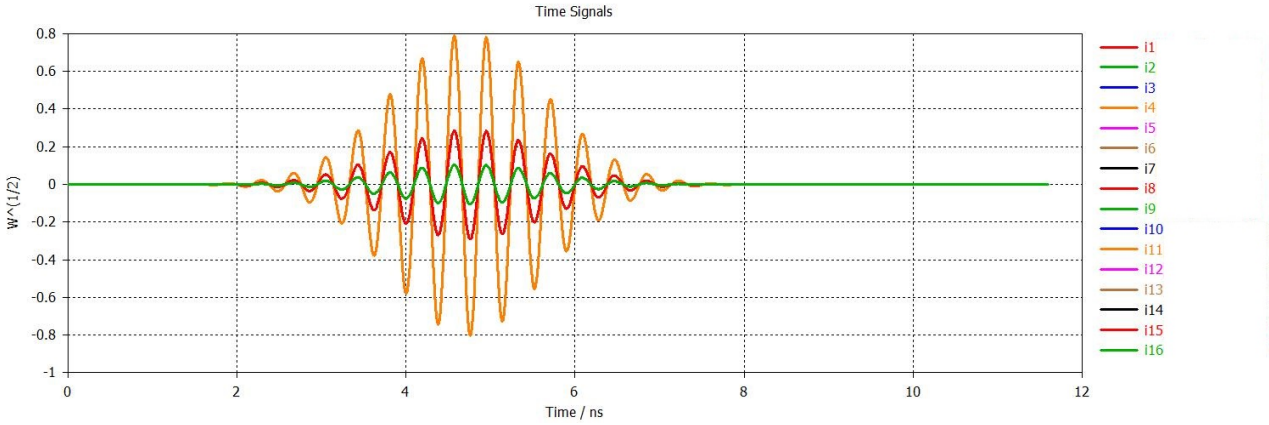

Figure. 4.1. Taylor pattern excitation signals for the phased array antenna elements (16 active elements) with various amplitude levels

All simulation results and analyses are presented for the following performance parameters and metrics for the defined phased array antenna:

- Reflection coefficient (S_{11}parameters)
- Mutual coupling between elements (S_{ij}parameters)
- Correlation coefficient for MIMO performance
- Diversity gain of MIMO antenna elements
- Farfield results (radiation pattern achieved)
- Surface wave flow between elements

However, the first criterion to look at in all simulation results is the acceptableness of S_{11} parameter; i.e., if it is below -10 dB within 2.5 GHz - 2.7 GHz frequency, then the other results can be shown and analyzed. Thus, the reflection coefficient plot is analyzed first. Mutual coupling plots are shown only for 4x4 phased array antenna using the same ground plane, isolated ground plane, and metallic slot insertion between elements which

have individual ground planes. The reason to show mutual coupling only for 4x4 array antenna is the inadequate computing power and RAM memory on the device that was used to simulate the phased arrays. The simulation of 4x4 phased array using "Frequency Domain Solver" which produces each element coupling results takes about 8 hours and for 6x6 phased array simulation could take about 7 days if the computer does not run out of hard memory.

4.1 Square truncated capacitively pin-fed circularly polarized patch antenna dimensions

CST microwave studio software tool is used to design the phased array antenna, simulate it, and acquire the necessary data for analysis. The square truncated capacitively pin-fed circularly polarized patch antenna element is not designed entirely from scratch but is built upon the "Antenna Magus" antenna library tool [46] since the primary aim of the thesis is to construct an array from a number of antenna elements, not a single antenna. The dimensions of the antenna element from the library are modified to fit into the desired phased array antenna module.

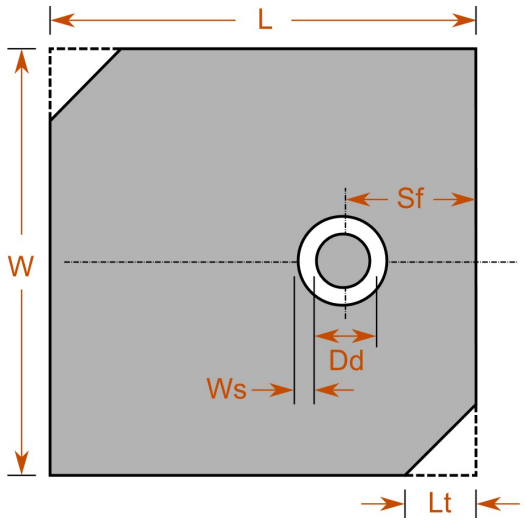

Figure. 4.2. Square truncated capacitively pin-fed circularly polarized patch antenna top view [46]

The square truncated capacitively pin-fed circularly polarized patch antenna element is chosen to make an array for its directive radiation pattern, as shown in **Figure 4.5**, and for its performance bandwidth which is about 12% of operating frequency, as shown in

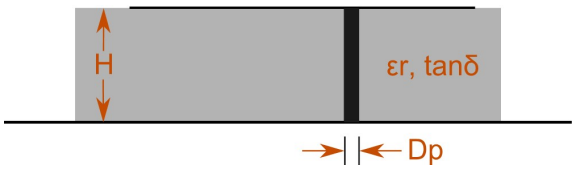

Figure. 4.3. Square truncated capacitively pin-fed circularly polarized patch antenna side view [46]

Figure 4.4 (BW > 250 MHz from 2.5 GHz to 2.7 GHz). The detailed element performance parameters are indicated in **Table 4.1**. The dimensions for the patch antenna are given in **Table 4.1** as well as in **Figures 4.2 and 4.3** associated with labels indicated in the table. A few parameters of the patch are modified throughout the iterations, hence updated tables are presented with the changed parameter.

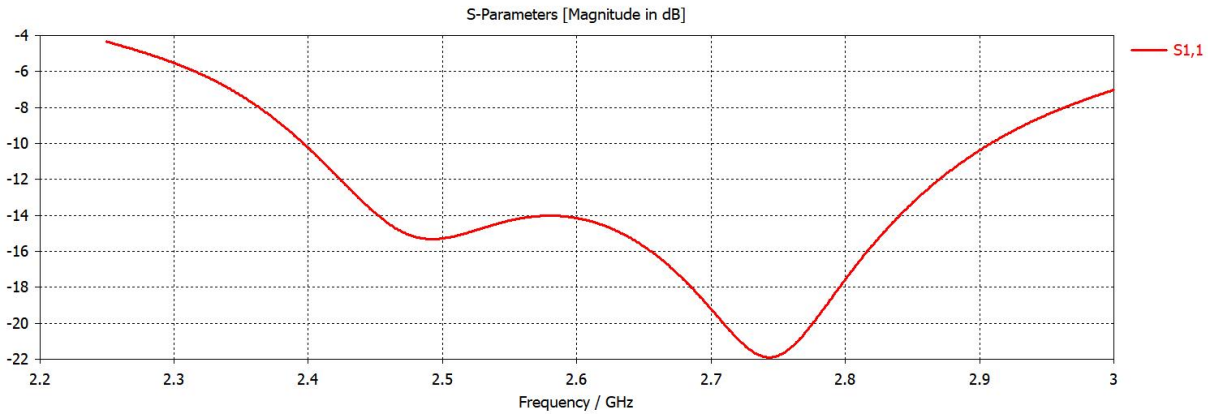

Figure. 4.4. Reflection coefficient of the patch element with dimensions indicated in Table 4.1, assuming center frequency being 2.5 GHz

As mentioned in previous sections, B7 (Uplink: 2500 – 2570 MHZ and Downlink: 2620 – 2690 MHz) is the band of interest. The patch antenna dimensions are calculated basing 2.5 GHz as the centre frequency even though this statement is not entirely accurate (Centre frequency for B7 is 2.6 GHz). The reason for doing so is that the array construction using multiple elements where (if element dimensions are calculated based on 2.6 GHz) each element impedance shifted about 100 MHz from the frequency of interest, leading to a reflection coefficient of -10 dB level shift from 2.5 GHz to 2.6 GHz as a starting frequency, as indicated in **Figure 4.6**. Thus, 2.5 GHz frequency is set as the centre frequency to yield a -10 dB level ranging from 2.5 GHz till 2.7 GHz.

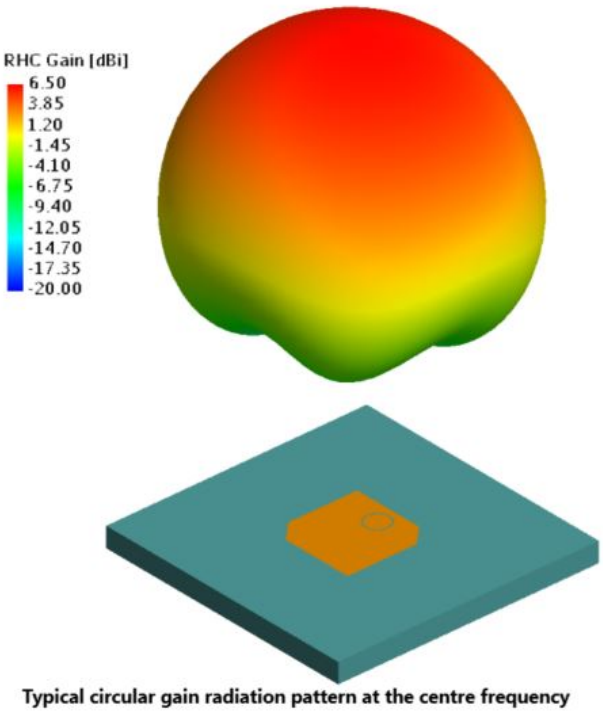

Figure. 4.5. 3D radiation pattern of square truncated capacitively pin-fed circularly polarized patch antenna [46]

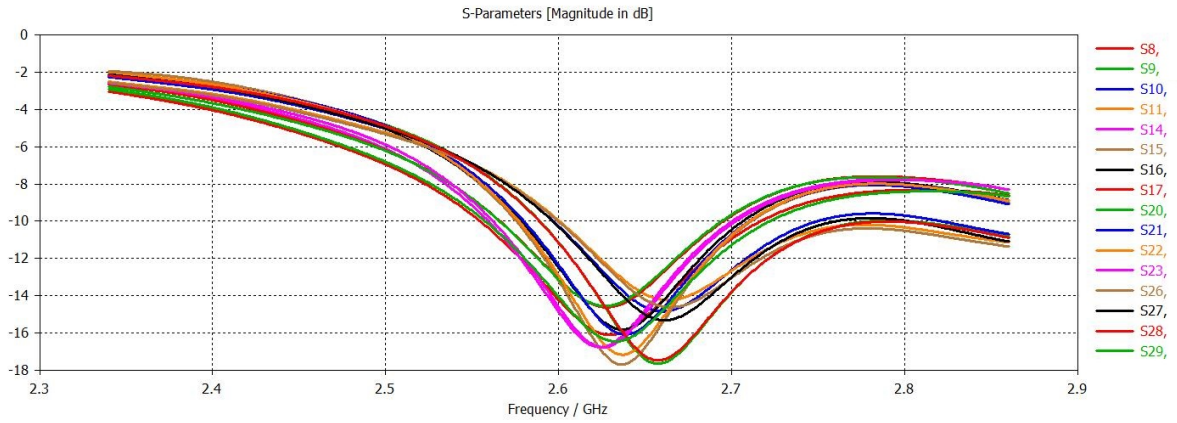

Figure. 4.6. S11 parameters of an 6x6 array antenna whose elements are designed setting the center frequency at 2.6 GHz. All active elements' reflection coefficients are shown with 100 MHz shift from 2.5 GHz to 2.6 GHz on a -10 dB level)

4.2 Common Ground Plane 4x4 (16 active elements) Phased Array Antenna Simulation Results

This section presents 4x4 (16 active elements) phased array antenna simulation results when the same ground plane is shared between elements at 2.5 GHz frequency. The

Parameter Name	Value	Description
L	24.3mm	Patch width
W	24.3 mm	Patch length
Lt	6.6 mm	Truncation length
Sf	4.56 mm	Feed inset
Dp	0.571 mm	Pin diameter
H	7.2 mm	Substrate height
ϵr	4.4	Relative permittivity
Dd	5.068 mm	Diameter of the coupling disc
Ws	0.38 mm	Width of the slot
F	2.5 GHz	Dimensions based frequency
Polarization	Circular	Polarization type
Radiation Pattern	Single Broadside Lobe	Radiation attern
Gain, dBi	6.5	Main beam gain
Performance Bandwidth	10 % -15%	BW :250 MHz to 300 MHz
Complexity	Moderate	Complexity level
Impedance	50 Ω	Antenna impedance

Table 4.1: Square truncated capacitively pin-fed circularly polarized patch antenna element dimensions and performance parameters [46]

impedance simulation result (S_{11}parameters) is not within B7 range for the shared ground case, thus only S_{11} parameters, surface wave flow, and mutual coupling results and analysis are provided. MIMO performance metrics such as diversity gain and correlation coefficients are not produced for this set up since it does not meet the first criterion mentioned above.

The following phased array antenna is constructed from single patch antenna elements with mentioned dimensions (Table 4.1) and with substrate height and length for each element being equal to H = L = 62.30 mm. The array size can be found by multiplying

62.30 mm x 4 = 249.2 mm since there are 4 elements with identical substrate and element dimensions.

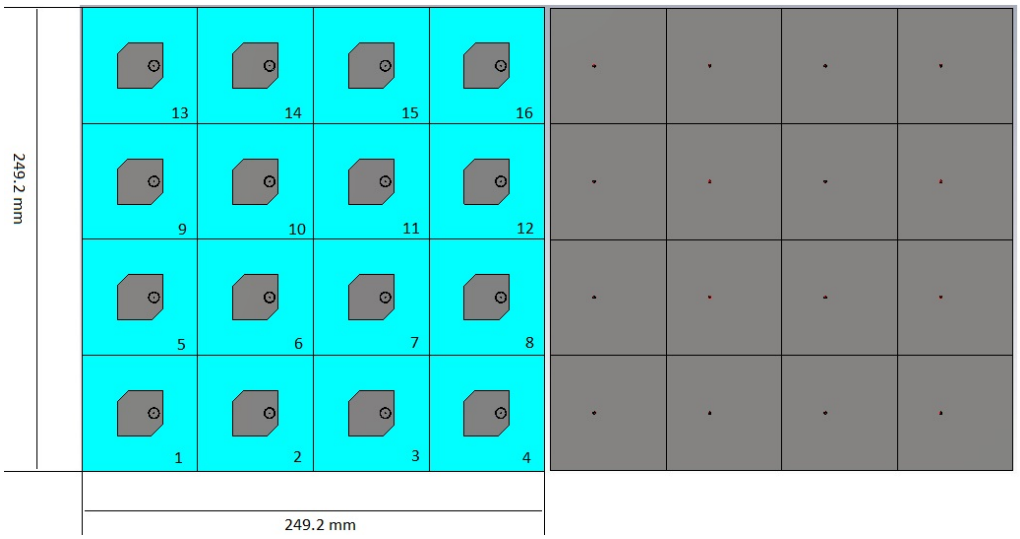

Figure. 4.7. Front (On the right) and back (on the left) views of the 4x4 phased array antenna (16 elements' numbers indicated) with shared ground plane between elements.

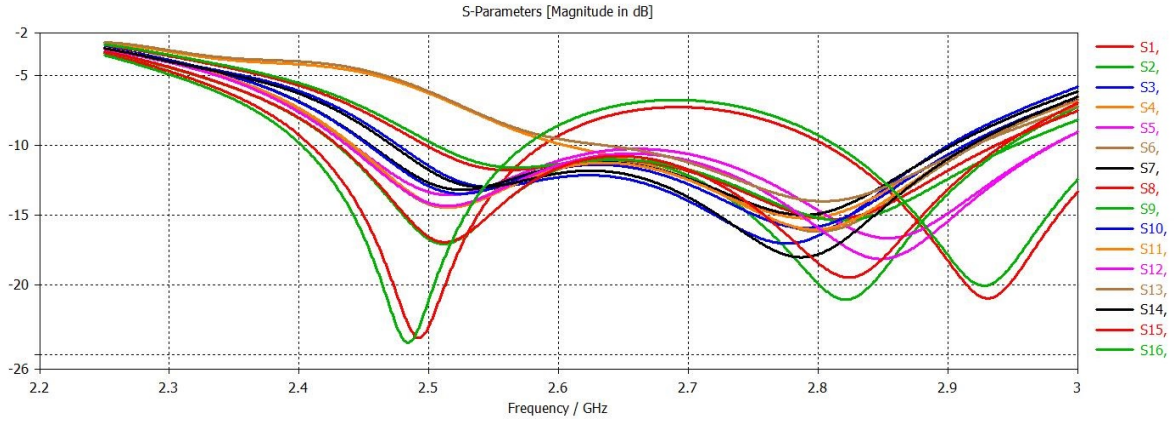

Figure. 4.8. Reflection coefficients of the 16 elements with a shared ground plane between them. The curves are not below the -10 dB level within the B7 frequency range

The reflection coefficients of each element on the array set do not satisfy the requirement which is at least a -10 dB level for the S_{11} parameters from 2.5 GHz to 2.7 GHz. As can be seen, the 1^{st} and 16^{th} elements have almost identical curves which are well above the limits within 2.6 GHz to 2.7 GHz. The others have a similar pattern, but with a -10 dB level starting from 2.65 GHz instead of 2.5 GHz. The reason of having similarities in the patterns between the 1^{st} and 16^{th} elements is the surface wave flow impact as shown in **Figure 4.12**.

The amplitude level for the 1^{st} and 16^{th} elements is 0.1 $W^{\frac{1}{2}}$ while the 6^{th}, 7^{th},10^{th}, and 10^{th} elements have the highest levels, as depicted in **Figure 4.11**. Thus, the surface wave flow within the elements located at the centre is high, leading to impedance change whereas the 1^{st} and 16^{th} elements at the edge are less impacted and their curves have a similar pattern as in the case the patch element was excitepd alone, as shown in **Figure 4.4**.

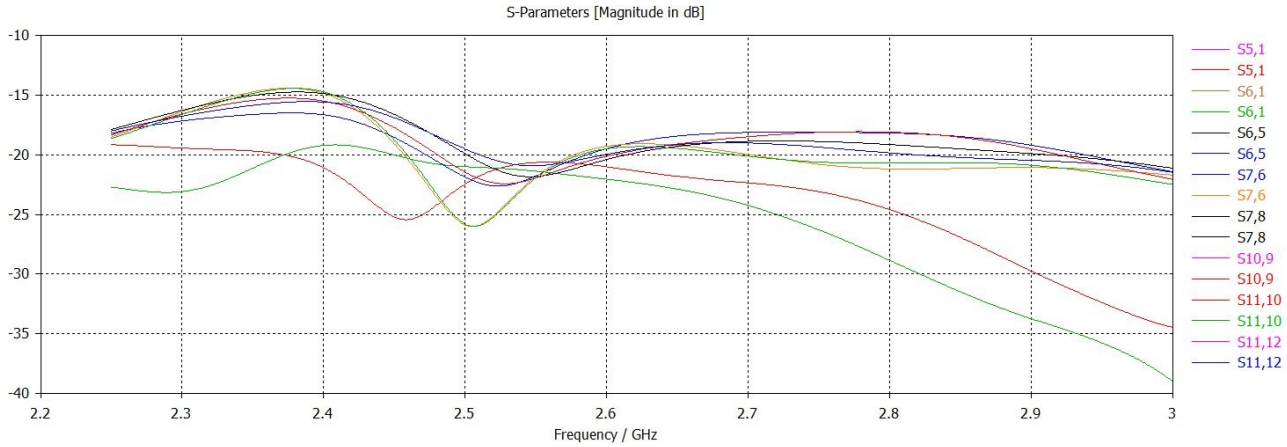

Figure. 4.9. Mutual coupling results for 8 elements. The coupling levels are high between the 5^{th},6^{th},7^{th},8^{th},9^{th},10^{th},11^{th}, and 12^{th} elements because of high amplitude levels; on the other hand, the impact of the 5^{th} and 6^{th} elements is low on the 1^{st} element

The phased array antennas under investigation are built on a dielectric substrate, which has a considerable effect on the antenna performance. One of the negative effects introduced by the substrate is the surface waves which propagates along the substrate with low loss and parallel to the surface. They are created due to internal electromagnetic wave reflections at two different media [15] (between the ground plane (metal) and the air), as shown in **Figure 4.10**

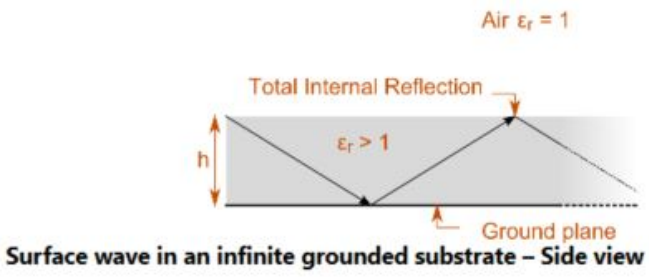

Figure. 4.10. Surface wave caused by internal reflection of electromagnetic waves on two different medias: metal and air [47]

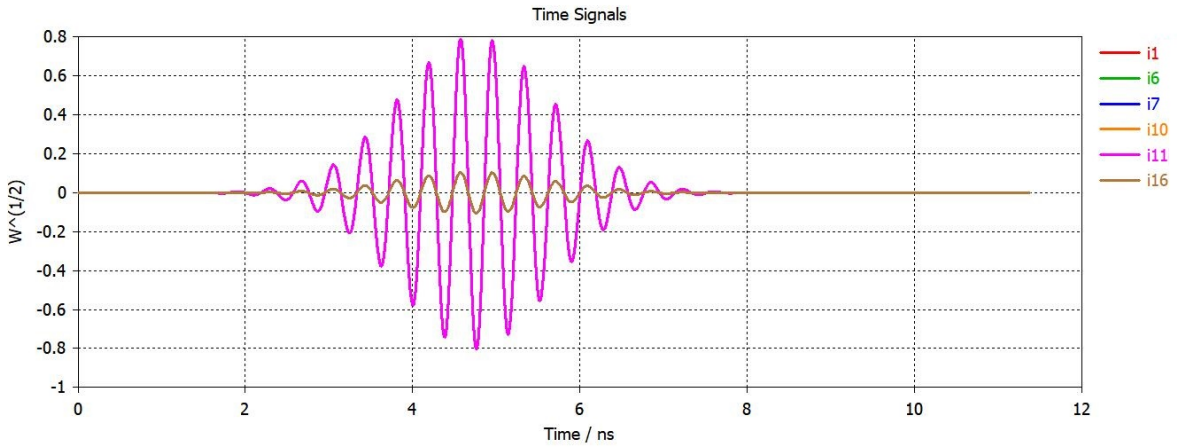

Figure. 4.11. Excitation signals for the 1^{st}, 6^{th}, 7^{th},10^{th}, 10^{th}, and 16^{th} elements of the phased array antenna

CST studio tool can produce mutual coupling results for all 16 elements with every element impact to each other. It produces a huge number of curves per element showing the effects of the 2^{nd}, 3^{rd}, 4^{th}...16^{th} element on the 1^{st} element's (S_{12}, S_{13}, S_{14}...S_{16}). Given the high number of combinations, only few considerably high impact elements are presented. It has been experimentally seen that the 6^{th}, 7^{th}, 10^{th}, and 11^{th} elements have high impact on each other as well as on their neighboring elements since they have the highest amplitude levels due to the "Taylor" excitation (**Figure 4.11**) implementation. Low level amplitude elements have less effect on the other elements (for instance, the 5^{th} element on the 1^{st} element), as shown in **Figure 4.9**.

For this setup, the mutual coupling results do not meet the requirement listed in **Table 3.1** where the target for the B7 (Band 7) range is -20 dB. The reason could be the implementation of a common ground plane for all elements. The ground plane is used to create directive radiation where the patch radiates forwards with low- level back lobe. The radiation power of each element varies, creating different voltage levels on the ground plane. Ideally, all 16 elements' ground voltage levels should be identical. However, when there is a voltage difference, a current flows on the ground plane since current is the rate at which electric charge flows. Therefore, in the next chapter, the results for isolated ground and metallic slots placed in 4x4 phased array set up are presented and analyzed to evaluate whether they can reduce the surface wave flow on the antenna operating bandwidth. However, before moving to these design strategies, let us analyze the simulation results for the common ground plane 6x6 (16 active elements) phased array

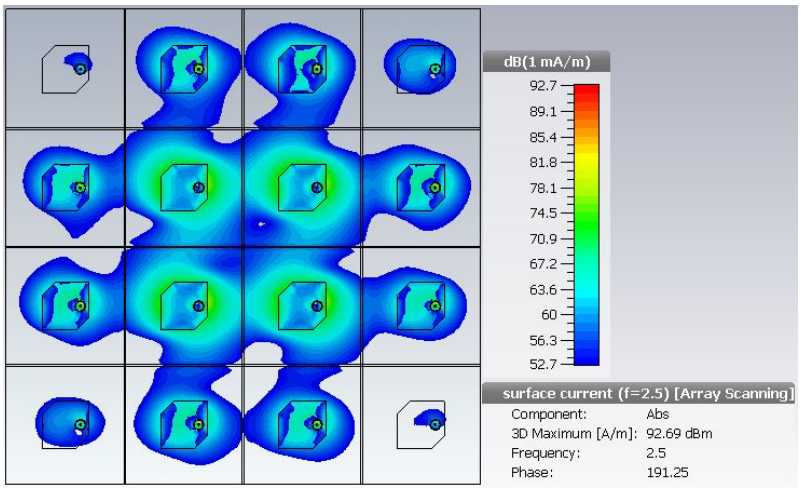

Figure. 4.12. Surface wave flow between the 16 elements of the shared ground plane antenna at 2.5 GHZ frequency with 0° beamforming. The amplitudes of the elements located at the edge are low so does the surface wave flow intensity

antenna.

4.3 Common Ground Plane 6x6 (16 active elements) Phased Array Antenna Simulation Results

This section describes the 6x6 (16 passive elements and 16 active elements) phased array antenna construction using the antenna element mentioned in Section 4.1. The patch dimensions listed in Table 4.1 are used in this section, without any adjustments by the author. Even though the array is called 6x6, there are only 34 elements (Figure 4.13); only 16 of them are active transmitters and receivers which are numbered, while the other 18 of them are passive and do not transmit nor receive (Figure 4.14).

The reason for having 18 passive elements stems from the experiment on the 4x4 array antenna (Section 4.2) which shows that elements at the edge of the array get considerably low levels of amplitudes, which isolates them in impedance values from the other elements, as shown in Figure 4.8. Therefore, in order to achieve higher amplitude levels for the elements at the edge, one can surround the active elements with passive elements in which "Taylor" excitation pattern assigns relatively higher amplitudes to the elements at the edge, as shown in Figure 4.16. The amplitude levels are about twice higher than the edge elements in the 4x4 phased array set up. The rest of this section consists of two subsections

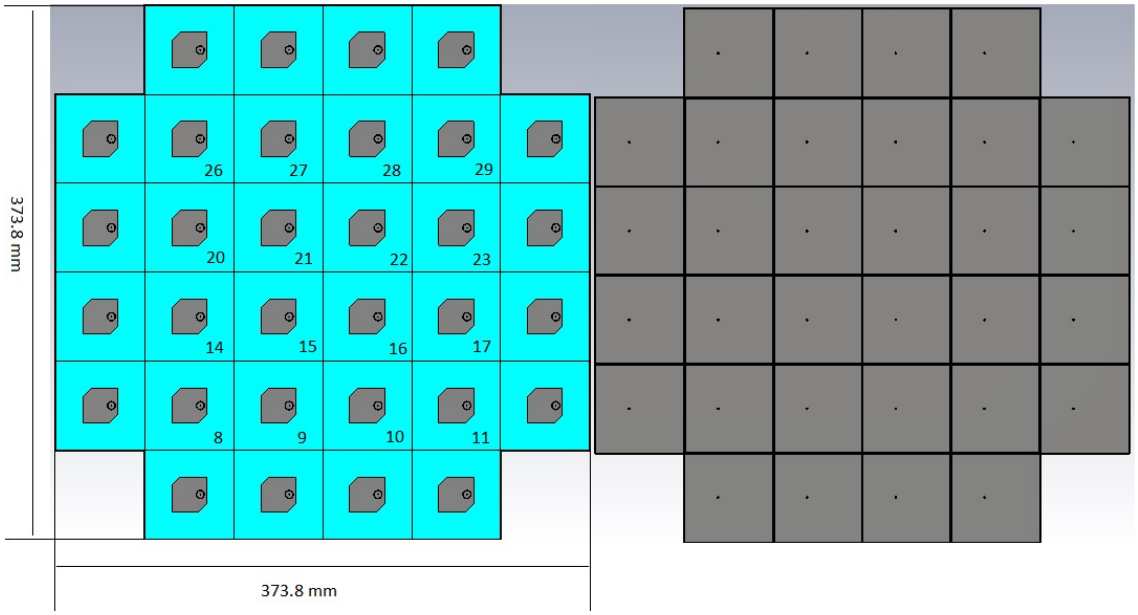

Figure. 4.13. Front and back view of the 6x6 (16 active elements) phased array antenna with only active elements numbered on the shared ground plane

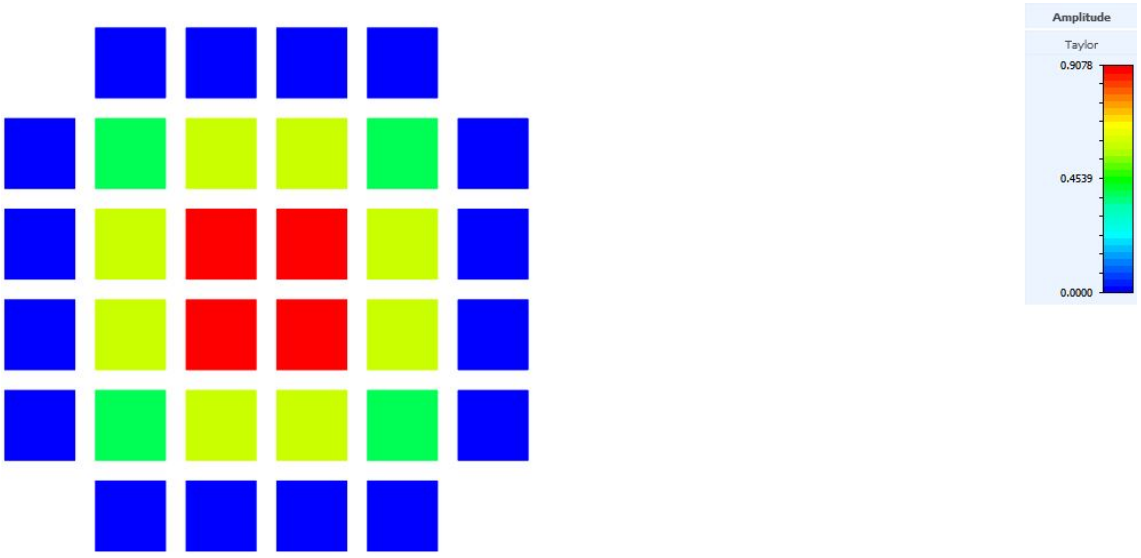

Figure. 4.14. 6x6 phased array antenna "Taylor" excitation view. The highest amplitude levels are at the four elements at the centre; the other elements have lower amplitudes

where the first step with ϕ , $\theta = 0°$ beamforming has acceptable results to proceed to the second step with ϕ , $\theta = 5°$ beamforming and its impact on the simulation results.

Another reason to include passive elements and to place them strategically is to create the same environment for elements located at the edge. Each corner of elements at the centre are surrounded by four elements and the ones at borderline are surrounded by three elements. However, the corners of the elements at the edge are surrounded

by only two elements. In order to achieve the beamforming effectively, each element should have less undesired interference to each other and the amplitudes, phases should be distributed accordingly. Creating the same environment for each element (surrounding each element from all corners) eases the accomplishment of effective beamforming and the array antenna efficiency versus scan angle since the reflection coefficients change as the scan angle changes.

4.3.1 ϕ , θ = 0° beamforming simulation results and analyses

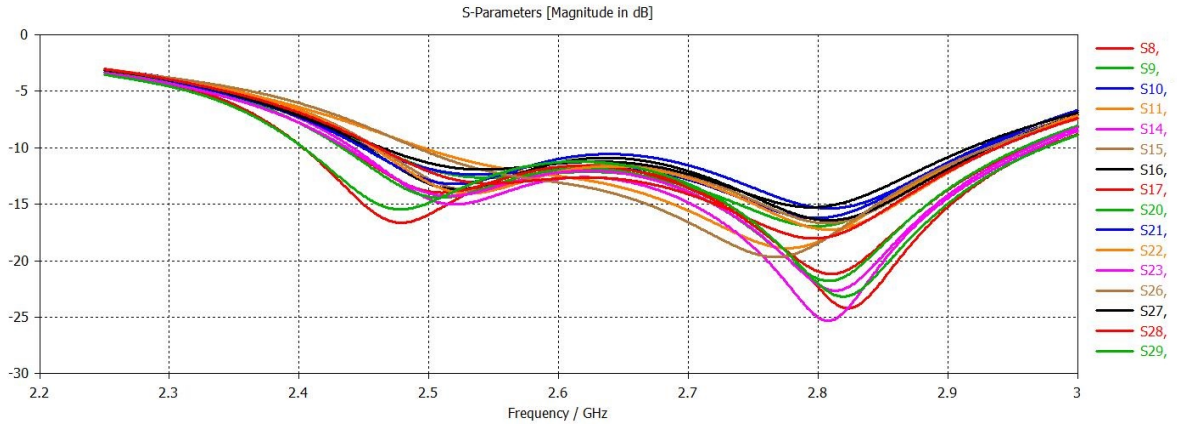

Figure. 4.15. Simulation results for (6x6 phased array) 16 active elements reflection coefficients with shared ground plane between elements with ϕ , θ=0° direction beamforming. The elements exhibit below -10 dB levels within the B7 frequency range

From the simulation results, it is seen that the antenna bandwidth (reflection coefficient) is at an acceptable level within the frequency range of interest (2.5 GHz - 2.7 GHz), as shown in **Figure 4.15**. Therefore, other results such as surface wave, radiation efficiency along with total efficiency and radiation patterns are shown. The mutual coupling plot is not presented due to the incapability of the author's personal computer to produce the result.

The simulation results for the reflection coefficients of the elements confirm the assumption that the introduction of passive element creates a similar environment for each element and assigns relatively high amplitudes to the elements located at the edge, leading to the highly correlated overall performance of the array antenna. The surface wave flow shows the interaction of the edge elements due to the higher amplitude levels compared to an array set up discussed in Section 4.2. Some of the passive elements, especially the

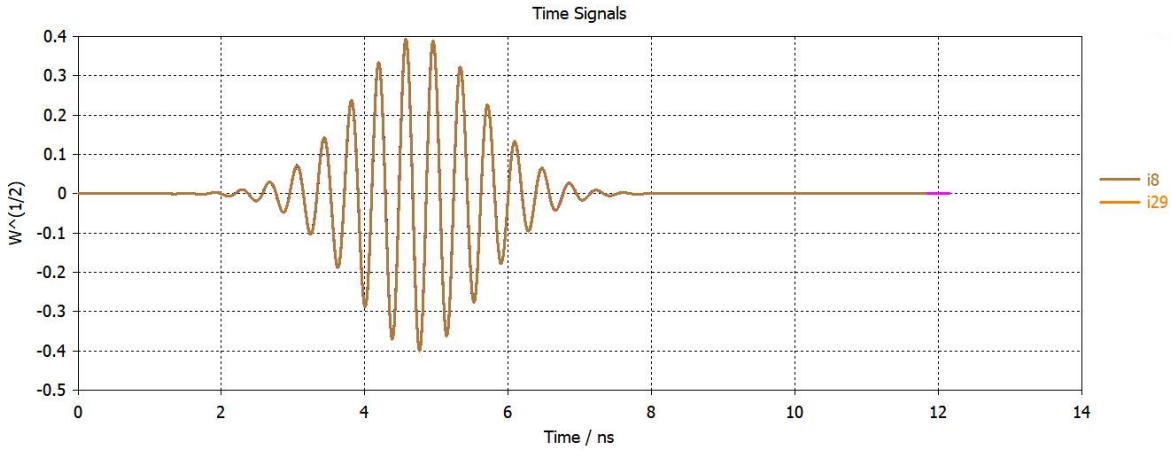

Figure. 4.16. 6x6 phased array's 8^{th} and 29^{th} elements at the edge, each assigned with 0.4 $W^{\frac{1}{2}}$

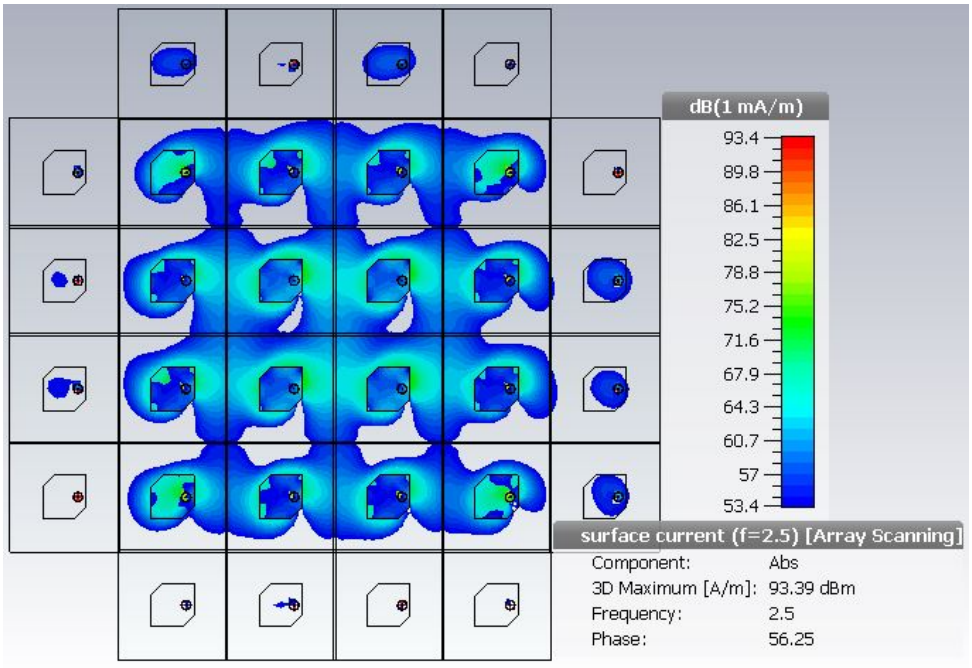

Figure. 4.17. Surface wave flow of common ground plane array antenna on 2.5 GHz frequency with ϕ , $\theta = 0°$ beamforming. The array has 36 elements but only 16 of them are active, the rest is passive but surface wave leaks to passive elements too.

ones on the right side and on the top, exhibit coupled surface current density since the high-intensity surface wave travels to the neighbouring element via the substrate and the common ground.

The total efficiency and radiation of the antenna vary starting from almost 95% to 90% from 2.5 GHz to 2.7 GHz, respectively (Figure 4.19). The radiation efficiency is the

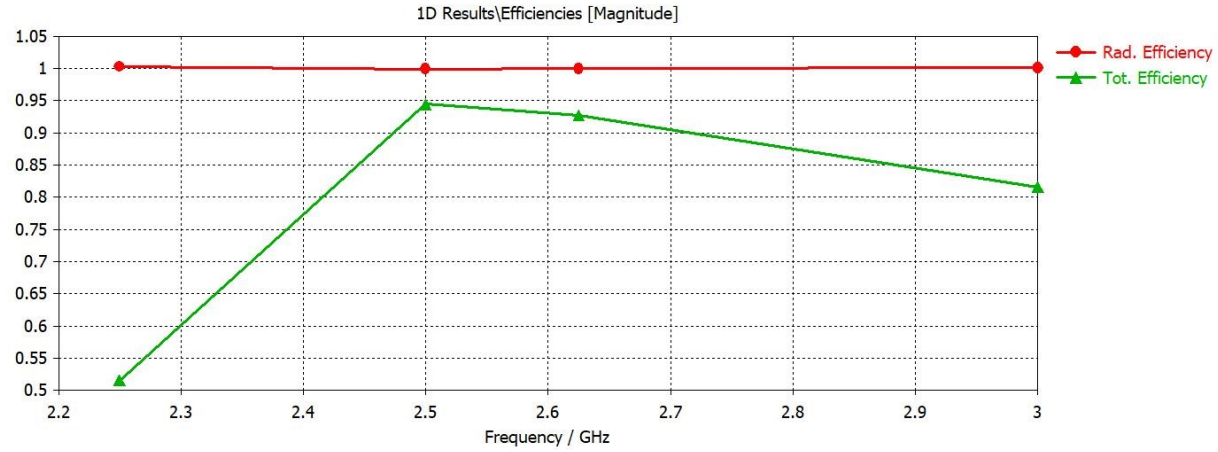

Figure. 4.18. Radiation and total efficiency of 6x6 phased array within the desired frequency band B7 (2.5 GHz - 2.7 GHz) with linear scale, 1 being 100 % efficiency.

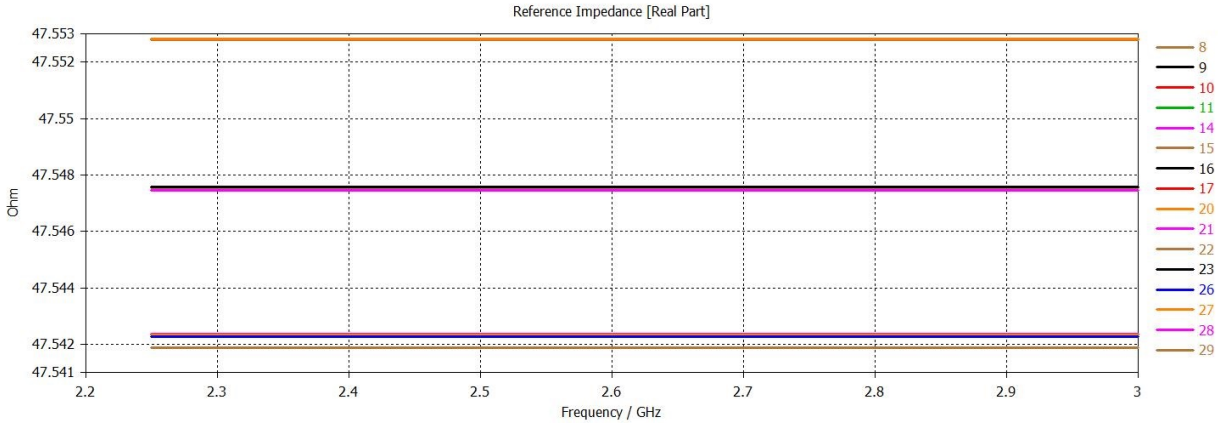

Figure. 4.19. 6x6 phased array 16 active element impedance representation. All the active elements' impedance values (load impedance) are close to 50Ω (input impedance)

efficiency of the antenna to convert the electric signal into the electromagnetic wave with a low loss. This array antenna radiation efficiency does not include the loss (in the form of heat) of the metallic elements, hence showing almost 100% efficiency. The efficiency results are calculated from S_{11} parameter values of the array antenna. The shared ground plane set up for 6x6 phased array on ϕ, $\theta = 0°$ beam direction showed acceptable parametric results according to the requirements listed in **Table 3.1**. Thus, in the next subsection, the experiment to beamform in ϕ, $\theta = 5°$ direction is carried out and the corresponding results are analyzed.

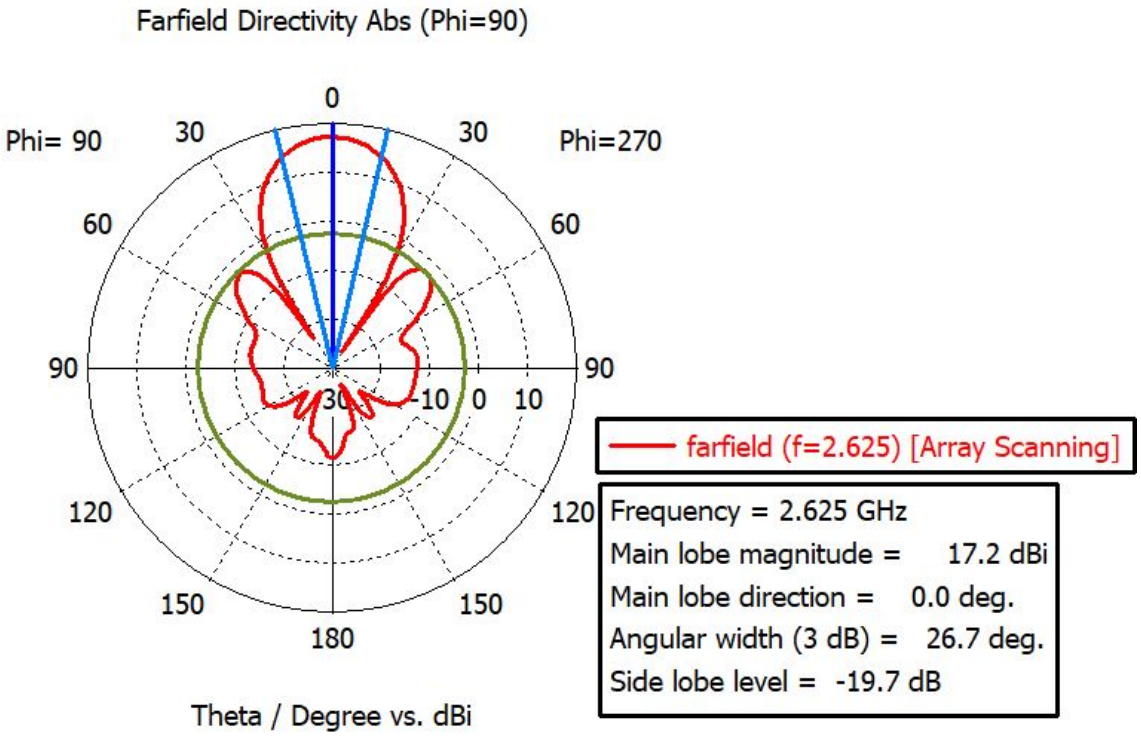

Figure. 4.20. 2D radiation pattern of 6x6 phased array antenna with the blue lines representing the angular width of the beam at 2.625 GHz frequency (Downlink Frequency of B7 band [7]). The main beam directed to 0° with magnitude achieves 17.2 dBi and a side lobe level of -19.7 dB

4.3.2 ϕ , θ = 5° beamforming simulation results and analysis

This subsection focuses on the result of impedance bandwidth, surface wave flow and radiation pattern of the phased array antenna whose main beam is steered to 5° in both ϕ and θ planes. To achieve the beam steering, each element on the array is assigned a specific phase value.

The antenna bandwidth plot shows that the 11^{th} element S_{11} parameter has a value higher than -10 dB within the frequency range of interest. The reason for this could be the signal phase distribution versus surface current flow. When the port is fed, the signal has a particular phase. This phase may lead to either a constructive or a destructive wave. In this case, it could be acting destructively with other surface wave flows generated by neighboring elements around it; an example thereof is visible in **Figure 4.23** where the 11^{th} element has a low intensity surface wave flow compared to the result of the ϕ , θ= 0° case (Figure 4.17).

The radiation pattern does not show exactly 5° in the azimuth and elevation planes due

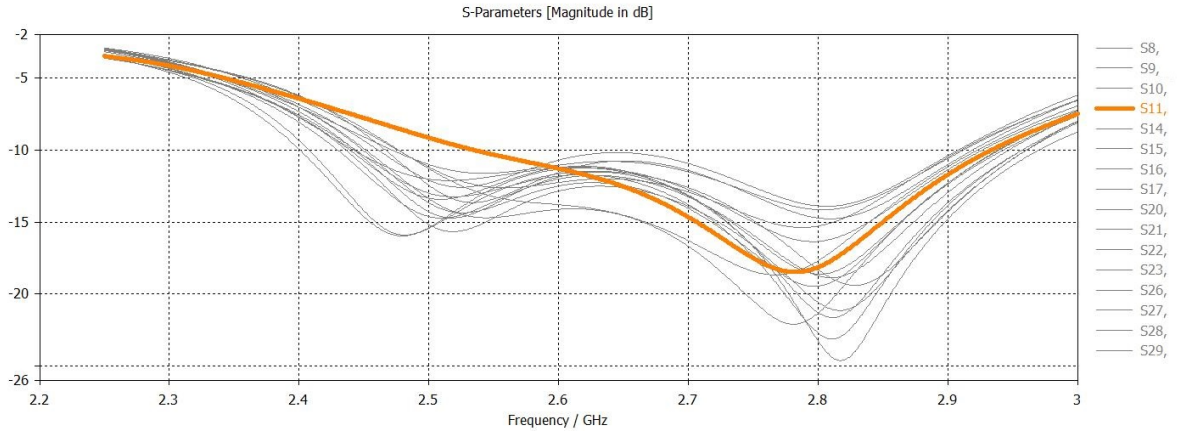

Figure. 4.21. Reflection coefficients of the (6x6 phased array) 16 elements with shared ground plane between the elements with 5° beamforming.

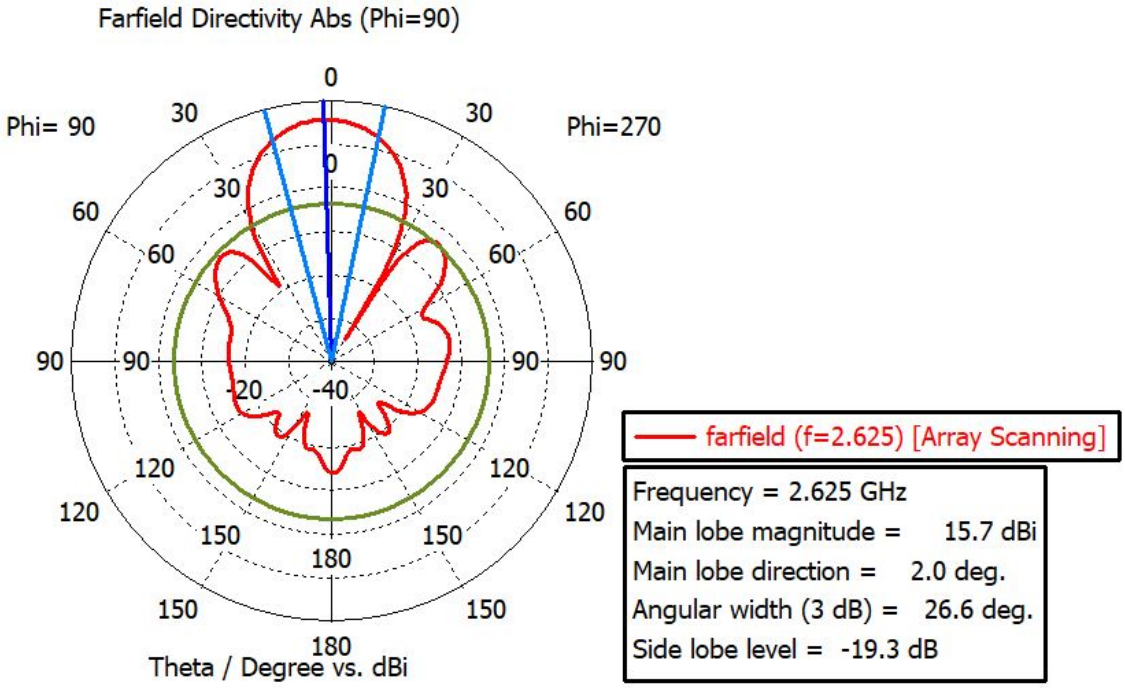

Figure. 4.22. 2D radiation pattern of 6x6 phased array antenna with blue lines representing the angular width of the beam at 2.625 GHz frequency (Downlink Frequency of B7 band [7]). The main beam is directed to 2° even though 5° beamforming phase distribution is applied for each element. The achieved magnitude is 15.7 dBi and the side lobe level is -19.3 dB

to the high side lobe levels, as **Figure 4.22** shows. High side lobe levels can be caused by the surface current on the array set up which impacts each element's radiation pattern. The initial phased array designs with both 4x4 and 6x6 constellations do not satisfy the

requirements listed in Table 3.1. Therefore, additional experiments have been carried out and are reported in the next chapter; these experiments deal with modifications to the phased array designs in terms of isolated ground plane and metallic slot usage between the elements.

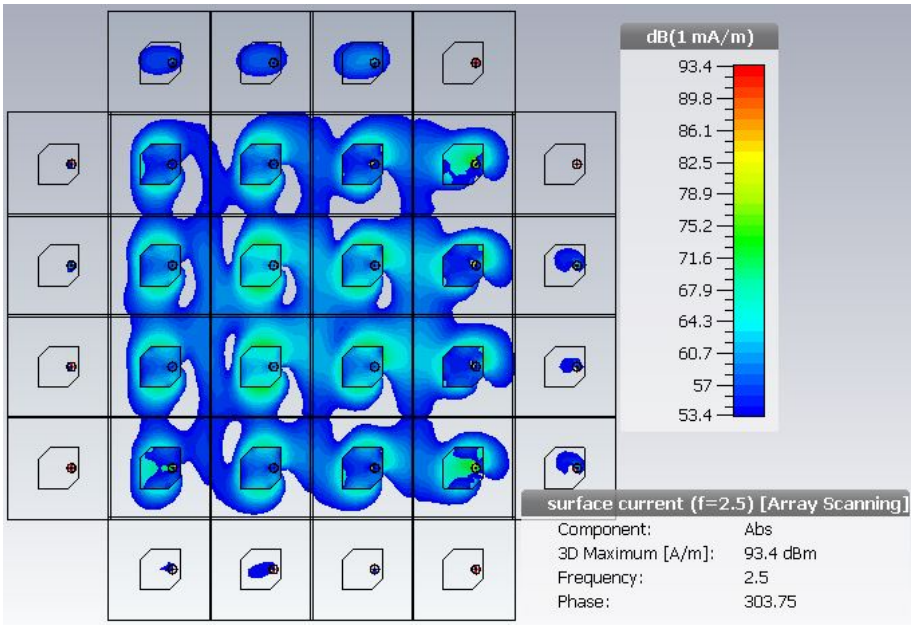

Figure. 4.23. Surface wave flow of common ground plane array antenna on 2.5 GHz frequency with ϕ , $\theta = 5°$ beamforming. The array has 36 elements but only 16 of them are active; the other ones are passive but surface wave still leaks to passive elements.

Chapter 5

Optimized Results: Antenna Design, Simulation and Analysis

The phased array design using the shared ground plane affected the antenna bandwidth when the beam is steered to ϕ, θ = 5°. In this chapter, experiments are continued on 4x4 and 6x6 phased arrays in two sections with each section presenting selected experimental iterations. The first section describes a 4x4 phased array design, initially with shared ground; in a second design, metallic slots are placed between elements to reduce the surface wave flow impact on antenna bandwidth when the main beam direction changes. The same procedure is followed for the 6x6 phased array. Within these iterations, the dimensions of the patch element (and thus of the array antenna) are adjusted to improve the performance and meet the requirements. Each parameter dimension that has been modified from an original value is experimentally swept with different values to meet the requirements. These sweep results are not presented in the thesis but only the final values that lead to the desired results are analysed.

In this chapter, the same criterion applies to show the parametric and performance metrics simulation results as was listed in Chapter 4. Mutual coupling results are shown only for 4x4 phased array set up and the diversity gain and correlation results are presented for a 6x6 phased array having isolated ground planes with slots inserted between elements since this is the best result achieved so far with beamforming ϕ, θ = 20°. Within the iterations, the beam is steered with steps 0°,10° and 20° if the initial criteria are within the limit.

5.1 4x4 (16 active elements) Phased Array Antenna Simulation Results and Analysis

This section includes two subsections where the individual ground plane usage per element and slots placement between elements are presented. Each subsection consists of the patch element dimension updated table. The ground plane size is mentioned in Table 5.1 and each ground plane is separated 7.5 mm apart from each other. Various spacing distances are practised with CST Studio; 7.5 mm separation resulted in a better mutual coupling.

5.1.1 Individual Ground Plane 4x4 (16 active elements) Phased Array Antenna Simulation Results

In this subsection, the only change in the design from the shared ground plane case is the isolation of the ground plane. Therefore, the same dimensions mentioned in **Table 4.1** are maintained with only one additional parameter which is the size of the individual ground planes for each element.

Parameters	**Performance Indicator Value**
Ground plane	54 mm

Table 5.1: Square truncated capacitively pin-fed circularly polarized patch antenna element's single ground plane size (each element ground plane size is identical).

The reflection coefficient results in **Figure 5.1** share a similar pattern with the results of the 4x4 phased array that used the shared ground plane. As explained in Section 4.2, the "Taylor" excitation applies relatively low amplitude level to the elements located at the edge. However, **Figure 5.1** shows that only the 1^{st} and 16^{th} elements have different pattern and values of S_{11} parameter, while the 4^{th} and 13^{th} elements have the same amplitude values as the 1^{st} and 16^{th} elements. H-plane represents the magnetic component of electromagnetic wave has distribution on x,y and z-axises. The reason for having various patterns between the 1^{st}, 16^{th} and the 4^{th}, 13^{th} elements could be the maximum radiation on x-axis component of H-plane, as shown in **Figure 5.5**. Magnetic field distribution that collectively creates the radiation on H-plane for the 4^{th} and 13^{th} elements does not seem to be equally assigned.

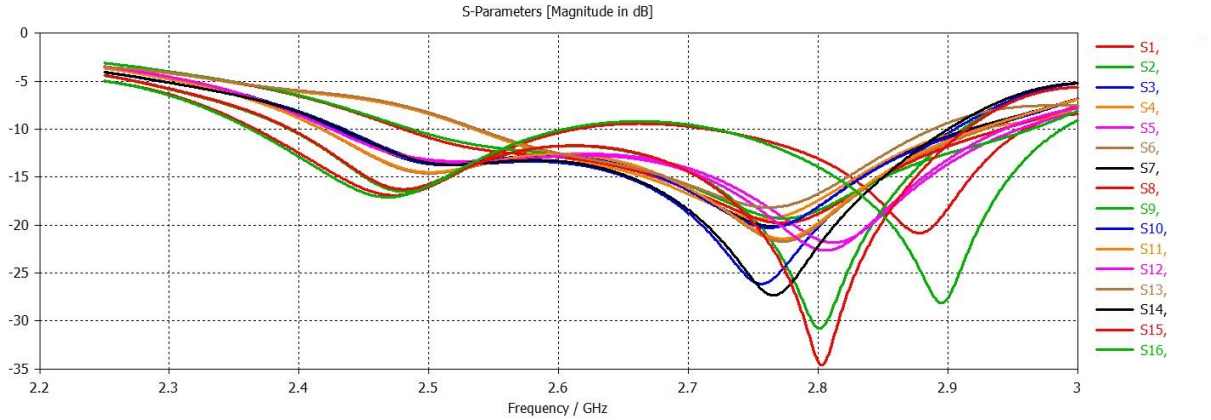

Figure. 5.1. Simulation results of the reflection coefficients for the 4x4 phased array with individual ground planes (16 active elements) on ϕ, θ= 0° beamforming with 2.5 GHz-2.7 GHz frequency range that of interest.

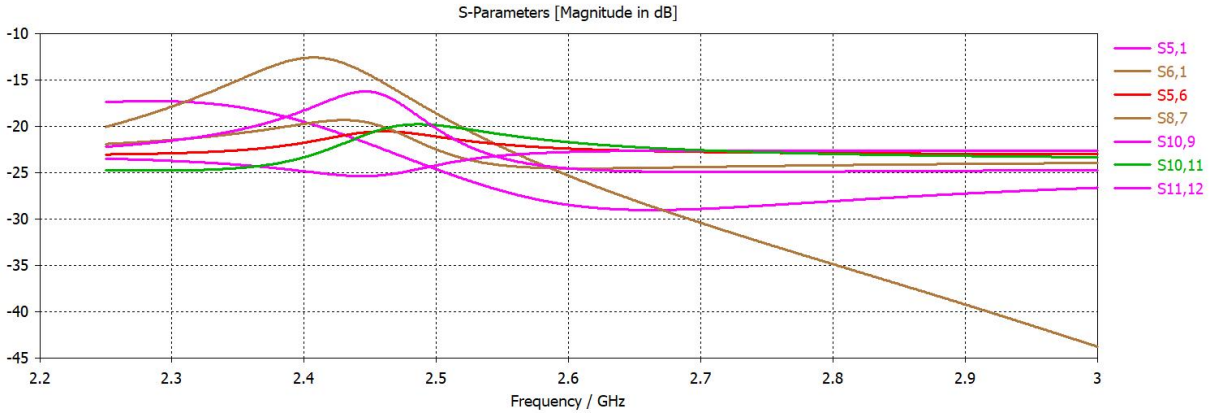

Figure. 5.2. Mutual coupling results for 8 elements within 2.5 GHz - 2.7 GHz. The coupling levels are high between the the 5^{th}, 6^{th}, 7^{th}, 8^{th}, 9^{th}, 10^{th}, 11^{th}, and 12^{th} elements because of high amplitude levels; on the other hand, the impact of the 5^{th} and 6^{th} elements is low on the 1^{st} element

The mutual coupling results presented in **Figure 5.2** meet the requirement listed in Table 3.1 which is -20 dB for each element within 2.5 GHz -2.7 GHz, except the coupling between the 6^{th} and 1^{st} elements. The coupling level decreases drastically between the 6^{th} and 1^{st} elements after ca. 2.53 GHz. This could be due to an unoptimized element dimensions which can be corrected with a few parametric sweeps. The results presented in **Figure 5.2** show a ca. 4 dB improvement as compared to that of Section 4.2. The surface wave flow via the substrate and the ground plane have been decreased with isolated ground plane since the media through which surface current flows gets separated, as shown in

Figure 5.4.

Even though using an isolated ground plane implementation improves some of the parameters results in the 4x4 phased array, it does not lead to the desired reflection coefficient values within the B7 frequency band. Therefore, in the next subsection, the array antenna with metallic slots placed between the elements is presented and analyzed.

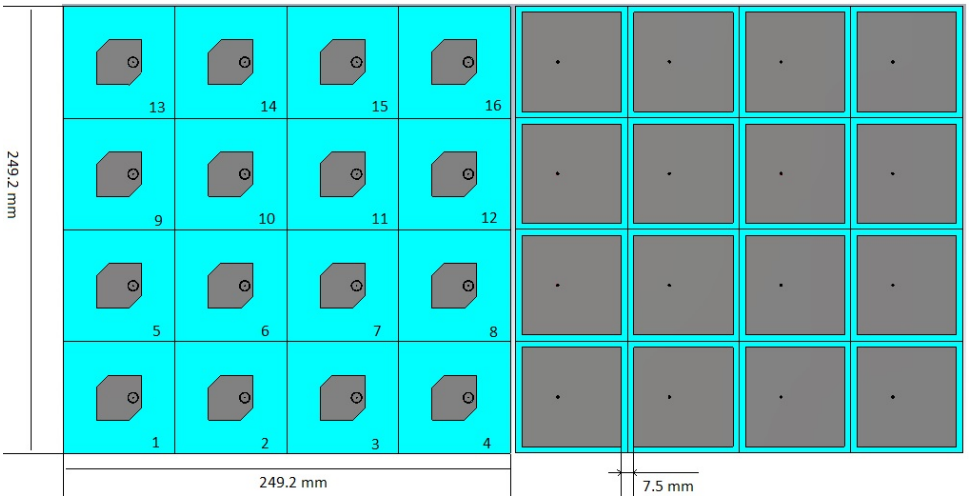

Figure. 5.3. Front and back views of 4x4 (16 active elements) phased array antenna with only active elements numbering on an isolated ground plane

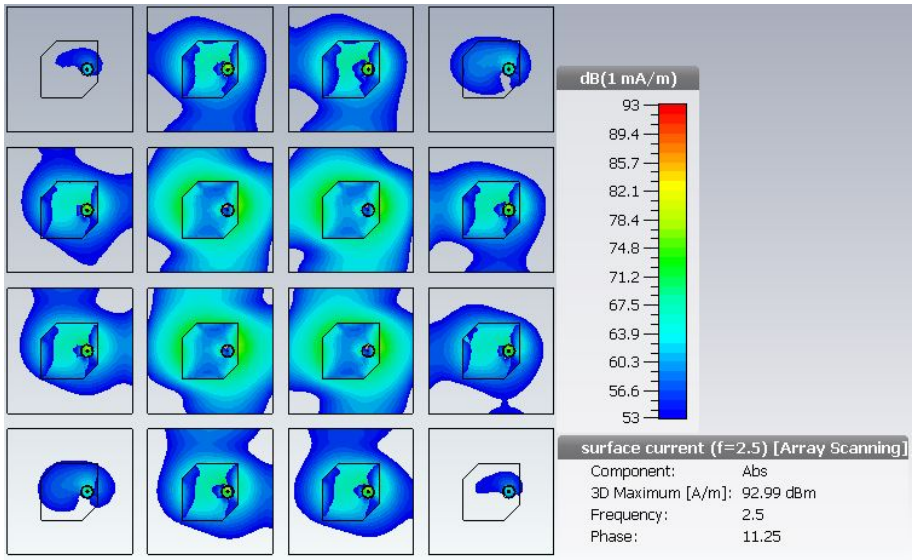

Figure. 5.4. Surface wave flow between individual ground planes used in the 16 element array antenna on 2.5 GHZ frequency with 0° beamforming.

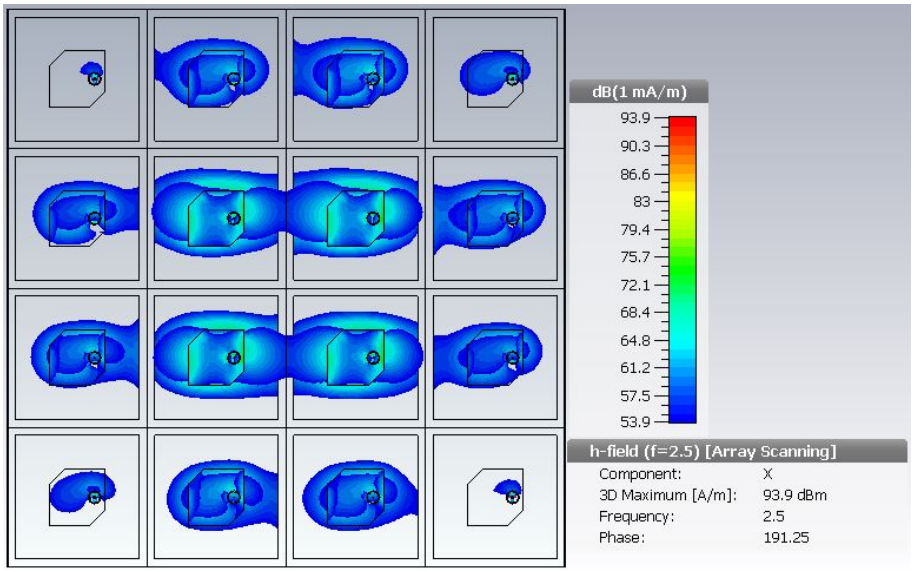

Figure. 5.5. 4x4 phased array radiation on x-axis component of H-plane. The magnetic field distribution is low on the 4^{th} and 13^{th} elements compared to the 1^{st} and 16^{th} elements

5.1.2 Individual Ground Plane with Metallic Slots 4x4 (16 active elements) Phased Array Antenna Simulation Results

This subsection presents the 4x4 phased array antenna design with the patch element whose dimensions are modified from the original one. Besides that, metallic slots are placed on the bottom and the right-hand side of the patch element (**Figure 5.6**), hence when the array is constructed from multiple elements, they would be shielded with slots from all sides, except the elements at the border line, as shown in **Figure 5.7**. The reason to insert metallic slots between the elements is to reduce the impact of surface current on the impedance of the array antenna versus the scanning angle. Within this subsection, only S_{11} and mutual coupling results are presented since the reflection coefficient results did not meet the requirements to proceed with the analyses for other metrics.

The patch element that was mentioned in Chapter 4 is taken as a reference but selected parameters are adjusted. All the mentioned parameters in Table 5.2 are optimized and they have been swept with various values to identify the value that would satisfy the requirements set in Table 3.1. The individual swept values of the parameters and their outcome are not presented in this thesis due to limited space to present each iteration.

The reflection coefficient results in **Figure 5.8** shows the curves below -10 dB from 2.4 GHz up to 2.84 GHz. However, the B7 frequencies are 2.5 GHz - 2.7 GHz and the

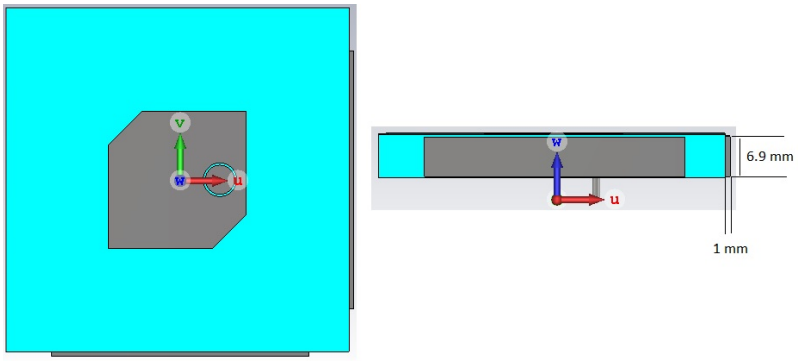

Figure. 5.6. A Patch antenna element with metallic slots on the bottom as well as on the right-hand side, which is used to make a 6x6 array antenna

Parameter Name	Value	Description
L	23.96 mm	Patch width
W	23.96 mm	Patch length
L_t	5.8 mm	Truncation length
H	7.5 mm	Substrate height
GND	54 mm	Ground Plane
$Slot_L$	26 mm	Slot length
$Slot_W$	1 mm	Slot width
$Slot_H$	6.9 mm	Slot Height

Table 5.2: Square truncated capacitively pin-fed circularly polarized patch antenna element's modified parameters

impedance bandwidth of the array antenna is shifted by ca. 40 MHz. This is because of the patch element length and width change from 0.202λ to 0.19λ. Thus, the smaller the size, the higher the impedance bandwidth.

The mutual coupling between elements is improved by 3 dB starting from 2.54 GHz to 2.7 GHz, as shown in **Figure 5.9**, when slots are inserted between the elements as compared to only using individual ground plane (**Figure 5.2**). As was mentioned, the patch length and width size change shifts the desired results. Since the 4x4 phased array antenna does not result in satisfying the requirements, the 6x6 phased array with individual ground plane and metallic slots is presented and analyzed in the next section.

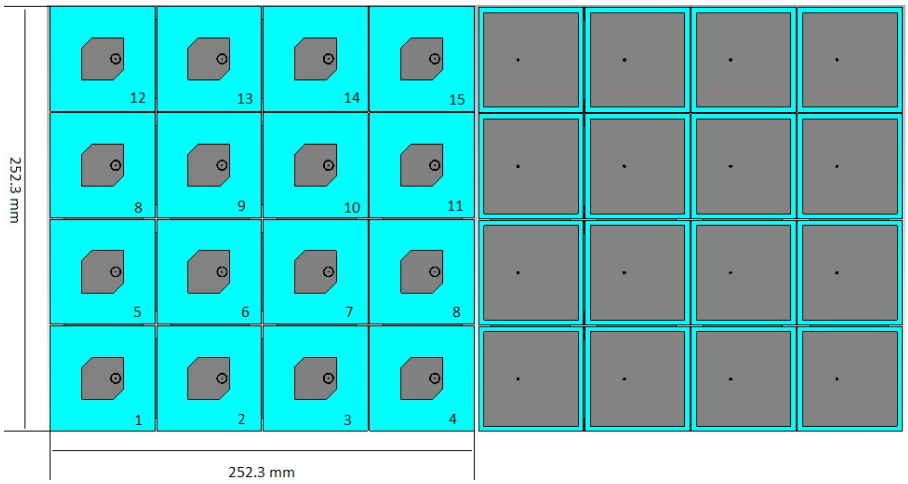

Figure. 5.7. 4x4 isolated ground plane phased array antenna with metallic slots placed between the elements.

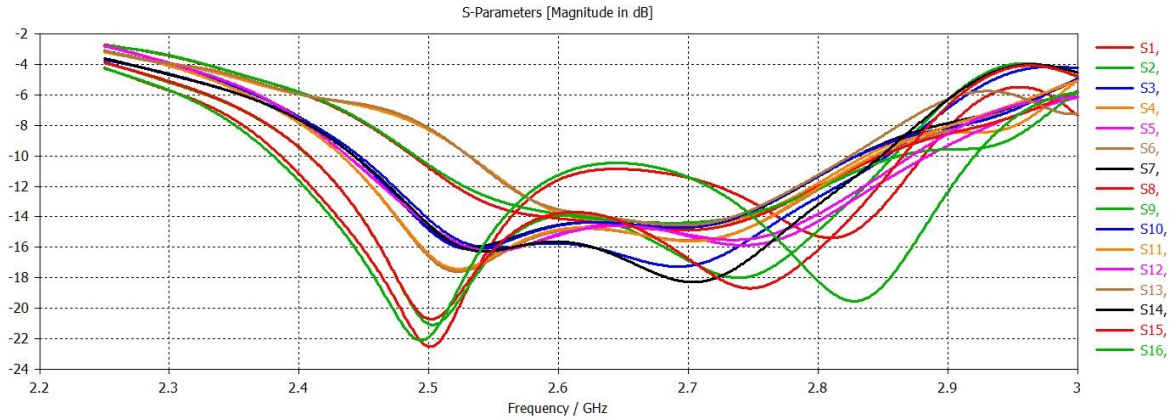

Figure. 5.8. 4x4 isolated ground plane phased array antenna reflection coefficients of each element. The frequency range of interest is 2.5 GHz - 2.7 GHz

5.2 6x6 (16 active elements) Phased Array Antenna Simulation Results

This section presents the simulation results and analyses for the 6x6 phased array in two subsections wherein the first subsection presents the isolated ground plane array antenna and the second subsection presents the isolated ground plane array with metallic slots inserted. The patch element dimension modifications including the ground plane size and separation are the same as in **Section 5.1**.

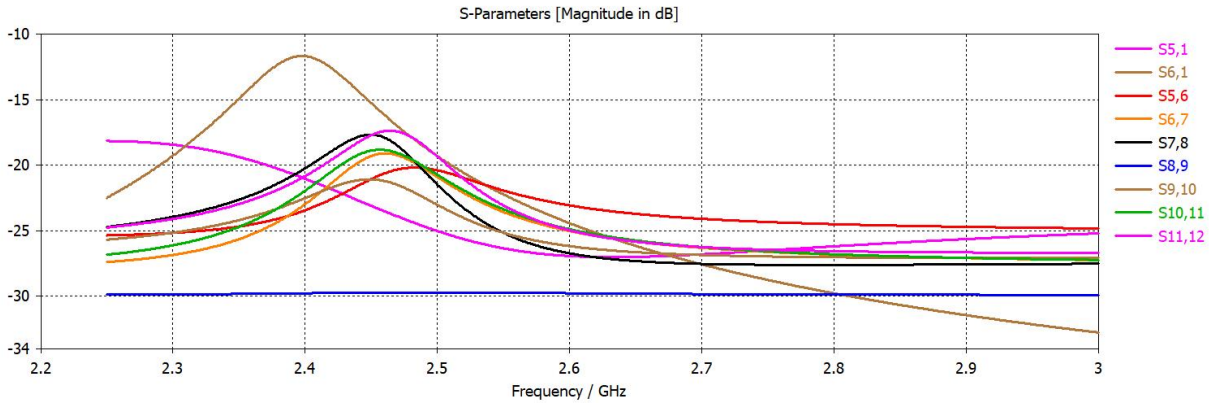

Figure. 5.9. Mutual coupling results for 8 elements. The coupling levels are high between the 5^{th}, 6^{th}, 7^{th}, 8^{th}, 9^{th}, 10^{th}, 11^{th}, and 12^{th} elements because of high amplitude levels; on the other hand, the impact of the 5^{th} and 6^{th} elements is low on the 1^{st} element within 2.5 GHz - 2.7 GHz

5.2.1 Individual Ground Plane 6x6 (16 active elements) Phased Array Antenna Simulation Results

The dimensions listed in Table 4.1 remains but only ground plane size being 54 mm and beamforming in ϕ , θ= 0°,5° and 10° are performed. Since all required parameters passed for 0° beamforming, the same parameters were simulated for ϕ , θ =5° beamforming with only S_{11} parameters and the radiation pattern results discussed. As S_{11} parameter result passes in ϕ , θ =5° beamforming, without further results, the antenna is simulated for ϕ , θ = 10° beamforming where only S_{11} parameters and the radiation pattern results are presented due to degraded results of reflection coefficients as it is the first criterion to analyze further.

Parameters	**Performance Indicators**
Ground plane	54 mm
Beamforming, ϕ , θ	0°,5°,10°

Table 5.3: Square truncated capacitively pin-fed circularly polarized patch antenna element single ground plane size (each element individual ground plane's size is identical).

The bandwidth of the array antenna is at an acceptable level within 2.5 GHz - 2.7 GHz when ϕ, θ= 0° beamforming is performed. As was mentioned in Chapter 4, the amplitude levels for the edge elements are high enough to follow a similar pattern in

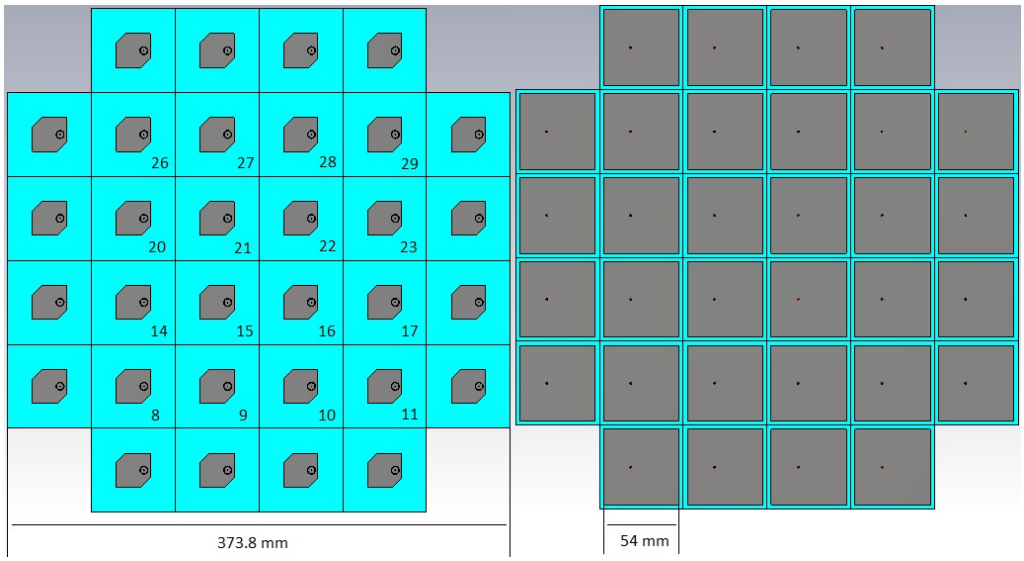

Figure. 5.10. Front and back view of 6x6 (16 active elements) phased array antenna with only active elements numbering and isolated ground planes

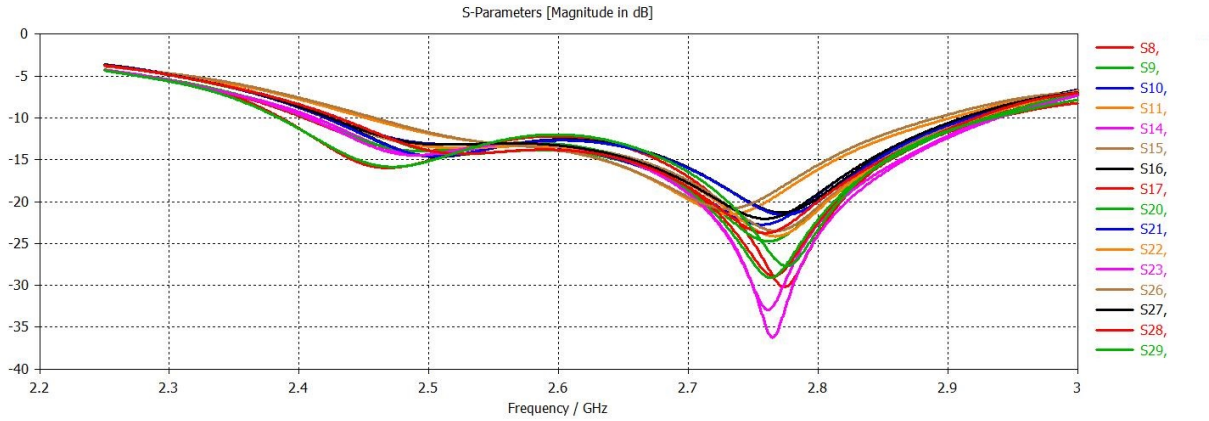

Figure. 5.11. Reflection coefficients of (6x6 phased array) 16 elements with individual ground planes on each patch with ϕ , θ= 0° beamforming.

reflection coefficient result. Individual ground plane usage for 6x6 phased array increased the bandwidth of the array antenna to about 40 MHz in Uplink frequencies, making it 2.460 GHz as shown in **Figure 5.12**, while the design with shared ground plane discussed in Section 4.3 has a operational bandwidth starting exactly from 2.5 GHz not leaving any room for unexpected antenna interference or other RF phenomena. Moreover, the reflection coefficient results within the B7 frequencies showed 1.5 dB improvement for the isolated ground plane case throughout the band as compared to the shared ground plane design (**Figure 4.15**).

The surface wave simulation results shown in **Figure 5.22** show that individual ground

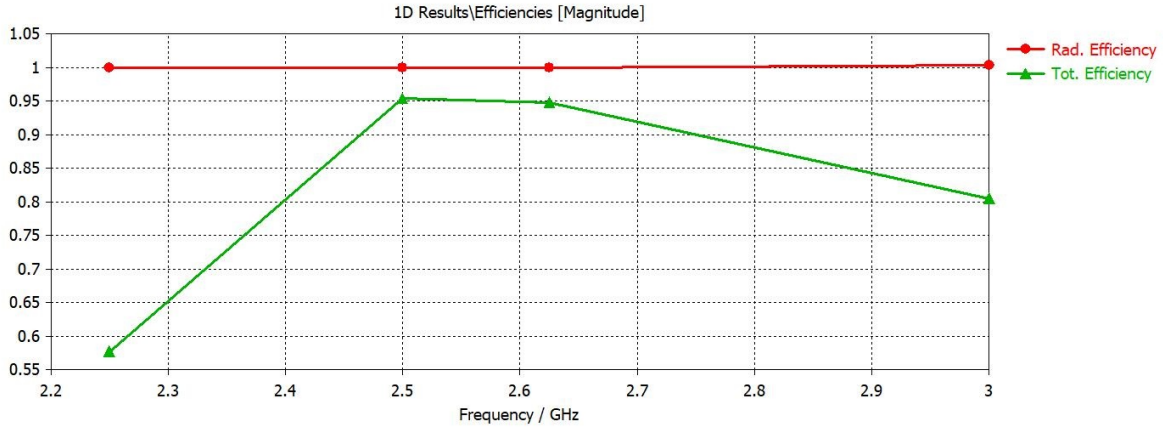

Figure. 5.12. Radiation and total efficiency of 6x6 phased array within desired frequency band B7 (2.5 GHz - 2.7 GHz) with linear scale, 1 being 100 % efficiency

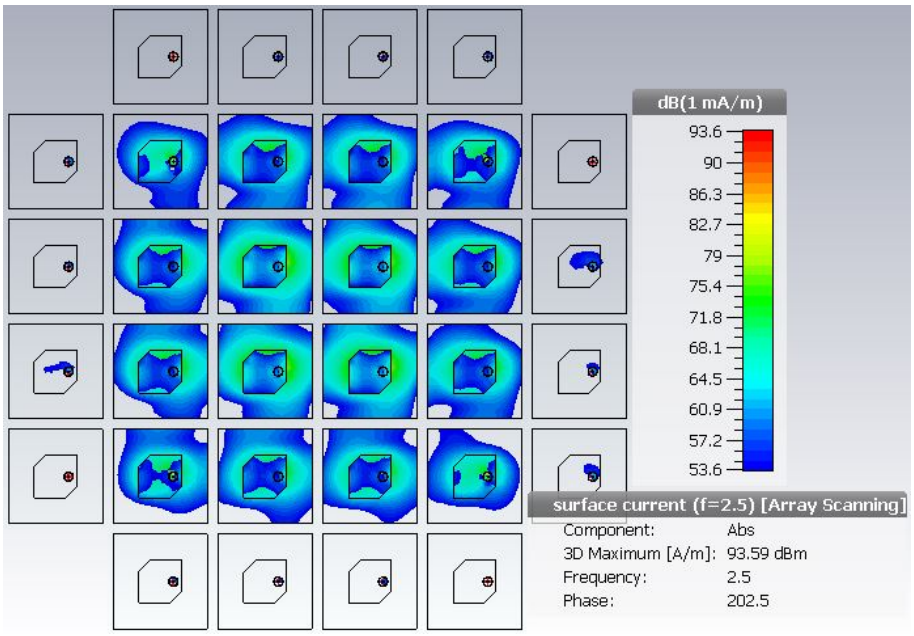

Figure. 5.13. A surface wave flow of isolated ground plane array antenna on 2.5 GHz frequency with ϕ , θ= 0° beamforming. The array has 36 elements but only 16 of them are active, the rest is passive but surface wave leaks to passive elements too.

plane usage decreased the surface current leakage to passive elements compared to the case where the same ground plane was used for all elements (Section 4.3). It makes the bandwidth of antenna more robust against the main beam scanning angle.

The radiation pattern results show a back lobe level increase for the individual ground plane design as compared to the shared ground plane case, as shown in Figure 5.14. As was mentioned in **Section 4.2**, the ground plane reflects the radiation energy going back

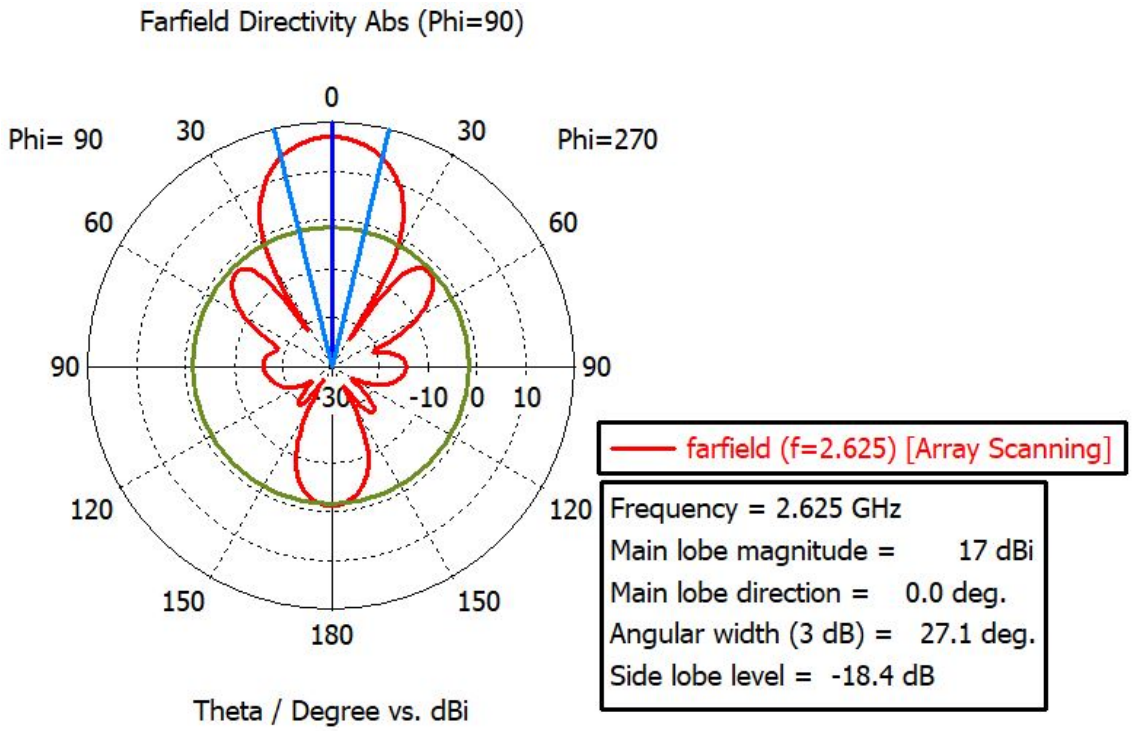

Figure. 5.14. 2D radiation pattern of 6x6 phased array antenna with blue lines representing the angular width of the beam at 2.625 GHz frequency (Downlink Frequency of B7 band [7]). The phase distribution is applied for each element to steer the beam in ϕ, θ= 0° direction. The achieved main lobe magnitude is 17 dBi and the side lobe levels are -18.4 dB

to forwards. The 7.5 mm separated ground planes are not able to reflect the full energy forwards hence, some of the energy goes backwards forming a back lobe. However, the back lobe and side lobe levels are 30 dB down from the main lobe magnitude, which means the energy radiating to an undesired direction is significantly low.

The simulation results for ϕ, θ= 5° beamforming satisfy the requirements listed in Table 3.1. Therefore, as a next step, the same phased array antenna is simulated with ϕ, θ= 5° beamforming and its results are analyzed in the next subsection.

ϕ , θ = 5° beamforming simulation results

The dimensions of the antenna are not adjusted but only 5° beamformed in ϕ and θ planes. The surface wave and efficiency plots are not depicted, only S_{11} and radiation pattern are shown since other simulation results are identical as in the ϕ, θ=0° beamforming design.

The reflection coefficient results for each element show a -10 db level in the 2.5 GHz

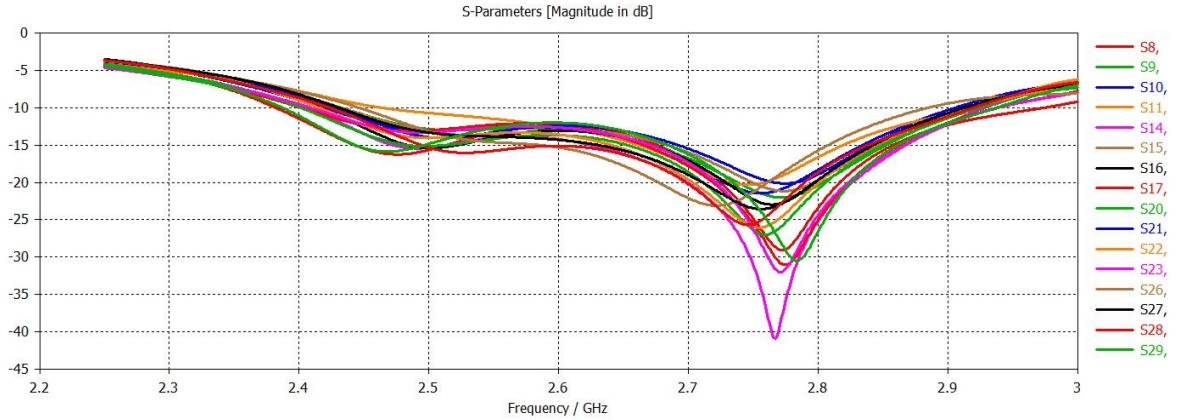

Figure. 5.15. Reflection coefficients of (6x6 phased array) 16 elements with individual ground planes on each patch with ϕ , θ= 5° beamforming.

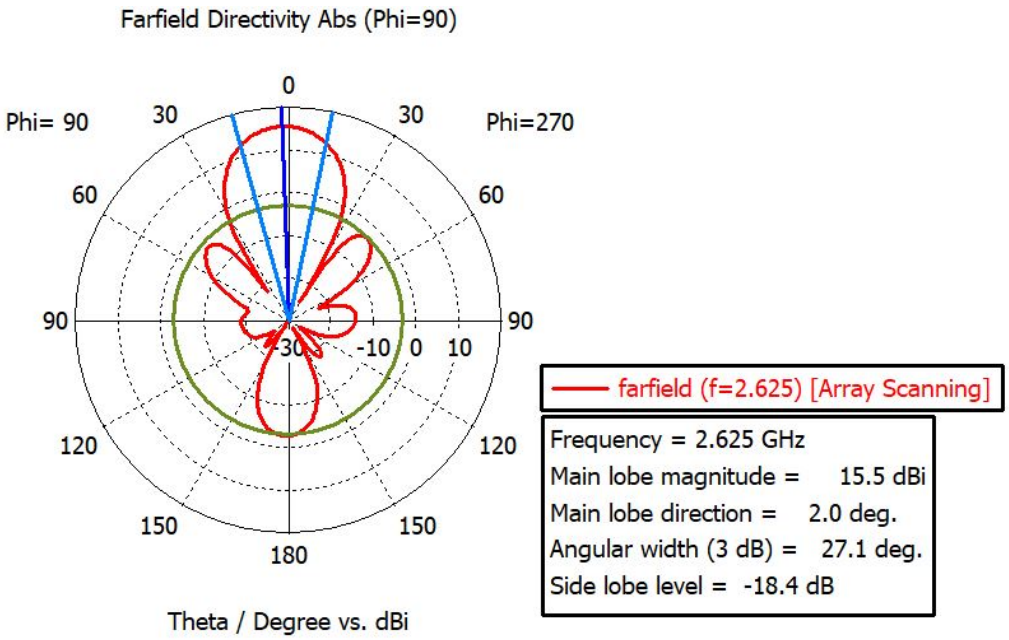

Figure. 5.16. 2D radiation pattern of 6x6 phased array antenna at 2.625 GHz frequency (Downlink Frequency of B7 band [7]). The main beam is directed to 2° even though 5° beamforming phase distribution is applied for each element. The achieved magnitude is 15.5 dBi and the side lobe level is -18.4 dB

- 2.7 GHz frequency range, which satisfies the requirement. The radiation pattern of the array antenna shows the main beam steered to ϕ , θ= 2° even though the elements are assigned phase values that should have produced ϕ , θ= 10° beamforming. The reason for not achieving exactly ϕ , θ = 10° could be the back lobe appearance where some part of the energy is not reflected back from the ground plane forwards, which contributes to the

beamforming. The simulation results in this subsection meet the requirements hence, as a next step, the same phased array is simulated to form a beam in ϕ , θ = 10° and its results are analysed in the next subsection.

ϕ , θ = 10° beamforming simulation results

In this subsection where the phased array main beam is steered to ϕ , θ = 10°, only S_{11} parameters and radiation pattern are shown since array antenna reflection coefficients are not below -10 dB as required to further analyze the other results.

The reflection coefficients results in **Figure 5.17** show that all elements are below -10 dB except 11^{th} element within B7 frequency range. A similar case has been witnessed in Section 4.3.2 and it was explained that phased distribution for each element may result in interacting with surface wave constructively or destructively. The 11^{th} element located at the edge may be interacting destructively with radiations around it such that the impedance curve is affected undesirably.

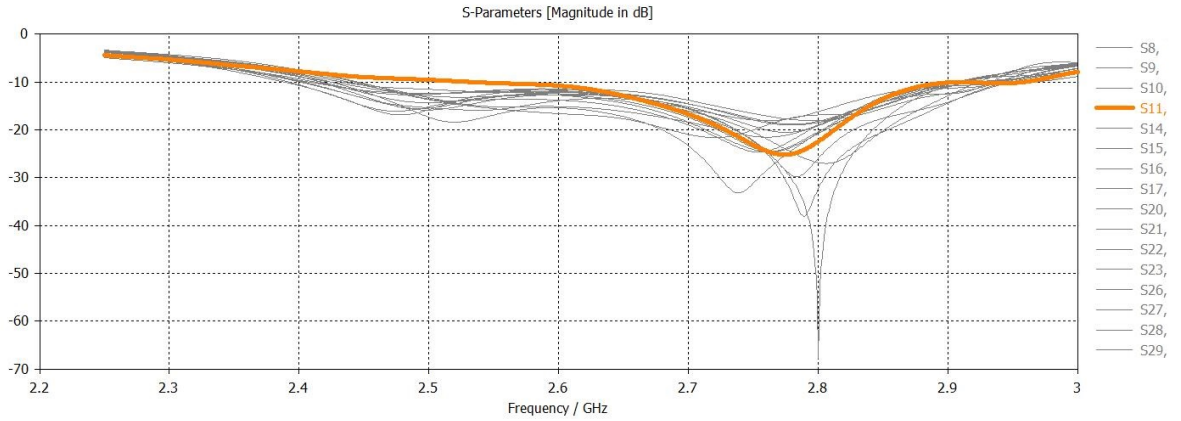

Figure. 5.17. Reflection coefficients of (6x6 phased array) 16 elements with individual ground planes on each patch with ϕ , θ = 10° beamforming.

The radiation pattern shows high back lobe with side lobes 30 dB down from the main beam magnitude. Elements of the phased array are assigned signals with particular phases that should have produced 10° beamforming in ϕ and θ planes but 4° beamforming is accomplished. The same explanation which was presented for the ϕ, θ = 5° simulation results and analysis (**Section 5.2.1**), applies to the result discussed here.

The highest scan angle achieved so far that keeps the antenna bandwidth below -10 dB is 5° in ϕ and θ planes. In order to increase the scanning angle while keeping the reflection

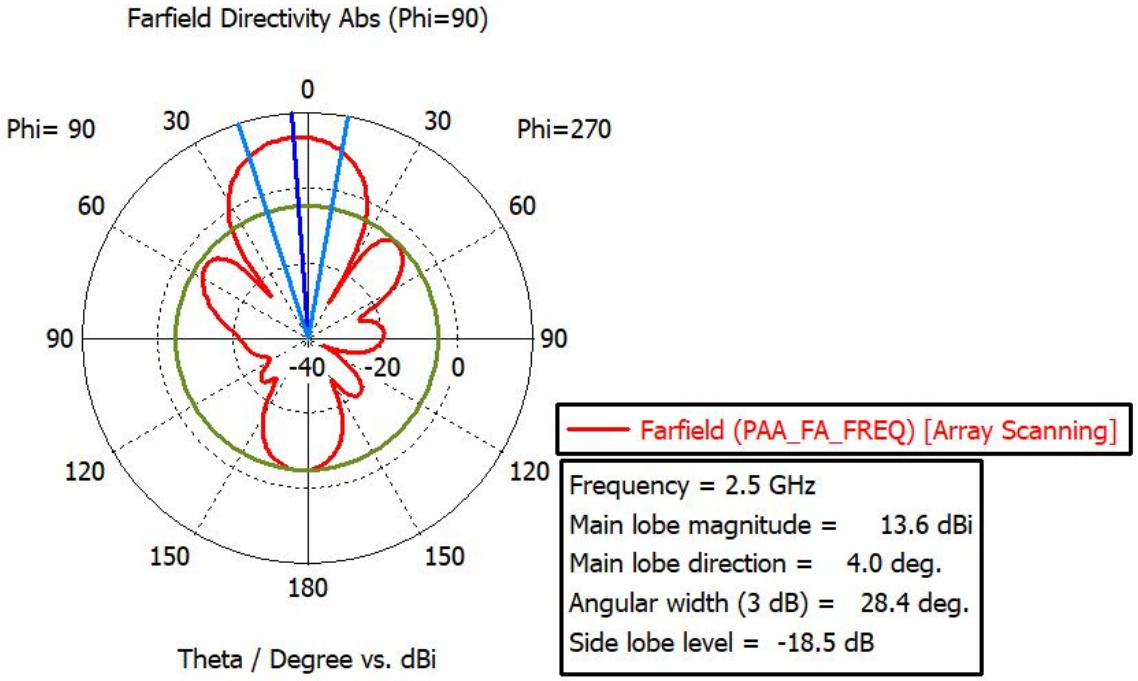

Figure. 5.18. 2D radiation pattern of 6x6 phased array antenna at 2.625 GHz frequency (Downlink Frequency of the B7 band [7]). The main beam is directed to 4° even though 10° beamforming phase distribution is applied for each element. The achieved magnitude is 13.6 dBi and the side lobe level is -18.5 dB

coefficients below -10 dB, the array antenna design is changed by adding metallic slots between the elements, which is discussed in the next subsection.

5.2.2 Individual Ground Plane with Metallic Slots 6x6 (16 active elements) Phased Array Antenna Simulation Results

This subsection presents the simulation results and analysis for the 6x6 phased array antenna whose patch element parameters are modified according to Table5.2 and where metallic slots are inserted to reduce the surface current effect on the antenna bandwidth change when the main beam is steered. Each parameter in Table5.2 is modified for that particular purpose. When a 6x6 isolated ground plane phased array antenna was simulated without any parameter change but with slots placed, the reflection coefficient results decreased abruptly as the main beam is steered to ϕ, θ = 10° direction. Therefore, the following dimensions are changed for that particular purpose:

- The patch element [46]: The size of the patch radiator element has a direct relation

with the resonance frequency where the small patch element moves the resonance to a higher frequency while the opposite is true when the size is large [46]. In this section, the patch element size is decreased to 23.96 mm from 24.3 mm as the reflection coefficients were out of the B7 frequency.

- The truncation length [46]: The resonant frequencies of the two modes may be separated further by increasing the truncation length. In this design, the truncation length is decreased from 6.6 mm to 5.8 mm to bring two resonant frequencies closer since they were too far apart a shown in **Figure 5.19**

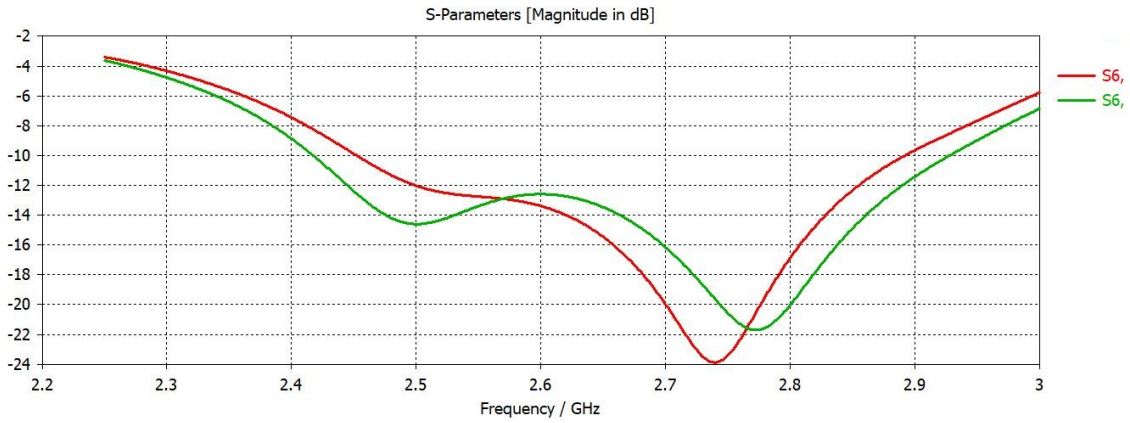

Figure. 5.19. Single patch element truncation length impact on reflection coefficient [46]. The green line shows 6.6 mm and the red line 5.8 mm truncation length. The two resonant frequencies are brought closer with truncation length = 5.8 mm (Red curve)

- The Substrate height [46]: Increasing the substrate height results in lowering the reflection coefficient down (more than -10 dB) with slight bandwidth reduction. Since the decreased truncation length brings two resonant frequencies together, increased substrate height from 7.2 mm to 7.5 mm keeps them under -10 dB in higher scanning angles.

- Metallic slots: Slot dimensions are chosen by sweeping various values and identifying the optimal one. The length of the slot is slightly longer than the size of the radiating element as it acts as a surface wave reflector. The width is chosen to be 1 mm since widening the slot length increases the separation between elements, leading to poor beamforming. The height value is optimized to the substrate height. The slots are inserted from the bottom and from the right side of the patch to reduce the surface wave flow impact from the elements around it.

This subsection presents simulation results for beamforming in ϕ , $\theta = 10°$ and ϕ, $\theta = 20°$ directions since 0° and 5° beamforming results are identical to the ones presented in Section 5.2.1. Analysis of the reflection coefficients, surface wave flow, and radiation pattern results are provided for both 10° and 20° beamforming. However, MIMO performance indicators such as correlation coefficient and diversity gain results are presented for the array antenna design that supports ϕ , θ =20° beamforming.

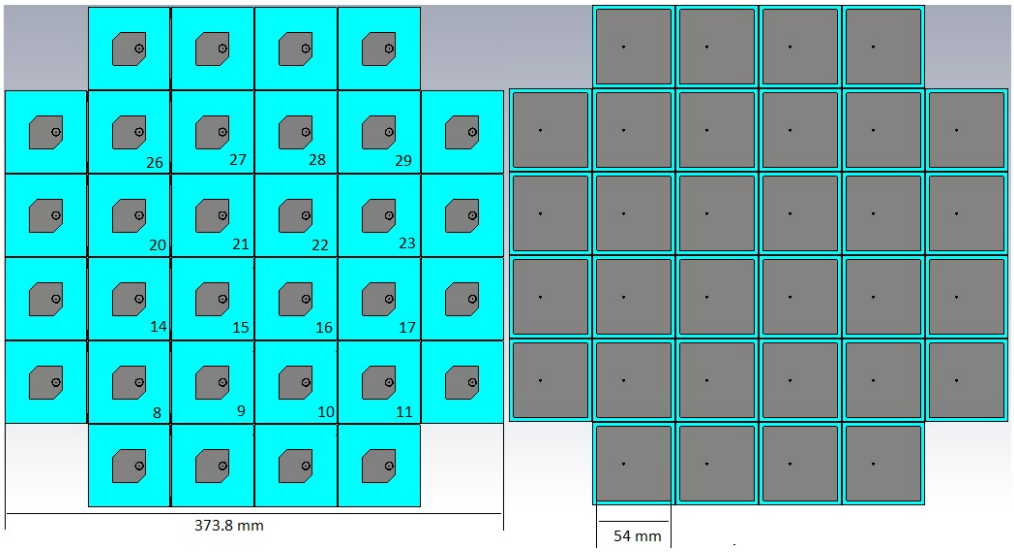

Figure. 5.20. 6x6 phased array antenna with isolated ground plane as well as with metallic slots between elements

ϕ , θ =10° beamforming simulation results

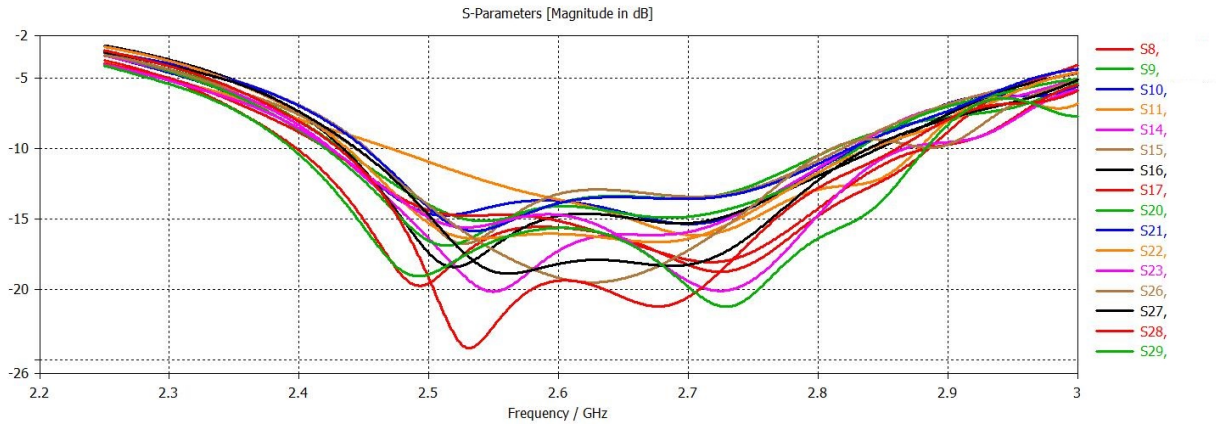

Figure. 5.21. Reflection coefficients of 6x6 phased array antenna with isolated ground plane as well as with metallic slots between elements on ϕ , θ = 10° beamforming

Reflection coefficients of each element are in below -10 dB in the B7 frequency range (2.5 GHz- 2.7 GHz). The metallic slots reduce the surface current flow between phased array antenna elements by absorbing and reflecting the radiation that reaches the slots. Metallic slots are inserted only between active elements, not among active and passive ones, since slot placement between passive and active elements showed a negative effect on the radiation pattern.

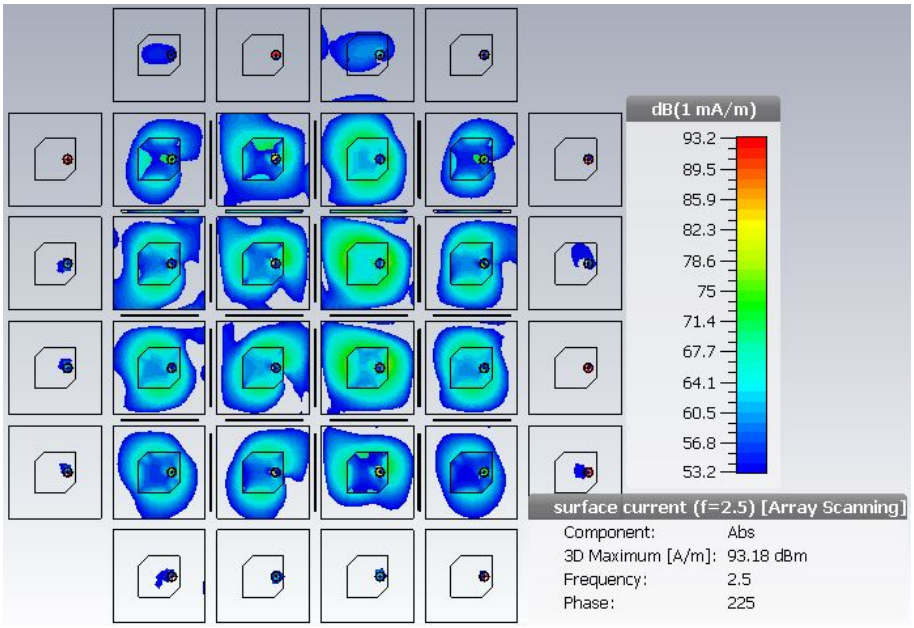

Figure. 5.22. A surface wave flow of isolated ground plane array antenna with metallic slots placed between elements on 2.5 GHz frequency with ϕ , θ= 10° beamforming. The array has 36 elements but only 16 of them are active, the rest is passive but surface wave leaks to passive elements too.

The radiation pattern shows the main beam direction ϕ , θ = 4° even if each element is assigned phase values that would steer the main beam to ϕ , θ = 10°. One of the reasons is using an isolated ground plane that does not reflect the full energy forwards but because of gaps; some part of the energy radiates back as discussed in the previous section. Another reason is the impact of the metallic slots on the radiation pattern. When each element is radiated, some part of the energy is absorbed and radiated by the slot as well. Thus, the created pattern is a combination of the actual radiating element pattern with metallic slot added. **Figure 5.23** shows back lobe and side lobe levels below 30 dB from the main beam magnitude but the radiation pattern overall has imperfections because of the metallic slots.

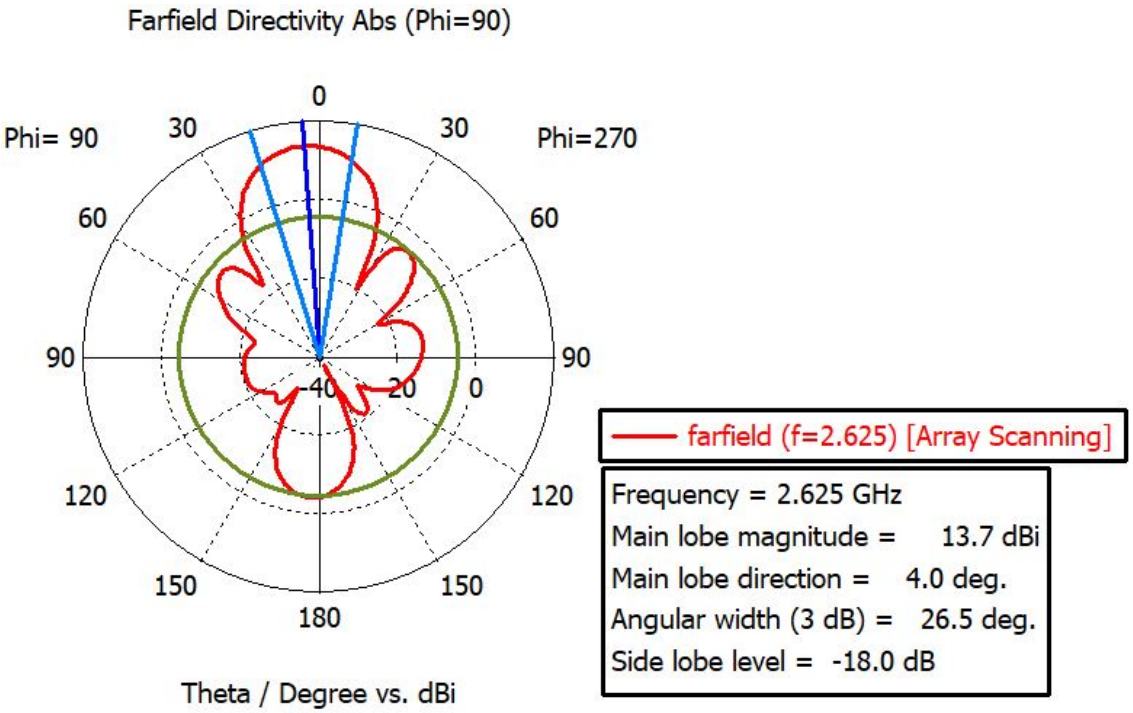

Figure. 5.23. 2D radiation pattern of 6x6 phased array antenna at 2.625 GHz frequency (Downlink Frequency of the B7 band [7]). The main beam is directed to 4° even though 10° beamforming phase distribution is applied for each element. The achieved main lobe magnitude is 13.7 dBi and the side lobe level is -18.0 dB

ϕ , θ =20° beamforming simulation results

Within this subsection, surface wave flow analysis is not presented since ϕ, θ = 20° beamforming showed identical result as in **Figure 5.22**. However, reflection coefficient results, radiation pattern, as well as correlation coefficient and diversity gain are presented and analyzed.

The reflection coefficients are below -10 dB from 2.5 GHz to 2.7 GHz frequency but pretty close to the limit. The curves do not follow a similar pattern as shown in **Figure 5.24** due to the heterogeneous phase distribution that results in constructive and destructive behaviour in radiation.

The radiation pattern shows that side lobes are close to the main beam. It was mentioned previously that such imperfection is caused by the metallic slots and their effect on the radiation pattern can be reduced by decreasing the slot width. When the slot width is small, energy is reflected and only some portion is radiated from the slot. The **Figure 5.25** shows the main lobe magnitude 11.2 dBi with sidelobe levels -17.9 dB. "Taylor"

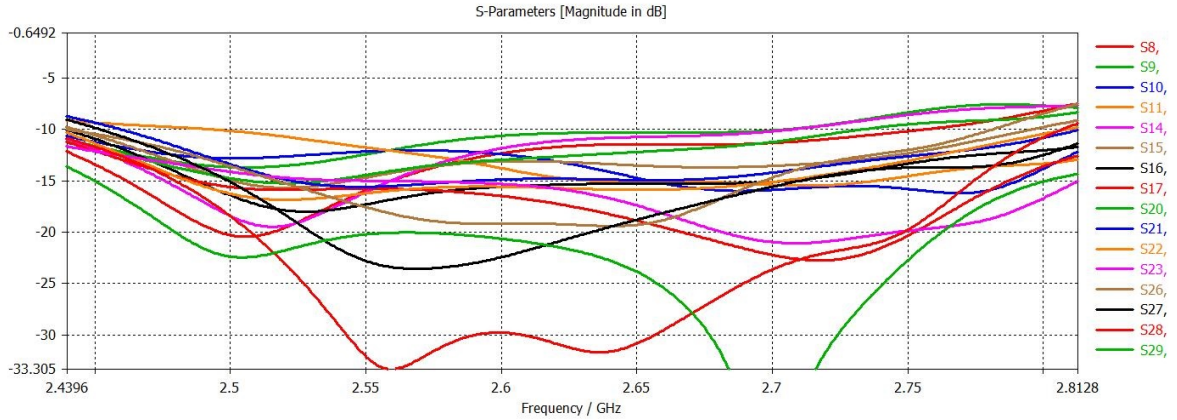

Figure. 5.24. Reflection coefficients of 6x6 phased array antenna with isolated ground plane as well as with metallic slots between elements on ϕ, θ = 20° beamforming

distribution should have kept the side lobes levels 30 dB less from the main lobe but the actual difference is 29.1 dB when the side lobe level (-17.9 dB) is subtracted from the main lobe magnitude (11.2 dBi).

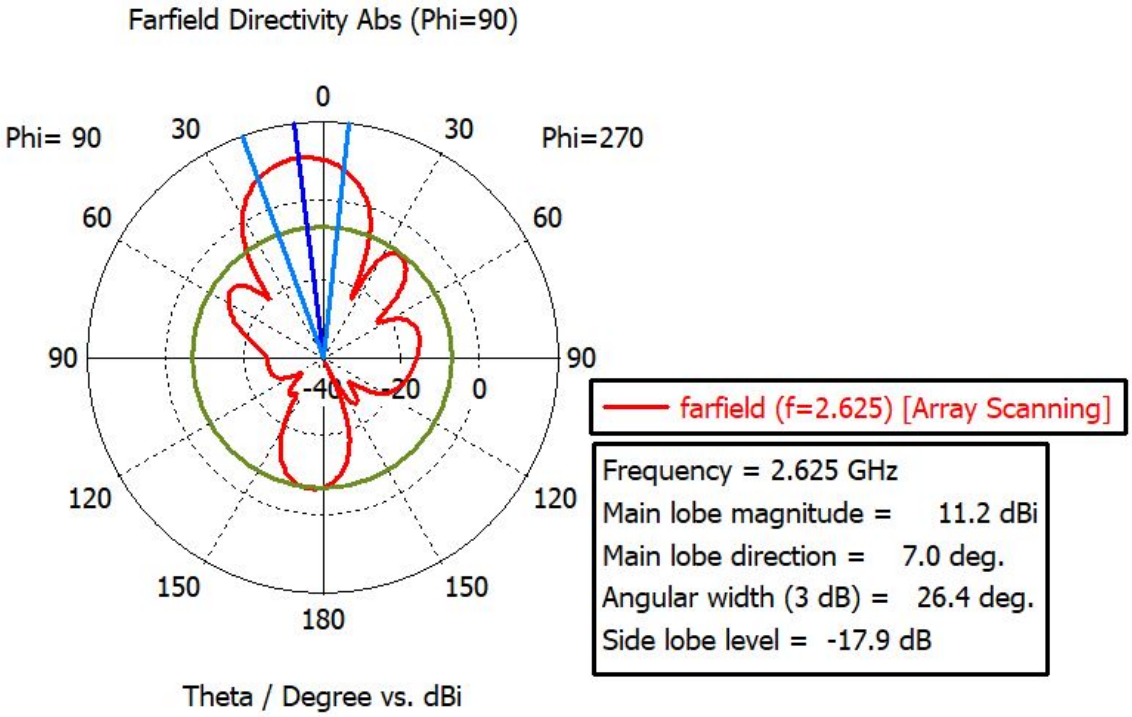

Figure. 5.25. 2D radiation pattern of 6x6 phased array antenna at 2.625 GHz frequency (Downlink Frequency of the B7 band [7]). The main beam is directed to 7° even though 20° beamforming phase distribution is applied for each element. The achieved main lobe magnitude is 11.2 dBi and the side lobe level is -17.9 dB

The best result achieved in beamforming using the phased array antenna is in ϕ, θ

= 20° direction. Therefore, MIMO performance metric results are also discussed in this subsection. It has been stated that MIMO performance of the antenna is in a higher priority than beamforming, hence beamforming analyses are finished and MIMO performance metrics are discussed further.

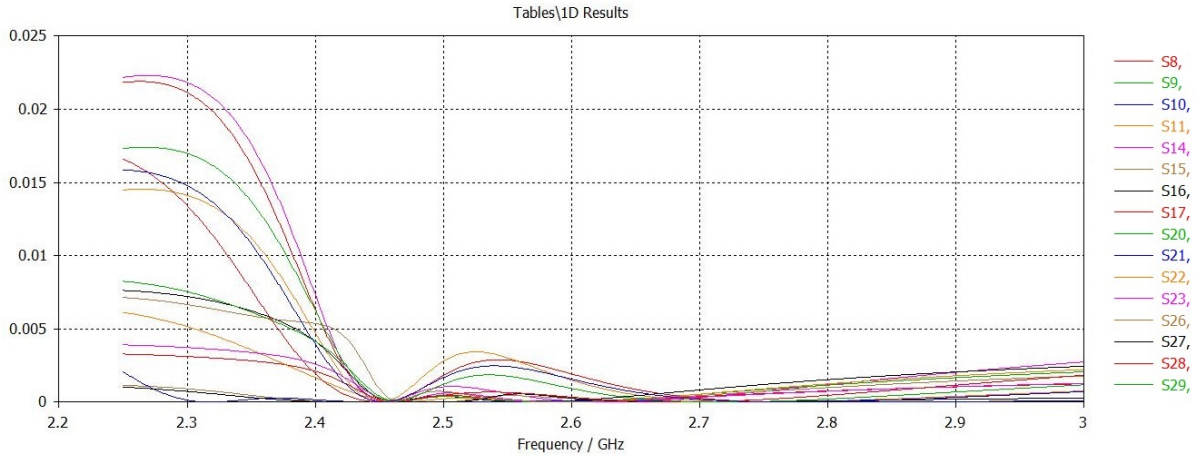

Figure. 5.26. Correlation coefficients of 16 elements in 6x6 phased array antenna with isolated ground and the metallic slots between elements

Correlation coefficient and diversity gain are discussed; the requirements were set in Section 3.3 in Chapter 3. The correlation coefficient can be calculated using the reflection coefficient of each element or using the radiation pattern of the elements. When it is calculated using the radiation pattern, the correlation coefficient shows how much each element's radiation pattern affect each other when they are excitepd at the same time. The result in **Figure 5.26** is produced by CST studio using S_{11} parameters of 16 elements and all the 16 curves are below the correlation limit (0.3) listed in Table 3.1. This shows low correlation of the signals in each antenna element and high enough diversity gain.

Since MIMO systems implement multiple antennas, transmitting the same signal from each antenna element (spatial multiplexing) increases the reliability of the entire system as well as the diversity of the received signal. The diversity gain of the phased array antenna which is calculated from the correlation coefficient results and is shown in **Figure 5.27**. It is calculated considering the correlation between one element and neighboring elements on the right and the top. For instance, the diversity gain of the 8^{th} element is calculated between the 9^{th} element and the 14^{th} element separately to identify to what extent they are diverse. The result achieved is a bit below (i.e. 9.98 dB) than the limit

(10 dB in Table 3.1) between the 16^{th} and the 22^{th} elements from 2.5 GHz-2.6 GHz frequency range. However, the rest of the elements show 10 dB diversity gain in the B7 frequency range. It should be noted that the higher the diversity gain , the better the spatial multiplexing performance. For the phased array antenna investigated in this thesis with 16 active elements, the radiating element spacing is set to 0.75λ to support both beamforming (0.5λ required) and MIMO (1λ) technology. 10 dB diversity gain may be improved further by increasing the distance between the elements but leads to degradation of beamforming performance. When the elements are spaced 1λ away, diversity gain increased to about 12 dB, which is a marginal rise from what is achieved (10 dB). Therefore, 10 dB diversity gain is deemed as the golden balancing point to benefit greatly from MIMO and beamforming features for this phased array antenna.

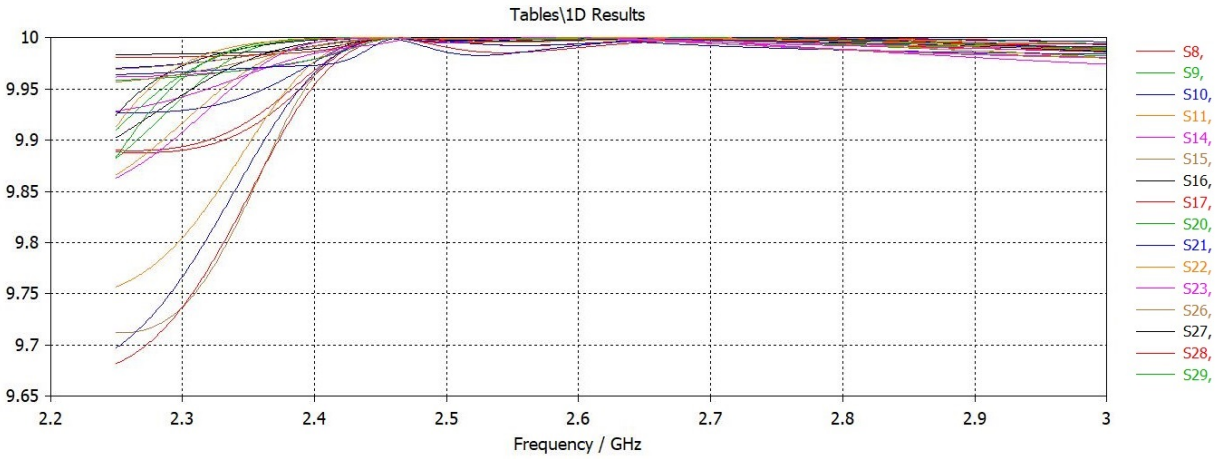

Figure. 5.27. Diversity gain of 16 elements in 6x6 phased array antenna with isolated ground and the metallic slots between elements. The graph shows diversity between one element and neighboring elements on the right and the top.

Chapter 6

Conclusion and Future Work

The introduction of 5G technology with its low latency and high data rate exchange using MIMO and beamforming is enabling new applications such as drone and robot delivery by means of remote control over the base station. Therefore, compact, highly efficient and low cost but high-performance array antennas need to be optimized for such drones and delivery robots.

The goal of this thesis was to design circularly polarized phased array antenna for drones and delivery robots (A well know example of such delivery robots are that of Starship [10]) that would support MIMO and beamforming technologies on 5G network. However, MIMO and beamforming technologies require different element spacing in the array set. Hence, before designing and simulating the proposed antenna, previous research in the field has been analyzed, and the requirements for the phased array antenna have been set.

The main goal of the thesis was to propose a 6x6 (16 active elements) phased array antenna. To work towards this, two types of phased array antennas 4x4 (16 active elements) and 6x6 (16 active elements) have been designed from the microstrip patch element that was obtained from "Antenna Magus" library [46]. Initially, both 4x4 (16 active elements) and 6x6 (16 active elements) arrays have been simulated without any adjustments to the antenna element obtained from "Antenna Magus" where elements had the same ground plane. Using the shared ground plane set up did not produce results that satisfy the requirements; for the 4x4 (16 active elements) array and 6x6 (16 active elements) array, the reflection coefficients were below -10 dB only on 0° beamforming. The reason being high mutual coupling because of the shared ground plane.

To try overcoming this, the following modifications were introduced to the antenna element:

- Shared ground plane is isolated for each element to reduce the mutual coupling between elements;
- Metallic slots are placed between elements to decrease the effect of surface current flow on array antenna operational bandwidth when the beam is steered.

To reduce the mutual coupling between the elements, ground plane has been isolated for each radiating element and beamforming reached practically 2° on ϕ and θ planes even though 5° beamforming phase values were assigned to each element on 6x6 (16 active elements) phased array antenna. It is because of the isolated ground plane that does not reflect all the applied energy forwards but passes the radiation backwards through the gaps between ground planes, creating a back lobe. 4x4 (16 active elements) array antenna did not pass any requirements for the parameters listed in Table 3.1 on both shared ground plane and the isolated ground plane set up due to high amplitude variation between centre elements and edge elements when "Taylor" excitation is used. Thus, making 6x6 array where 16 elements are passive and 16 of them are active resulted in less difference on amplitude levels between the elements.

To combat surface current that negatively impact antenna bandwidth when the main beam is steered to various directions, metallic slots were placed between elements to mitigate the surface current influence. Consequently, the beam steering of 7° on ϕ and θ planes was achieved even though 20° beamforming phase values were assigned to each element on 6x6 (16 active elements) phased array antenna while 4x4 phased array had reflection coefficients below -10 dB only on 0° beamforming and did not show acceptable results for further angle beamformation. The beamforming performance did not meet the requirements of steering the beam to +45 to -45° but MIMO performance satisfied the requirements set in Chapter 3 (Table 3.1) with correlation coefficients being below 0.005 and diversity gain results being above than 9.95 dB within B7 frequency (2.5 GHz -2.7 GHz) range.

6.1 The future steps

The investigations that have been conducted and the design proposals on 6x6 phased array antenna can be applied to any other kind of phased array antenna. These design iterations pave the way for further improvements of phased array antenna designs, especially the ones that are designed to operate under sub-6 GHz spectrum bands. The current phased array works on B7 uplink and downlink, but as a next step, different antenna element with the wider operational band will be investigated based on the proposals provided in this thesis. In the future following steps are planed to perform

- Choose wideband (to cover all LTE and 5G sub-6 GHz bands) patch antenna even though the radiation directivity is poor;
- Implement the metallic slot placement between elements to reduce the surface wave;
- Use two types of substrate materials on top of each other with two different permittivity values where the radiating element resonates the passive radiator creating a capacitive coupling as shown in Figure 6.1;
- Print the designed antenna and carry out RF measurements with Vector Network Analyzer (VNA) and using a signal generator to generate CW signal for every port with calculated phase values.

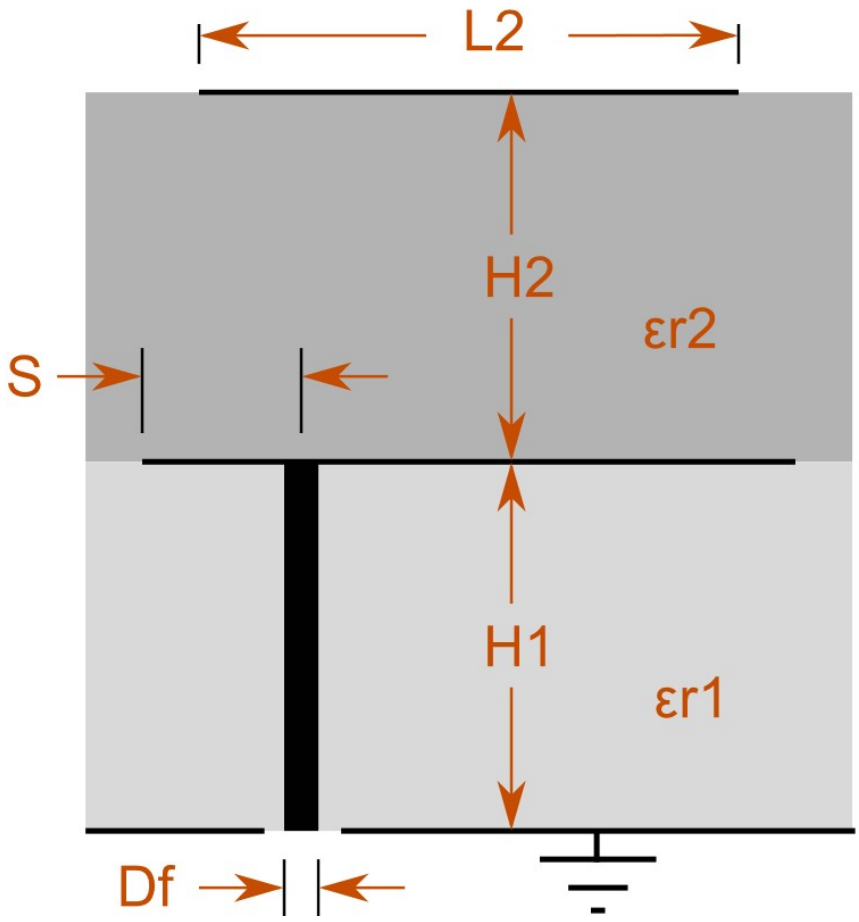

Figure. 6.1. Stacked pin-fed rectangular patch antenna element. The active radiating element is placed between two different substrate materials. There is a passive radiator which is capacitively coupled to the active radiator

Bibliography

[1] The Statistics Portal. (2018). Number of mobile phone users worldwide from 2015 to 2020 (in billions), [Online]. Available: https://www.statista.com/statistics/274774/forecast-of-mobile-%5C%5Cphone-users-worldwide/ (visited on 05/04/2019).

[2] J. Wannstrom. (2013). 3GPP LTE-Advanced, [Online]. Available: http://www.3gpp.org/technologies/keywords-acronyms/97-lte-advanced (visited on 05/04/2019).

[3] Dr.Amitabha Ghosh, "Massive MIMO for the New Radio Overview and Performance," *IEEE 5G Summit*, pp.1–15, Jun.2017.

[4] Mohammad S. Sharawi, Eva Rajo-Iglesias. (2016). MIMO antennas, [Online]. Available: https://www.igi-global.com/chapter/mimo-antennas/136613 (visited on 05/04/2019).

[5] Erik Dahlman, Stefan Parkvall, Johan Sköld, *4G LTE/LTE-Advanced for Mobile Broadband*. pp.57-59, Press Elsevier, Number of Pages= 447,ISBN = 978-0-12-385489-6, Mar.2011.

[6] Chuck Powell, "Technical Analysis:Beamforming vs. MIMO Antennas," *Radio Frequency Systems*, pp.10–17, Mar.2014.

[7] Wikipedia. (2019). 5G NR frequency bands, [Online]. Available: https://en.wikipedia.org/wiki/5GNRfrequencybands (visited on 05/04/2019).

[8] Kathrein. (2019). 5G Antenna Modules, [Online]. Available: https://www.kathrein.com/ (visited on 05/04/2019).

[9] Millimeter Wave Antennas. (2019). 5g antenna modules, [Online]. Available: https://www.miwv.com/millimeter-wave-products/antenna-products (visited on 05/04/2019).

[10] Starship. (2019). Starship Delivery Robots, [Online]. Available: https://www.starship.xyz/company/ (visited on 05/04/2019).

[11] Qorvo. (2017). How Carrier Networks Will Enable 5G, [Online]. Available: https://www.qorvo.com/design-hub/blog/how-carrier-networks-will-enable-5g (visited on 05/04/2019).

[12] 5G Forum, "5G Vision, Requirements and Enabling Technologies," in *5G White Paper :5G Vision, Requirements and Enabling Technologies*, Republic of Korea, Oct. 2016, pp. 2–12.

[13] Takashi Yanagi, Toru Fukasawa, Hiroaki Miyashita, and Yoshihiko Konishi, "Measurement using the S-parameter method for radiation characteristics and mutual coupling of multiport antennas on a small ground," *2012 International Symposium on Antennas and Propagation (ISAP)*, pp.1003–1006, Dec.2012.

[14] Tyler F. Chun ; Alexis Zamora ; Bao Jun Lei ; Reece T. Iwami ; Wayne A. Shiroma, "An Interleaved, Interelement Phase-Detecting/Phase-Shifting Retrodirective Antenna Array for Interference Reduction," *IEEE Antennas and Wireless Propagation Letters*, vol. 10, pp.919–922, Sep.2011.

[15] R. Garg, P. Bhartia, I. Bahl and A. Ittipiboon, *Microstrip Antenna Design Handbook*. pp.41-43, Artech House, Number of Pages= 490,ISBN = 0-89006-513-6, Mar.2001.

[16] Wikipedia, "IBM and Ericsson Announce 5G mmWave Phased Array Antenna Module," *Microwave Journal*, Feb.2017.

[17] Arismar Cerqueira S. Jr., "Antenna Development for 5G Networks," in *2017 SBMO /IEEE MTT-S International Microwave and Optoelectronics Conference (IMOC)*, Águas de Lindoia, Brazil, Aug. 2017, pp. 3–5.

[18] Yaohui Yang , Zhiqin Zhao , Zaiping Nie, "Closely spaced multi-band MIMO antenna for mobile terminals," in *2017 Progress In Electromagnetics Research Symposium - Spring (PIERS)*, St Petersburg, Russia, May 2017, pp. 1222–1226.

[19] Gunjan Srivastava , Akhilesh Mohan, "Compact MIMO Slot Antenna for UWB Applications," *IEEE Antennas and Wireless Propagation Letters*, vol. 15, pp.1057–1060, Oct.2015.

[20] Mojtaba Kiani-Kharaji, Hamid Reza Hassani , Sajad Mohammad-Ali-Nezhad, "Wide scan phased array patch antenna with mutual coupling reduction," *IET Microwaves, Antennas & Propagation*, vol. 12, pp.1932–1938, Sep. 2018.

[21] C. X. Mao, Q. X. Chu, Y. T. Wu, Y. H. Qian, "Design and investigation of closely-packed diversity UWB slot-antenna with high isolation," *Prog. Electromagn. Res. C*, vol. 41, pp.13–25, Jun.2013.

[22] S. Zhang, Z. N. Ying, J. Xiong, S. L. He, "Hybrid fractal shape planar monopole antenna covering multiband wireless communications with MIMO implementation for handheld mobile devices," *IEEE Trans. Antennas Propag*, vol. 62, no. 3, pp.1483–1488, Mar.2014.

[23] C. X. Mao, Q. X. Chu, "Compact Coradiator UWB-MIMO Antenna With Dual Polarization," *IEEE Trans. Antennas Propag*, vol. 62, no. 9, pp.4474–4480, Sep.2014.

[24] Mukesh Kumar Khandelwal, Binod Kumar Kanaujia, and Sachin Kumar, "Tapering of Antenna Array for Efficient Radiation Pattern," *e-Journal of Science and Technology (e-JST)*, vol. 8, no. 2, pp. 36-40, Feb.2013.

[25] D.B. Hou, S. Xiao, B.Z. Wang et al., "Elimination of scan blindness with compact defected ground structures in microstrip phased array," *IET Microw. Antennas Propag.*, vol. 3, no. 2, pp. 269-275, Mar.2009.

[26] Y. Hajilou, H.R. Hassani, B. Rahmati, "Mutual coupling reduction between microstrip," in *2012 6th European Conference on Antennas and Propagation (EUCAP)*, Prague, Czech Republic, Mar. 2012, pp. 1–4.

[27] K. Wei, J. Li, L. Wang et al., "Mutual coupling reduction by novel fractal defected," *IEEE Trans. Antennas Propag.*, vol. 64, no. 10, pp. 4328-4335, Oct.2016.

[28] Y. Fu, N. Yuan, "Elimination of scan blindness in phased array of microstrip patches using electromagnetic bandgap materials," *IEEE Antennas Wirel. Propag. Lett.*, vol. 3, no. 1, pp. 63-65, 2004.

[29] G. Donzelli, F. Capolino, S. Boscolo et al., "Elimination of scan blindness in phased array antennas using a grounded-dielectric EBG material," *IEEE Antennas Wirel. Propag. Lett.*, vol. 6, pp. 106-109, Apr.2007.

[30] E. Rajo-Iglesias, Ó Quevedo-Teruel, L. Inclán-Sánchez, "Mutual coupling reduction in patch antenna arrays by using a planar EBG structure and a multilayer dielectric substrate," *IEEE Trans. Antennas Propag.*, vol. 56, no. 6, pp. 1648–1655, Jun.2008.

[31] M.H. Awida, A.H. Kamel, A.E. Fathy, "Analysis and design of wide-scan angle wide-band phased arrays of substrate-integrated cavity-backed patches," *IEEE Trans. Antennas Propag.*, vol. 64, no. 60, pp.3034–3041, Jun.2013.

[32] K. Buell, H. Mosallaei, K. Sarabandi, "Metamaterial insulator enabled superdirective array," *IEEE Trans. Antennas Propag.*, vol. 22, no. 4, pp. 1074-1085, Apr.2007.

[33] A. Habashi, J. Nourinia, C. Ghobadi, "Mutual coupling reduction between very closely spaced patch antennas using low-profile folded split-ring resonators (FSRRs)," *IEEE Antennas Wirel. Propag. Lett.*, vol. 10, pp. 862-865, Aug.2011.

[34] M.C. Tang, Z. Chen, H. Wang et al., "Mutual coupling reduction using metastructures for wideband dual-polarized high-density patch arrays," *IEEE Trans. Antennas Propag.*, vol. 65, no. 8, pp. 3986-3998, May.2017.

[35] H. Qi, X. Yin, H. Zhao et al., "Mutual coupling suppression between two closely spaced microstrip antennas with an asymmetrical coplanar strip wall," *IEEE Antennas Wirel. Propag. Lett.*, vol. 15, pp. 191-194, Jun.2015.

[36] G. Yang, J. Li, D. Wei et al., "Study on wide-angle scanning linear phased array antenna," *IEEE Trans. Antennas Propag.*, vol. 66, no. 1, pp. 450-455, Jan.2018.

[37] U. Yang, J. Li, S.G. Zhou et al., "A wide-angle E-plane scanning linear array antenna with wide beam elements," *IEEE Antennas Wirel. Propag. Lett.*, vol. 16, pp. 2923-2926, Sep.2017.

[38] B.A. Arand, A. Bazrkar, A. Zahedi, "Design of a phased array in triangular grid with an efficient matching network and reduced mutual coupling for wide-angle scanning," *IEEE Trans. Antennas Propag.*, vol. 65, no. 6, pp. 2983-2991, Jun.2017.

[39] Mukesh Kumar Khandelwal, Binod Kumar Kanaujia, and Sachin Kumar, "Defected Ground Structure: Fundamentals, Analysis, and Applications in Modern Wireless Trends," *International Journal of Antennas and Propagation*, vol. 2017, pp. 2-3, Feb.2017.

[40] Mohammad S. Sharawi, Eva Rajo-Iglesias, "Printed Multi-Band MIMO Antenna Systems and Their Performance Metrics," *IEEE Antennas and Propagation Magazine*, vol. 55, no. 5, pp.218–232, Oct. 2013.

[41] Antenna Theory. (2015). Antenna-theory, S-parameters, [Online]. Available: http://www.antenna-theory.com/definitions/sparameters.php (visited on 05/04/2019).

[42] ACER. (2019). Aspire 5 A515-51G Tech Specs, [Online]. Available: https://www.acer.com/ac/en/GB/content/model/NX.GS3EK.001 (visited on 05/04/2019).

[43] Aras Saeed Mahmood , Dlnya Aziz Ibrahim, "Non-Uniform Chebyshev Excitation of a Linear Broadside Antenna Array Operating at 1.8GHz," *Global Journals*, vol. 16, no. 5, pp. 19-23, Jan.2016.

[44] Mohamed F. A. Ahmed, Osama M. Haraz, Georges Kaddoum, Saleh A. Alshebili, Abdel-Razik Sebak, "On Using Gaussian Excitation Amplitudes to Improve the Antenna Array Radiation Characteristics," in *2014 IEEE Asia-Pacific Conference on Applied Electromagnetics (APACE)*, Johor Bahru, Malaysia, Dec. 2014, pp. 131–134.

[45] Gert Paparisto, Joel Kirshman, David Vye. (2017). Capitalize on EDA When Developing MIMO, Phased-Array Antenna Systems, Part 1, [Online]. Available: https://www.mwrf.com/software/capitalize-eda-when-developing-mimo-phased-array-antenna-systems-part-1 (visited on 05/04/2019).

[46] CST Studio. (2019). Patch Square Truncated Capacitively Pin Fed, [Online]. Available: https://www.cst.com/solutions/article/patch-square-truncated-%5C%5Ccapacitively-pin-fed-antenna-magus (visited on 05/04/2019).

[47] Antenna Magus. (2019). Planar antennas and surface waves, [Online]. Available: http://www.antennamagus.com/applicationnotes.php?page=apps (visited on 05/04/2019).